Institut für Biochemie der Medizinischen Fakultät Charité
der Humboldt-Universität zu Berlin

DISSERTATION

Structures of protein targeting complexes

Zur Erlangung des akademischen Grades
doctor rerum naturalium (Dr. rer. nat.)

im Fach Biologie

eingereicht an der

Mathematisch-Naturwissenschaftlichen Fakultät I

der Humboldt-Universität zu Berlin

von
Mario Halic
geb. 06.04.1976 in Cakovec, Kroatien

Präsident/Präsidentin der Humboldt-Universität zu Berlin

Prof. Dr. Jürgen Mlynek

Dekan/Dekanin der Mathematisch-Naturwissenschaftlichen Fakultät I

Prof. Dr. Thomas Buckhout

Gutachter: 1. Prof. Dr. Peter-M. Kloetzel

2. Prof. Dr. Klaus Peter Hofmann

3. Prof. Christian Spahn

eingereicht: 31.01.05
Datum der Promotion: 12.10.05

Abstract

Cotranslational translocation of proteins across or into membranes is a vital process in all kingdoms of life. It requires targeting of the translating ribosome to the membrane by the signal recognition particle (SRP), an evolutionary conserved ribonucleoprotein particle. SRP recognizes signal sequences of nascent protein chains emerging from the ribosome. Subsequent binding of SRP leads to pausing of peptide elongation and docking to the membrane-bound SRP receptor. Here, the 12 Å cryo-electron microscopy structure of a targeting complex is presented consisting of mammalian SRP bound to an active 80S ribosome carrying a signal sequence. A molecular model of SRP in this functional conformation was generated. The model reveals how the S-domain of SRP contacts the large ribosomal subunit at the nascent chain exit site to bind the signal sequence, and that the Alu-domain reaches into the elongation factor binding site of the ribosome explaining its elongation arrest activity. A molecular model of the first steps of protein targeting is presented. Moreover, also the docking step has been visualized by solving a cryo-EM structure of the ribosome-SRP complex bound to the SRP receptor. This structure provides first hints regarding the mechanism of ribosome transfer to the translocon. As a side result the position of the functionally significant ribosomal protein L30e has been identified in the high resolution maps of the wheat germ ribosome.

Keywords:
SRP, SR, ribosome, signal sequence, protein targeting, cryo-electron microscopy

Zussamenfassung

Sowohl die kotranslationale Translokation von sekretorischen Proteinen durch die Membran als auch die Insertion von Membranproteinen sind essentielle Prozesse in allen lebenden Zellen. Sie erfordern die Sortierung des translatierenden Ribosoms zur Membran mittels des Signalerkenungspartikels (SRP), eines im Verlauf der Evolution konservierten Ribonukleoprotein-Partikels. SRP erkennt die Signalsequenz einer wachsenden Proteinkette, sobald diese aus dem Ribosom hervortritt. Die Bindung von SRP führt zum Anhalten der Peptidelongation (Elongationsarrest) und zum Andocken an den membrangebundenen SRP-Rezeptor (SR). In dieser Arbeit wird die 12 Å Kryo-Elektronenmikroskopie-Struktur eines Sortierungs-Komplexes dargestellt, der aus dem Säugetier-SRP gebunden an ein aktives Ribosom mit Signalsequenz besteht. Ein erstes molekulares Modell von SRP in dieser Konformation wurde erzeugt. Es zeigt wie die S-Domäne von SRP die große ribosomale Untereinheit nahe dem Peptidtunnel-Ausgang kontaktiert, um dort die Signalsequenz zu binden. Außerdem wird deutlich wie die Alu-Domäne von SRP in die Bindungsstelle für Elongationsfaktoren hineinreicht, wodurch die Elongationsarrest-Aktivität der Alu-Domäne erklärt wird. Auf dieser Basis konnte ein erstes Struktur-basiertes Modell der ersten Schritte der kotranslationalen Proteinsortierung entworfen werden. Darüberhinaus wurde auch der Schritt des Andockens an die Membran visualisiert, indem die Struktur des Ribosom-SRP-SR-Komplexes durch Kryo-EM gelöst wurde. Erste Schlüsse hinsichtlich des Mechanismus, der das Ribosom vom SRP zum Translokon transferiert, können hier gezogen werden. Als Nebenergebnis konnte durch die erreichte hohe Auflösung die Position des wichtigen ribosomalen Proteins L30e in der Kryo-EM-Struktur des Weizenkeim-Ribosoms idenifiziert werden.

Schlagworte:
SRP, SR, Kryo-Elektronenmikroskopie, Signalsequenz

Abbreviations

SRP	signal recognition particle
SR	SRP receptor
RNC	ribosome nascent chain complex
GTP	guanosine triphosphat
GDP	guanosine diphosphat
GMP-PNP	guanylyl-imidodiphosphate
GAP	guanine nucleotide activating protein
GEF	guanine nucleotide exchange factor
ER	endoplasmic reticulum
ATP	adenosine triphosphat
w/v	weight per volume
CTF	contrast transfer function
SC	fourier shell correlation

1 Introduction

1.1 Protein Targeting

Proteins are synthesized in the cytosol by ribosomes which are large macromolecular machines consisting of RNA and 50-80 proteins. Eukaryotic and prokaryotic ribosomes are very similar in design and function. Both are composed of small (30S in prokaryotes, 40S in eukaryotes) and large ribosomal subunit (50S in prokaryotes, 60S in eukaryotes) which join on the translated mRNA molecule. The mRNA codons are translated into amino acid sequence using the cognate tRNAs as adapters to add the correct amino acids to the growing polypeptide chain. The large subunit of the ribosome provides the peptidyl transferase activity while the small subunit binds mRNA and is the site of decoding. When the stop codon is recognized on the mRNA ribosomes release the protein, and subunits separate again.

Many proteins have not the cytoplasm but organelles or even the environment outside the cell as a destination and have to be transported there. Even though most secretory and membrane proteins are targeted to the endoplasmic reticulum (ER) membrane to be cotranslationally translocated, some are translated completely in the cytosol, and later, postranslationally, transported to their destination. This applies also to mitochondrial, chloroplast or nuclear proteins. The main advantage of cotranslational targeting is that the coupling of translation and translocation prevents misfolding of the proteins in the cytoplasm.

The essential signal for correct sorting of such proteins are hydrophobic N-terminal signal sequences typically comprising 15-20 amino acids: a short positively charged N-terminal region, a central hydrophobic core and a more polar C terminal part which has a cleavage site for signal peptidase. Signal sequences are very divergent and have two general features – hydrophobicity and α-helical conformation of the hydrophobic core. Disruption of one of these features leads to a non-functional signal sequences for cotranslational targeting [1]. While in eukaryotes signal sequences are usually located at the extreme N-terminus, in prokaryotes like E. coli SRP-dependent signal sequences are often a transmembrane helix within membrane proteins of the plasma membrane.

Nascent chains carrying signal sequences will be recognized by a signal sequence “binding factor” [2], later identified in a mammalian system as an 11S ribonucleoprotein particle and named signal recognition particle (SRP) [3]. SRP will recognize any signal sequence with a critical level of hydrophobicity. The question how SRP recognizes and binds almost any hydrophobic α-helix is currently unanswered. Binding of SRP will arrest elongation of the nascent peptide chain and target the complex to the membrane via GTP dependent interaction with the SRP receptor (SR). After the SRP-SR-nascent chain-ribosome complex interacts with the translocon, the signal sequence is released; the SRP-SR complex dissociates after GTP hydrolysis and translation resumes (fig.1).

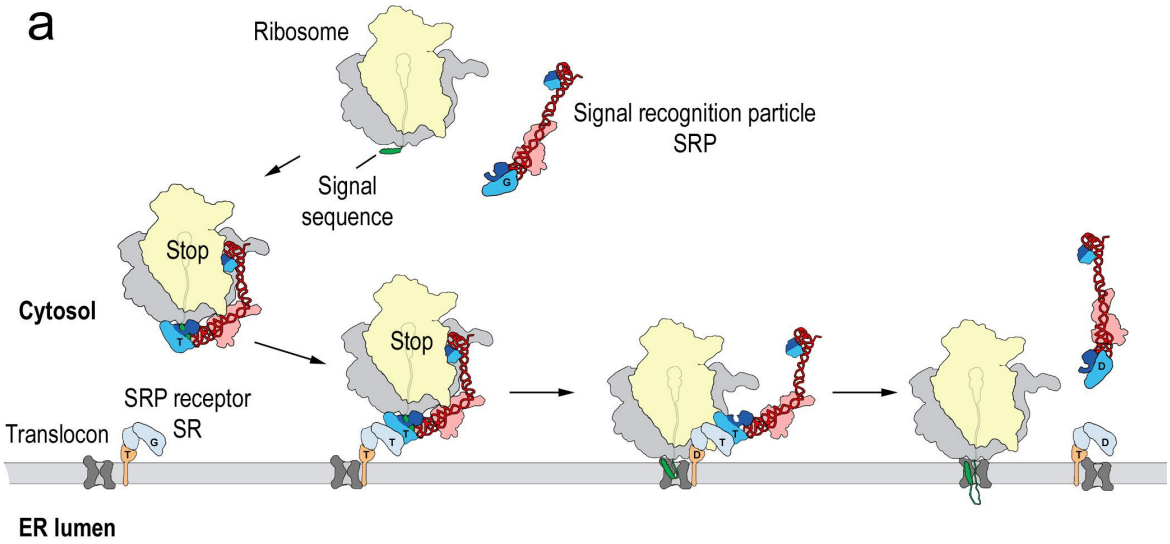

Figure 1: Signal sequence recognition and cotranslational targeting by SRP. (a) Schematic overview of cotranslational targeting of proteins destined for secretion or membrane insertion. SRP interacts with the signal sequence as soon as it emerges from the ribosomal polypeptide exit tunnel (step I). In eukaryotes peptide elongation pauses upon SRP / ribosome nascent chain (RNC) complex formation and the RNC complex is targeted to the ER membrane by the interaction with the SR (step II). GTP binding to SRP and SR has been shown to be a prerequisite for SRP/SR complex formation. The RNC is then transferred to the protein-conducting channel in the membrane (the translocon) (step III) and triggered by GTP hydrolysis in SRP and SR the SRP/SR complex dissociates (step IV). (b) Schematic overview of the mammalian SRP bound to the signal sequence carrying 80S ribosome (RNC) based on a cryo-EM structure. The SRP core as part of the S-domain is positioned near the tunnel exit of the large ribosomal subunit. The 40S and 60S ribosomal subunits are yellow and grey, respectively. The SRP RNA is shown in red and the SRP proteins are labelled as follows: SRP54NG (turquoise), SRP54M (dark blue), signal sequence (green), SRP19 and SRP68/72 (pink), SRP9/14 (turquoise/dark blue).

1.2 Signal recognition particle (SRP)

The signal recognition particle displays three main activities in the process of cotranslational targeting: (I) binding to signal sequences emerging form the translating ribosome, (II) pausing of peptide elongation, and (III) promotion of protein translocation through docking to the membrane-bound SRP receptor (FtsY in prokaryotes) and transfer of the ribosome nascent chain complex (RNC) to the protein-conducting channel [4].

These activities can be assigned to the two main domains of SRP separable by the micrococcal nuclease treatment [5]: the first domain, called S-domain, binds to signal sequences and promotes translocation [6]. In mammalian SRP, it includes about half of 7S RNA of SRP (~nucleotides 100-250) as well as the essential proteins SRP19, SRP54 (Ffh in prokaryotes), and the SRP68/72 heterodimer (fig. 2, 3a). While SRP19 is required for SRP assembly [7], SRP54 is the functionally most significant protein subunit of the S-domain: it recognizes the signal sequence [6] and interacts with the SRP receptor in a GTP-dependent manner [8]. SRP54 is composed of an N-terminal domain (N), a central GTPase domain (G) and a methionine-rich C-terminal domain (M) [9], which anchors SRP54 to SRP RNA [10]. In addition, together with a part of the RNA backbone [11], the

M-domain carries out the principal function of the signal sequence recognition [12] near the peptide tunnel exit site of the large ribosomal subunit [13].

The second main domain of SRP, called Alu-domain, mediates the elongation arrest activity [14]. It is supposed to enable efficient targeting by providing a time window during which the nascent chain can be targeted to the translocation site [15, 16, 17]. The Alu-domain contains the 5'- and 3'-part of 7S RNA (including Alu-like sequences) as well as the SRP9/14 heterodimer, which is essential for its activity [18].

1.2.1 SRP RNA

The presence and necessity of RNA in SRP is not completely understood yet. It seems that 4.5S RNA in *E.coli* stabilises the structure of the Ffh M-domain[19, 20]. In addition, kinetic studies show that RNA enhances association and dissociation of Ffh-FtsY complexes, and the positively charged N-terminal part of the signal sequence probably interacts with the negatively charged RNA backbone.

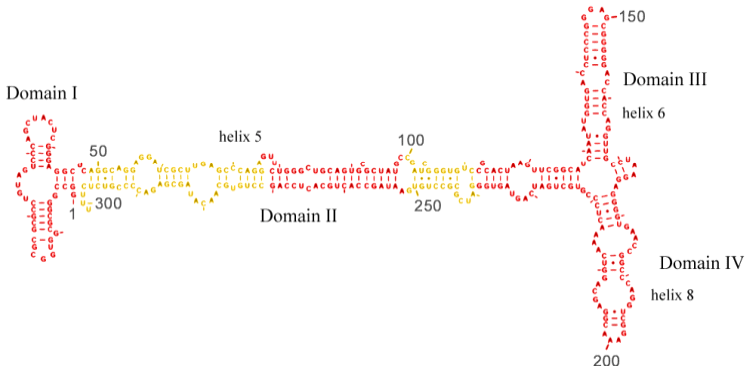

Figure 2: Secondary structure of the SRP RNA with RNA domains indicated

Structurally, the 300 nucleotide long human SRP RNA can be divided into four domains**[21, 22]**. Domain I consists of 5'- and 3'-ends of the molecule (helices 2-4 in mammalian SRP) and it builds the SRP Alu-domain. It seems that helix 1 is absent in eukaryotes. Domain II (helix 5) is the linker between the Alu-domain and the S-domain which consists of two RNA domains, domain III (helix 6) and domain IV (helix 8). Eukaryotes contain an additional helix 7 at the interface of domains III and IV. Only domain IV is conserved in all SRP RNA molecules.

1.2.2 Evolutionary conservation

Although SRP is essential and present in all kingdoms of life maintaining its general function, structurally it shows high diversity. Minimal SRP, as found in gram negative eubacteria such as *E. coli* consists of a 106 nucleotides long RNA (domain IV) and SRP54 homolog (Ffh) only (fig. 3c). *E. coli* SRP also completely lacks an Alu-domain, and there is no evidence for translational arrest

induced by SRP binding. In gram-positive eubacteria, like *Bacillus subtilis,* SRP has a more complex structure. The RNA is longer and it consists of domains I, II and IV and, in contrast to the gram-negative, has an Alu-domain. The presence of the SRP9/14 heterodimer has not been shown in gram-positive eubacteria, but a histone-like protein HBsu has been found to bind to Alu part of SRP RNA [23] (fig. 3c). HBsu is not a homolog of SRP9/14, but it has been suggested that it can fold into a tertiary structure similar to SRP9/14 [24], and might serve as their functional analog.

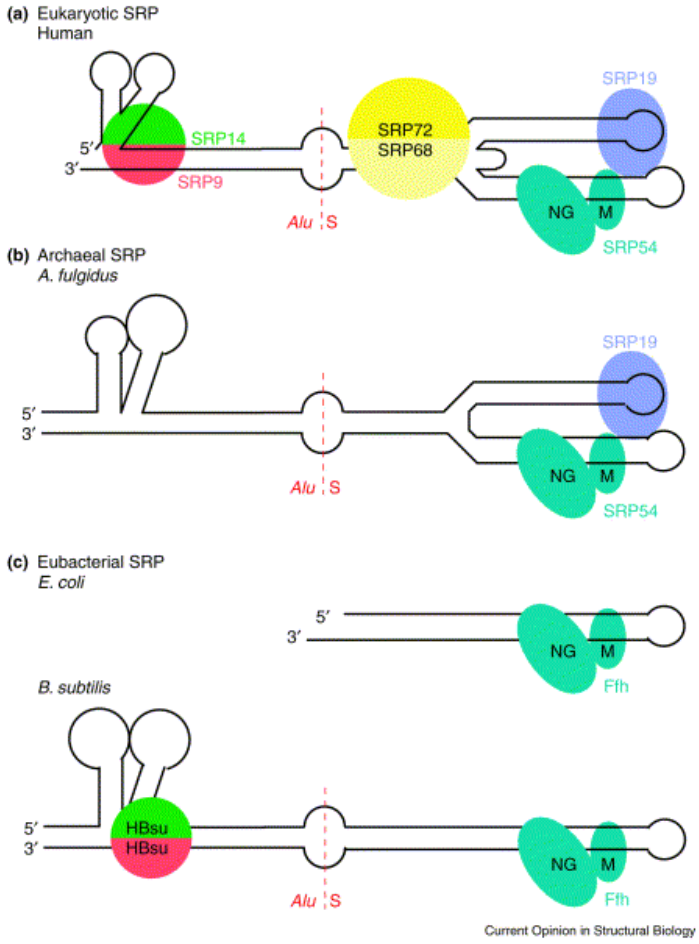

Figure 3: Evolutionary conservation of SRP. a) Eukaryotic SRP consists of six proteins and RNA divided into two main domains, S- and Alu-domain. b) Archaeal SRP with similar RNA structure, but with only two proteins, SRP54 and SRP19. c) Eubacterial SRP in gram-negative bacteria like E. coli represents a minimal SRP consisting of a SRP54 homolog (Ffh) and RNA domain IV only. Some gram-positive bacteria like B. subtilis have an Alu-domain with histone-like HBsu proteins instead of SRP9/14 [25]

Archaeal SRP is more similar to eukaryotic SRP (fig. 3b). Archaeal RNA secondary structure shows high similarity to the mammalian; it contains four domains divided in eight helical elements folding into S- and Alu-domain. It has only two proteins, SRP54 and SRP19, which is, like in eukaryotes, responsible for the assembly [26]. Moreover, archaeal SRP54 can functionally interact with mammalian signal sequences [27], showing its high evolutionary conservation.

Even certain eukaryotic SRPs display a high level of structural variety. For example SRP of *S. cerevisiae* has a 600 nucleotide long RNA, twice as long as the mammalian. Instead of the SRP9/14

heterodimer, *S. cerevisiae* SRP contains a SRP14 homodimer, and, in addition, the unique SRP protein SRP21. In contrast to the secondary structure of S-domain RNA, which is comparable to mammalian, the Alu-domain is far larger and more complex [28].

Nevertheless, high functional and structural conservation of the minimal SRP through all kingdoms of life has been experimentally revealed by replacement of subunits of mammalian SRP (SRP54) with bacterial homologs (Ffh) which leads to partially active chimeric SRP [29].

Recently, SRP has also been found in chloroplasts where it differs from the cytosolic in that it contains unique a 43kD [30] subunit and lacks an RNA. It is required for the posttranslational targeting to the thylakoid of chlorophyll proteins encoded in the nucleus, and the cotranslational targeting of proteins synthesized by the chloroplast ribosomes. Chloroplast SRP appears to be present in two forms [31]. Polytopic protein D1 is synthesized by the chloroplast membrane bound ribosomes and is cotranslationally integrated in the thylakoid membrane where it interacts with cpSecY, the translocation channel in thylakoid membrane [32, 33]. The targeting to the thylakoid cpSecY involves cpSRP54 (chloroplast homolog of SRP54), and it is independent from cpSRP43 [34]. Chloroplast ribosomes have the ability to pause the translation involving a light dependent regulation mechanism different from the elongation arrest. CpSRP composed of cSRP43 dimer and cpSRP54 is responsible for the posttranslational targeting of nuclear encoded photosystem proteins (light harvesting complexes) [35], after they have been imported into the stroma. It interacts with the substrate and forms a soluble intermediate transit complex. Both cpSRP43 and cpSRP54 are involved in the substrate binding [36], and are necessary for the posttranslational targeting [30]. Insertion into the membrane requires GTP and cpFtsY (SRP receptor homolog). Both SRPs have no overlapping functions. No SRP or SRP receptor was found in mitochondria.

1.2.3 SRP assembly

SRP is partially assembled in the nucleus and partially in the cytoplasm a in agreement with that, nuclear localization for SRP proteins SRP9/14, SRP68, SRP72 and SRP19 has been determined [37]. After the transport into the nucleus the subunits bind SRP RNA and form a pre-SRP which is exported to the cytoplasm and binds SRP54 [7, 37, 38].

SRP assembly starts during 7S RNA transcription by RNA polymerase III in the nucleolus, by binding of the SRP 9/14 heterodimer and formation of Alu-domain. Prior to transportation to the nucleus SRP9 and SRP14 form the heterodimer in the cytoplasm which is a prerequisite for the binding to 7S RNA [39].

The structure of the Alu-domain, which includes 56 nucleotides of the 5'-region of 7S RNA and the SRP9/14 heterodimer does not resemble a tRNA-like structure as previously suggested. Both proteins, SRP9 and SRP14 are structurally related and have an αββββα fold. The heterodimer binds primarily to the highly conserved core of the 5'-region of 7S RNA which consists of a three way junction in which two helical hairpins are connected to a third helical stem by a conserved U-turn [40]. The 5'-region of 7S RNA contains highly conserved nucleotides and it is capable to bind

SRP9/14 even in absence of 3'-region. The majority of protein-RNA interactions are made by the concave β-sheet of SRP14. The final assembly step requires the 3'-region of 7S RNA to which the 5'-region folds back. As a result, the stem leading to the S-domain emerges on the C-terminal side of SRP14 and the SRP9 β-sheet interacts with the 3'-region [40] (fig. 4). This backfolding of 7S RNA is probably the final but a reversible step of Alu-domain assembly. Intact Alu-domain is required for final 3' processing of SRP RNA in mammalian cells, and its export to the cytoplasm [41]. A compactly folded 5'-region of 7S RNA and SRP9/14 is shown to be necessary for the efficient transcription of SRP RNA [42], probably by direct interaction with the transcriptional machinery. Notably, the central question of how the Alu-domain exerts its activity and mediates the arrest of peptide elongation remains unanswered so far. Since its structure apparently doesn't resemble a tRNA-like fold it appears unlikely that the Alu-domain simply occupies the tRNA A-site of the ribosome as suggested before.

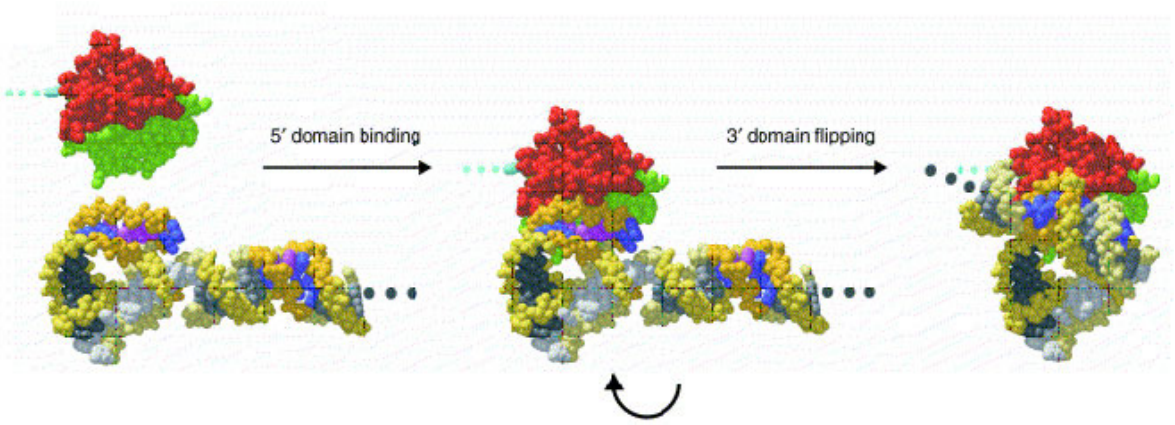

Figure 4: Mammalian Alu domain assembly. In a first step the heterodimer consisting of SRP9 (red) and SRP14 (green, with the important C-terminal tail in cyan) binds to 5'-region of the Alu RNA. In a second step the 3'-region of the Alu RNA flips by up to 180 and it is clamped against 5' Alu RNA. The RNA backbone is shown in yellow. Both 5'- and 3'-region of Alu RNA involved in protein binding are structurally conserved (orange) [25].

Sequences related to the Al-part of 7S RNA are dispersed through the mammalian genome. They originate from a reverse flow of the genetic information from 7S RNA to genomic DNA and amplification of 5'- and 3'-end of 7S RNA [43]. The Alu family of repetitive sequences is specific for rodent and primate genomes. The human genome has around 1 million copies of 300bp long Alu sequences which comprise over 10% of the genome. The function of these elements is unknown yet, but they are one of the major differences between human and other primate genomes. One of these Alu elements is BC200, which is specifically expressed in human neural cells from a single gene by RNA polymerase III. BC200 localises in neurons specifically in the somatic and/or dendritic domains and it is still actively retrotransposing. The tertiary structure of BC200 is related to the SRP Alu-domain, however it permits the binding of SRP9/14 heterodimer [44].

A central role in the SRP assembly can be assigned to SRP19. From *in vitro* reconstitution experiments it is known that binding of the mammalian SRP54 to 7S RNA requires SRP19 binding first [7]. However, archaeal SRP54, unlike eukaryotic, has significant affinity for 7S RNA even in an absence of SRP19. SRP19 is a single domain αβ-type protein with a three-stranded antiparallel β-sheet packed on one side against two helices. With its flexible loops, it recognizes a particular shape of the rigid stem-loop RNA. SRP19 homologues have been found only in organisms which have helix 6. Helix 6 is closed with an unusual GNAR (N is any nucleotide; R is G or A) type loop, where A is strictly conserved and necessary for SRP19 binding. SRP19 interacts with a major groove of this tetraloop and with a minor groove of helix 8 tetraloop. In addition it interacts with parts of the highly conserved symmetrical loop of helix 8 that are not interacting with SRP54 M-domain [45]. In that way it brings together both helices in a side-by-side position (fig. 5, 6).

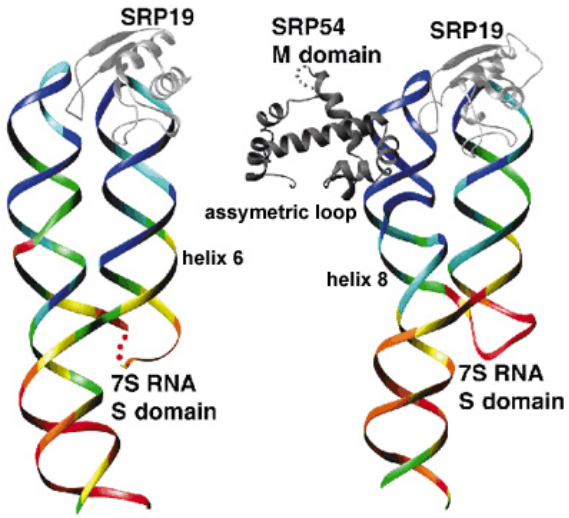

Figure 5: Structure of SRP S-domain assembly steps. On left side the structure of SRP19 in complex with helices 5-8 is shown. SRP19 binds to both helices and brings them together as a prerequisite for SRP54 binding. On the right side the structure of a ternary complex consisting of SRP19, helices 5-8 and SRP54M domain is shown. Note the change in the asymmetric loop arrangement upon SRP54 binding [46].

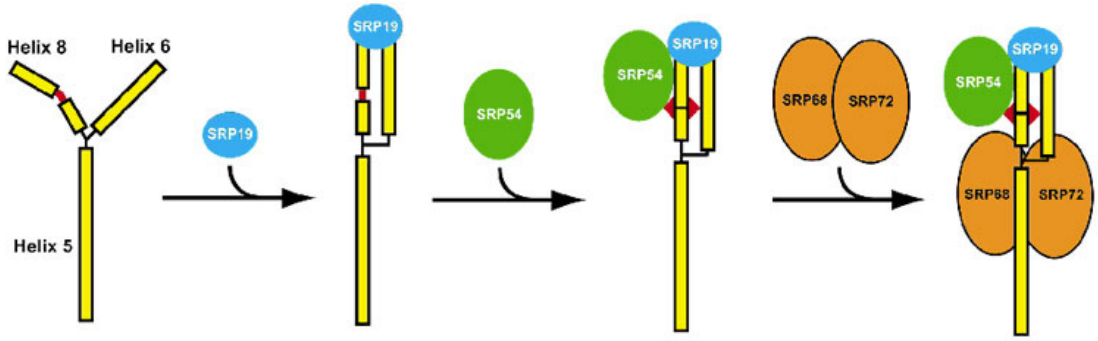

Figure 6: Model of SRP S-domain assembly. In a first step SRP19 brings helices 6 and 8 together. In a second step SRP54 binds to the symmetric and asymmetric loops and changes the asymmetric loop to a rigid conformation. In a last step the SRP68/72 heterodimer binds to the three -way junction [46].

The symmetric loop consists of four non-Watson-Crick base pairs which are conserved from eubacterial to human SRP RNA. Disruption of one of two base pairs, a sheared G-G pair or a reverse Hoogsteen A-C pair, eliminates protein binding and is lethal for the cell. SRP54 binds to these two loops and induces severe structural changes of the asymmetric loop. Two bases of it flip out and form an A-minor motif with helix 6 bases, which is only possible after SRP19 binding. In contrast to the well ordered symmetric loop the asymmetric loop is very flexible in free 7S RNA. SRP19 binding stabilizes the asymmetric loop of helix 8 via A-minor base triples with the helix 6 which is a prerequisite for SRP54 binding. The asymmetric loop has an evolutionary conserved 5'-side adenosine base which interacts with three universally conserved amino acids of the C-terminal part of SRP54 M-domain. This part of SRP54 M-domain forms a conserved arginine-rich HTH-motif which is involved in the RNA binding (αM2-αM5). SRP54 interacts with the minor groove of RNA with two helices αM3b and αM4 and in that way it brings asymmetric and symmetric loop together to form a stable protein-RNA interface (fig. 8). In contrast to RNA the SRP54 M-domain does not undergo large conformational changes upon binding [45, 46, 47].

In eubacteria without helix 6, the asymmetric loop is stabilized by magnesium ions. Currently no other function for SRP19 has been determined. It seems that helix 6/SRP19 is an evolutionary adaptation of SRP to enhance and control the kinetics of the assembly that cannot be done by metal ions.

SRP68 and SRP72 form a heterodimer in the nucleus only in a presence of 7S RNA, and as a dimer they bind to the three-way junction of the S-domain RNA. SRP68 binds first to RNA with its N-terminal region which is mainly positively charged. This is a prerequisite for the interaction of the C-terminal region of SRP72 with the C-terminal region of SRP68 in an hydrophobic manner [48]. SRP68/72 can be released from 7S RNA by high-salt treatment without dissociating into monomers.

It is not completely clear what the function of SRP68/72 is. Biochemical experiments [49] indicate that SRP68/72 interacts with the SRP receptor, and that it possibly participates also in the elongation arrest. SRP with an alkylated SRP68/72 heterodimer fails to target to the ER. SRP missing SRP68/72 or SRP reconstituted with SRP68/72 alkylated as a free protein, fails not only in targeting, but also in the elongation arrest. It has been proposed that SRP68/72 has also a role as guanine nucleotide dissociation factor [50].

1.2.4 SRP54 and signal sequence recognition

Signal peptide is recognized by SRP54 which together with the RNA helix 8 builds the minimal SRP. These two components are present in all SRPs. SRP54 is a multidomain protein consisting of three domains; an N-terminal four-helix bundle (N-domain), a GTPase domain (G-domain) and a C-terminal methionine-rich domain (M-domain). The N- and G-domain are usually treated as one domain (SRP54NG) responsible for the GTP regulation of protein targeting and the interaction with SR. The M-domain can be divided into two parts, the evolutionary conserved and rigid C-terminal

part which binds RNA helix 8, and the flexible N-terminal part which is responsible for the signal sequence recognition and binding as demonstrated by chemical cross-linking [12]. The M-domain contains typically a high percentage of methionine residues [10, 12]. About 16% of all M-domain residues in E. coli are methionine, a frequency about 6 time's higher than that of the average methionine occurrence in proteins. Methionine has a highly flexible hydrophobic side chain because it is unbranched and displays unique conformational properties of the thioether linkage [51]. This features led to the hypothesis that methionines and other hydrophobic residues are arranged so that their flexible side chains form the hydrophobic binding site for the signal sequence with sufficient plasticity to recognize the wide variety of signal sequences [9]. In T. aquaticus, methionine residues are often replaced by branched hydrophobic residues like Phe, Leu or Val, because at higher temperatures (optimal for T. aquaticus) increased thermal motion eliminates the need for more flexible methionine [4, 26].

Compared to prokaryotic Ffh, the eukaryotic SRP54 M-domain contains additional 100 residues which play a role in the signal sequence binding. Deletion of this C-terminal region leads to the abolishment of cross-linking to signal sequences [52]. It is possible that the C-terminus increases the hydrophobic surface area. However, the necessity for that is not clear since eukaryotic signal sequences are often shorter then transmembrane regions which act as signal sequences in prokaryotic inner membrane proteins.

In the last few years several crystal structures of SRP54 M-domains have been solved [1, 11, 46, 53]. While the C-terminal part of M-domain (Mc) is very similar and well ordered in all structures, the N-terminal part (Mn) shows differences, especially in the finger loop, which is closing the hydrophobic groove and significantly varies in diverse structures. Helices αM1, αM1b, αM2 and αM5 build the hydrophobic pocket closed by this flexible loop. In the T. aquaticus structure [1] the finger loop is well ordered as it binds into its hydrophobic pocket the helix of a neighbouring M-domain in the crystal resembling in that way the signal sequence binding. In the E. coli structure [11] the finger loop is disordered and in the S. solfactoricus [53] structure of the complete SRP core, the finger loop is closed (fig. 7, 8). These differences show the flexibility of the finger loop which might be the basis for binding a variety of signal sequences. The structures of the M-domain of T aquaticus and S solfatoricus may represent two functional states of M-domain; the open state occupied with the signal peptide, and the closed empty state. If this is true, the signal sequence binding induces severe structural changes in the N-terminal part of the M-domain (Mn) whereas the RNA binding C-terminal part seems to stay rigid (Mc). The N-terminal region of signal sequences contains positively charged residues which may contact RNA as suggested [11] (fig. 8).

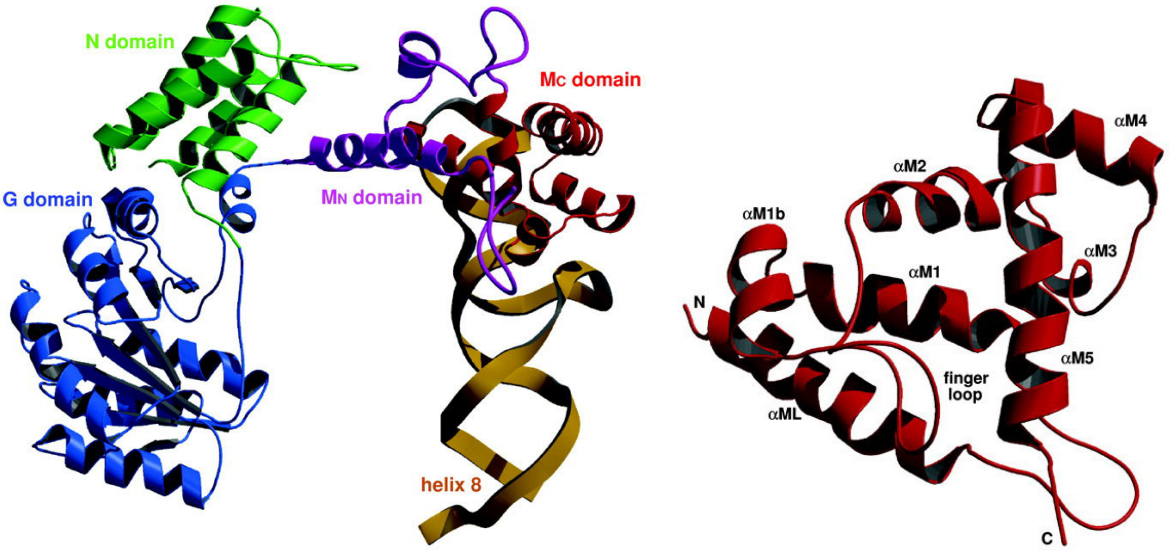

Figure 7: A) Crystal structure of SRP54 in complex with helix 8 in a ribbons representation of the N- (green), G- (blue), Mn- (purple) and Mc-domains (red) and helix 8 (orange). The novel N-terminal part of the M-domain contains the linker helix (αML) and the closed finger loop is highlighted in purple. B) M-domain in a top view compared with A. The finger loop on top is folded into the hydrophobic groove, which is lined by helices αM1, αM1b, αM2 and αM5 [53].

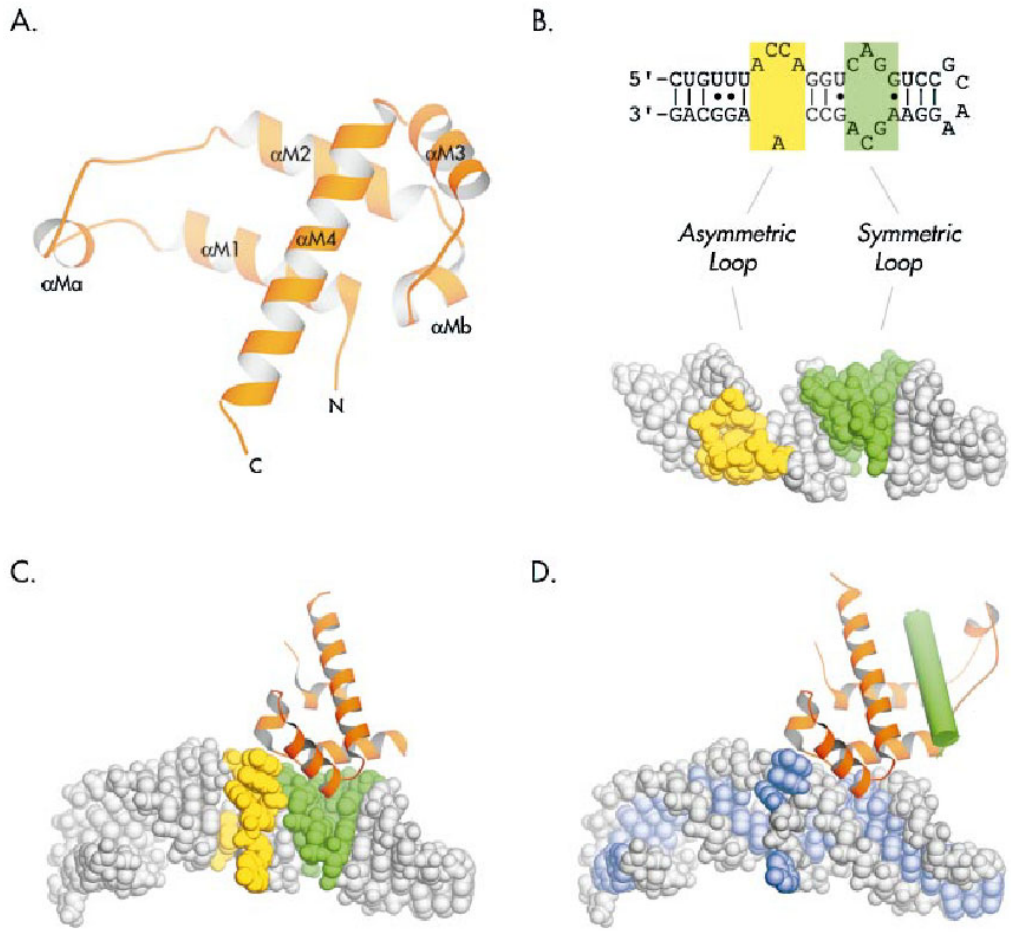

Figure 8: A) Crystal structure of the SRP54 (Ffh) M-domain from *T. aquaticus*. A) The loop connecting helices αM1 and αM2 is open in this crystal structure [1]. B) Secondary structure of the domain IV sequence, and the solution structure of apo form of the domain IV from *E. coli* SRP RNA[54]. Nucleotides within the symmetric loop are highlighted in green, and nucleotides within the asymmetric loop in yellow. C) The SRP54 M-domain in complex with domain IV from *E. coli* [11] with a disordered finger loop. Note the conformational changes in the asymmetric loop (yellow) upon SRP54 binding. D) Model of *T. aquaticus* M-domain together with the structure of *E. coli* M-domain with the signal sequence (green) modelled in the hydrophobic groove of the M-domain. The signal sequence could simultaneously contact the backbone of domainm IV RNA with its positively charged residues [26].

1.2.5 Elongation arrest

The advantage of cotranslational targeting is that coupling of translation and translocation prevents misfolding of newly synthesized protein in cytoplasm. But protein translation can be faster then the diffusion of SRP-RNC complex to the membrane. To prevent that, SRP retards the translation and in that way it enlarges the time window during which a nascent chain can be targeted before it reaches a critical length prone to fold or aggregate. Elongation arrest was discovered in an heterologous system containing the canine SRP and the wheat germ ribosome. Here the SRP completely stops the translation of the nascent peptides [15]. Later, it was also observed in a homologous and more physiological systems from yeast [17, 55] and also in the mammalian systems [16], and it is characteristic for all eukaryotic SRPs. In homologous systems the translational arrest is not very pronounced rather representing translation retardation, and it appears not to be essential for proper in vitro targeting [18]. It has been shown in yeast that defective translation arrest in vivo only slightly affects the translocation [17].

The Alu-domain of SRP, consisting of the 5'- and 3'-regions of 7S RNA and the SRP9/14 dimer, is responsible for the elongation arrest. SRP assembled without SRP9/14 is functional in protein targeting, but it lacks the elongation arrest feature. Even removal of the 20 C-terminal amino acids from SRP14 makes SRP non-functional in the elongation arrest. It has been suggested that the Alu-domain binds near the A-site on the ribosome, but the elongation arrest is still poorly understood. Since prokaryotic SRP lacks the Alu-domain it is one possibility that the elongation arrest is dispensable in prokaryotes. The elongation arrest main function is to enlarge the time window for targeting and prevent that the nascent chain reaches a length which can misfold or aggregate. Prokaryotic cells are in most cases significantly smaller then eukaryotic cells, and thus the time for diffusion to the membrane is smaller. Also, in prokaryotes bacterial DNA is anchored to the cytoplasmic membrane during coupled transcription/translation of membrane proteins which further reduces diffusion distance and, thus, this may allow cotranslational targeting without the need for the elongation arrest [4]. It has been shown that purified E. coli SRP is unable to arrest the translation in in vitro system although it properly binds to a signal sequence [56].

1.2.6 GTPase cycle and SRP receptor

The elongation arrest ability is abolished upon addition of microsomal membranes which led to discovery of the membrane bound SRP receptor (SR) [57]. SR is a heterodimeric complex formed by two subunits, the integral membrane protein SRβ and SRα. The assembly process includes cotranslational but SRP-independent targeting of SRα to the membrane. Within the SRα mRNA a stem loop structure similar to ribosomal frameshift structures causes pausing of the translation and allows folding of the N-terminal domain and interaction with SRβ before translation resumes [58]. In eukaryotes, SRα consists of three domains, the N-terminal X-domain which interacts with SRβ, the N-domain which builds a four helix bundle and the G-domain which binds GTP. The NG domain of the receptor is structurally and functionally homologous to the SRP54 NG domain. The bacterial homolog of eukaryotic SRα, FtsY, is a hydrophilic protein partially localized in the cytoplasm and partially at the membrane. However, a membrane anchoring protein homologous to SRβ has not been identified. Both, SRα and SRβ are GTPases.

GTPases are members of a protein family of highly conserved molecular switches responsible for the regulation of many complex functions such as cell cycling, protein synthesis and membrane trafficking. The general mechanism of GTPases (G-protein) is described in the molecular switch model [59, 60] where the enzyme goes through three conformational steps: GTP-bound, GDP-bound and empty. The G-protein is initially in an empty and inactive state and it gets activated through a conformational change by GTP-binding. Such an active G-protein interacts with a target molecule (GTPase activating protein or GAP) which induces hydrolysis of GTP and inactivates the G protein. The remaining GDP is then released and the G-protein returns into an empty state which is only a transient intermediate during exchange of GDP to GTP. This exchange is regulated by the guanine nucleotide exchange factor (GEF) which switches the G-protein back to the active state.

Protein targeting involves tree different GTPases (SRP54, SRα, SRβ) in eukaryotes and two in prokaryotes (FFH, FtsY). The GTPase cycles of SRP54 and SR do not follow the general model of the GTPase cycle but have several unique properties which led to the concerted switch model for SRP GTPases [60]. SRP54, SRα and their prokaryotic homologues constitute a new subfamily of small Ras-like GTPases [59] with relatively low affinity for nucleotides, and, in contrast to canonical GTPases, they are stable in the absence of the nucleotide. Biological relevance of this apo-form is not clear yet, but its stability is reflected by the fact that both GTPases have been crystallized in the empty state [61, 62]. Structurally, they are more similar to ATP-binding proteins than to other GTPases. Biochemical evidence shows that SRP54 and SRα do not depend on external GEFs in order to dissociate GDP [63, 64], but they have a built-in nucleotide exchange ability. It has been proposed that this activity is located in the unique insertion box domain (IBD) in the effector region of the GTPase [65, 66]. The IBD is a unique structural motif characteristic for the subfamily of SRP GTPases.

Mutation of a conserved glycine in the interface region between N- and G-domain of Ffh and FtsY severely weakens their ability to interact with each other. The same mutations in a conserved N-domain motif (ALLEADV) produced significant defects in signal sequence binding that correlate

with the severity of the mutation [67]. It has been suggested that this interface motif has a function in the communication between N-, G-, and M-domain and that it communicates signal-sequence binding by the M-domain to the NG-domain, thereby priming SRP for the subsequent interaction with SR.

The SRP-SR interaction takes place primarily via their NG-domains [68], but it is further modulated by the SRP RNA which catalyses complex formation [69]. Mutations of the 4.5S RNA which do not affect Ffh binding nor the SRP interaction with the ribosome affect the interaction between SRP and FtsY [70], which is in agreement with the proposed model,

GTP binding to SRP54 and SRα is a prerequisite for their complex formation, and GTP hydrolysis leads to complex dissociation. According to nucleotide cross-link data, GTP affinity of SRP54 is increased upon interaction with a ribosome carrying a signal sequence [71] and SRP is then in the activated GTP-bound form ready to interact with SRα. SRα is primed for complex formation by the interaction with translocon components [71, 72, 73, 74], since GTP binding of SRα is stimulated by addition of purified Sec61 which probably serves as GEF for it. When both, SRP54 and SRα are in GTP from, the complex can be formed.

The isolated NG domains are necessary and sufficient to form the complex in the presence of non hydrolysable nucleotides, although with slow kinetics [75], and it has been shown that they act as GAPs for each other [76]. The recent crystal structures of the interacting NG domains of SRP54/Ffh and FtsY in the GTP state showed that both N-domains rearrange towards the G-domains and that the complex forms an active site at the interface of the two proteins [77, 78] (fig. 9 The individual sites are so closely intertwined that the two nucleotides are hydrogen-bonded to each other via γ-phosphates and ribose moieties. In comparison to GTP-bound free NG domains, NG domains undergo severe conformational changes in highly conserved motifs upon complex formation. Catalytic residues in the IBD loop rearrange and align with respect to the bound substrate. Water molecules in the active site are in an ideal position for GTP hydrolysis, although a non-hydrolysing transition state is stabilized in the observed conformation. It is crucial in the physiological RNC-SRP-SR complex that GTP hydrolysis by SRP and SR is blocked until the signal peptide is released. This prevents complex dissociation prior to delivery of the nascent chain to the translocon. It is not clear how the release of the signal sequence in M domain is communicated to the NG domains to allow GTP hydrolysis. One possibility is that the presence of the signal sequence stabilizes a conformation of the NG twin that has no GTPase activity. To that end, the existence of several activation states has recently indeed been shown [79]. An exhausting mutational analysis of the NG twin structure interface resulted in a model describing discrete structural changes during NG interaction and reciprocal GTPase activation. According to that model the NG twin goes through several conformational states without GTPase activity which could serve as control points before reaching the activated state and complex dissociation.

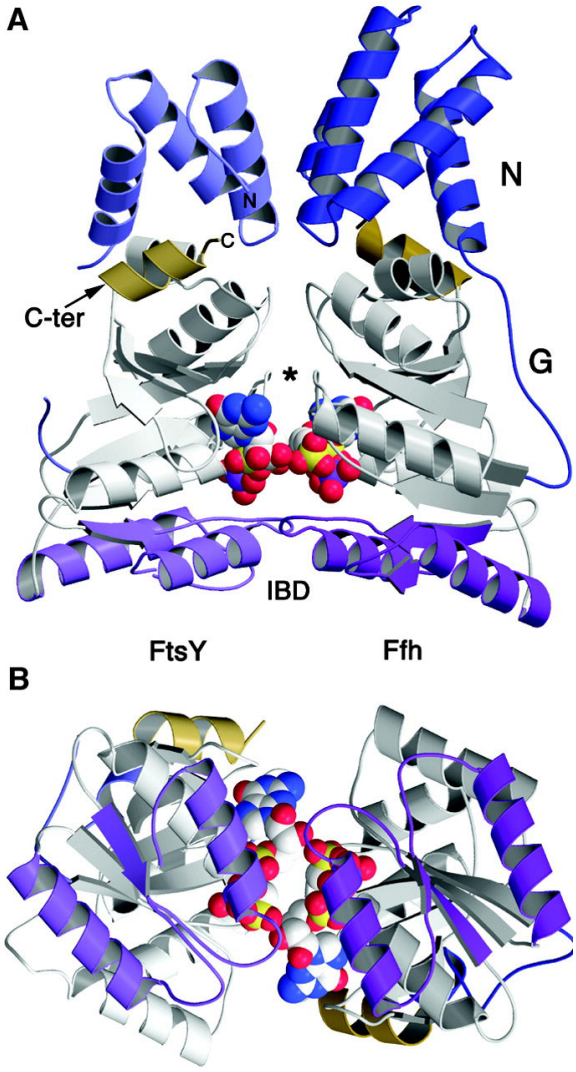

Figure 9: Structure of the heterodimeric FFH/FtsY NG domain complex. A) Ribbon representation viewed perpendicular to the dimer axis, which is vertical in the figure. The N domain (blue) and the C-terminal helices (golden) are at the top, and their IBD domains are at the bottom (purple). The two active sites are brought into direct apposition to form an active site chamber at the centre of G domain (grey) where the GMPPCP ligands are buried. The motif I P-loops of the two proteins pack adjacent to each other (*). The structure is highly symmetric with the exception of the smaller N domain of FtsY, and all secondary structure elements adopt the same orientation in both proteins. B) The structure viewed along the two-fold axis further highlights the symmetry of the complex. The viewpoint is toward IBD [77].

In eukaryotes the complexity of the targeting GTPase cycle is increased by one more GTPase, the Arf-like Srβ, the function of which is not entirely clear. The Arf subfamily of GTPases is absent in prokaryotes [80] and it has a higher affinity for nucleotides compared to the SRP family of GTPase. A recent crystal structure of the SRα-SRβ complex [81] revealed the spatial arrangement of the N-terminal SRαX1 domain and SRβ from *Saccharomyces cervisiae* (Fig. 4b). While the complex was purified in the presence of GDP, the structure clearly shows GTP in the active site suggesting catalytic inactivity of SRβ in complex with SRα. The interface between these two domains includes the entire switch 1 region of SRβ which is critical for GDP-GTP conformational switching. One important conclusion in agreement with previous findings [82] is that the interaction between the X domain of SRα and SRβ is nucleotide dependent and that it requires the GTP state of SRβ.

Furthermore, the crystal structure confirms that in contrast to SRP54 and SRα, SRβ requires both, a GAP and a GEF, to function as a GTPase switch. Recent data show that a subunit of the translocon, Sec61β, can function as a GEF for SRβ [83], which points at a role for SRβ in sensing the availability of a translocon. Interestingly, the ribosome has been suggested to function as a GAP for SRβ [84] implying that the SRα-SRβ complex would dissociate upon interaction with the RNC-SRP complex and subsequent GTP hydrolysis by SRβ. The dissociated SRβ in the GDP-state most likely stays bound to the ribosome since close proximity between SRβ in the GDP-state and a ribosomal protein (21 kD) has been shown by chemical cross linking [85].

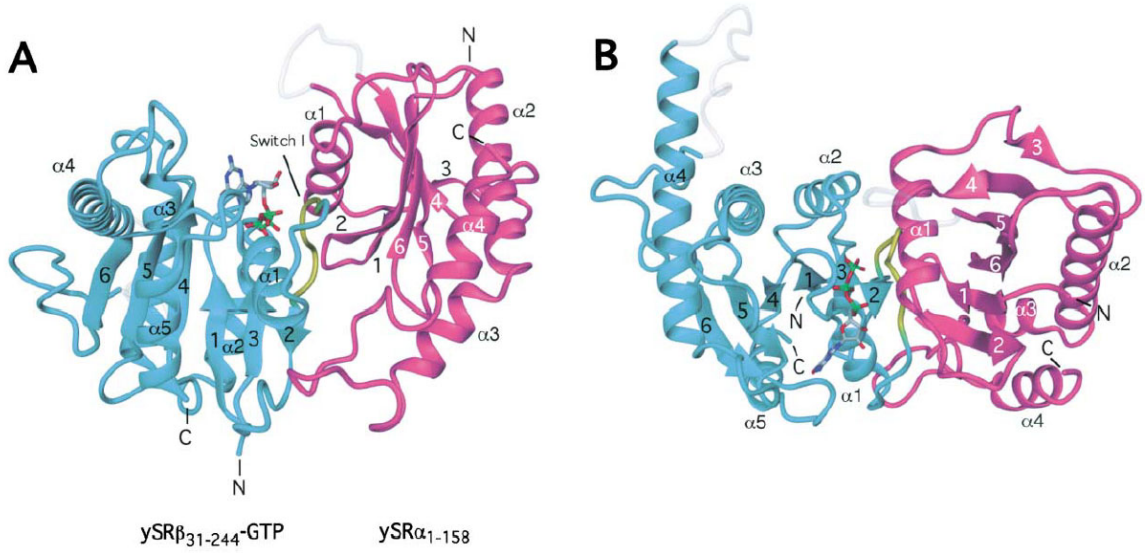

Figure 10: Structure of SRX-SRβ(GTP) complex. A) Structure of SRX-SRβ(GTP) complex from yeast. The SRβ subunit is shown in cyan and the SRX1 domain of SRα subunit in magenta. The GTP nucleotide is drawn in ball-and-stick representation. The switch 1 region (residues 64-72) of SRβ (yellow) forms the main interaction site with the SRα. Secondary structure elements are labelled. Unstructured loop regions are coloured gray. B) Same as A but rotated around horizontal axis counter-clockwise by 90° [81].

In the current model of the SRP cycle, SRP54 can interact in an empty state with the ribosome carrying the signal sequence. Assembly of the SRP-RNC complex slows down the elongation of the nascent chain and it induces stable GTP binding to SRP54. This results in the primed state of SRP54 with a conformation that does not yet allow GTP to access the catalytic centre, but is ready to interact productively with the SR. On the membrane side, the contact of SRβ with the translocon induces GTP binding by SRβ, which results in formation of the SRα-SRβ complex. The SRP-RNC complex is then targeted to the ER membrane where it interacts with SR. SRP54 and SRα NG-domains interact in a GTP-dependent manner which brings GTP into the catalytic centre. However, simultaneous GTP hydrolysis is blocked until the signal sequence is released. With all three GTPases in the GTP-bound state, the ternary complex is stably assembled. The synchronized GTP hydrolysis follows the release of the signal sequence to the translocation channel and results in the dissociation of SRP and SR from the ribosome and translocon while peptide elongation resumes.

The transfer of the nascent chain apparently precedes the GTP/GDP switch of all GTPases, since it also happens in the presence of non-hydrolysable GTP analogs.
In bacteria which lack SRβ, the SRα homolog FtsY exists in a soluble and a membrane-bound form. The soluble form of FtsY is not sufficient to dissociate SRP from RNCs but requires the context of the membrane. The membrane receptor for FtsY has not been identified yet, and it is possible, since there is only one target membrane in bacteria, that the FtsY ability to bind the membrane is sufficient for proper targeting to the bacterial SecYE translocon. Binding of FtsY to the membrane and the translocon induces GTP binding to FtsY and primes it for interaction with SRP.

1.3 Goals

Despite a large amount of functional data and a growing number of SRP sub-structures, several fundamental questions remain unresolved: How does SRP interact with the ribosome. How is translation arrest induced? How does SRP recognise and bind a signal sequence on the ribosome? How is signal-sequence binding coupled to GTP binding, a prerequisite for docking of SRP to its receptor (SR)? How does the SRP-RNC complex dock to the SR in GTP-dependent manner. And after docking to the membrane-bound receptor, how is the release of the signal sequence and transfer of the RNC to the translocon coordinated?

2 Materials and Methods

2.1 Purification of ribosome nascent chain complexes (RNCs)

For the generation of purified RNCs a wheat germ *in vitro* translation system (Ambion) was used programmed with truncated mRNA coding for the 90 N-terminal amino acids of the type-II membrane protein dipeptidylpeptidase B (DPAP-B) from *S. cerevisiae*. The mRNA carrying the code for an HA-tag was translated in the system and purified on a metal affinity column resulting in highly enriched RNCs.

2.2 Generation of DNA fragments by polymerase chain reaction

To make mRNA, a DNA fragment with N-terminal His- and HA-tags was generated by PCR from yeast genomic DNA using the forward primer DPHisHA and reverse primer DP90.

Oligonucleotide	Sequence (5'→ 3')	Comment
DPHisHA	taatacgact cactataggg accaaacaaa acaaataaaa caaaaacaca atgtct*catc* *atcatcatca* *tca***tacccat** **agatgttcca gattacg**ctga aggtggcgaa gaagaagttg	*His tag*, **HA tag**
DP90	ttgcagctcg tgatatttgg gatg	

The PCR easy kit was used to amplify DNA. The concentration of oligonucleotide primers was 1 μM with ca 10 nM template concentration. Prior to the reaction start Taq-polymerase (50 units/ml) was added. Polymerase chain reaction was made in 30 cycles with 45 s of denaturation at 95°C, followed by 45 s of primer annealing at 60°C, and 30 s of polymerase reaction at 72°C. Reaction was finished with 1 min at 72°C.

PCR products were checked on agarose gel.

2.2.1 Agarose gel electrophoresis

DNA and RNA are negatively charged molecules, and are moved by an electric field through a matrix of agarose. The migration of molecules depends on their size and on the size of pores of the agarose matrix which depends on agarose concentration.

The gels were made with 1-2% agarose (Seakem LE Agarose (Biozym, Hess. Oldendorf)) in TAE buffer and run for 20-40 min at 50 V. DNA/RNA molecules were stained with SybrGreen I/II (Molecular Probes) and visualized with 300 nm UV light.

2.2.2 Generation of RNA by DNA transcription

Subsequently, capped mRNA was synthesized using the Message Machine kit (Ambion). 1 μg of DNA was used in 20 μl reaction transcribing into 15-20 μg of mRNA.

2.2.3 Translation and RNC purification

To purify translating ribosomes, the mRNA was translated in a wheat germ *in vitro* translation system (Ambion). 6x 200 µl reactions were incubated for 45 min at 27ºC and terminated with 2 µl of 10 mg/ml cycloheximide. Reactions were spun through four 600 µl high salt sucrose cushion (50 mM Tris.Cl pH 7.0, 500 mM KOAc, 25 mM $Mg(OAc)_2$, 2 mM DTT, 1 M sucrose, 10 µg/ml cycloheximide) at 355000xg for 45 min (TLA100.2 at 100k). The supernatant was quickly removed to prevent resuspension of the pellet. Each pellet was resuspended in the 200 µl ice-cold 250 buffer (50 mM Tris.Cl pH 7.0, 250 mM KOAc, 25 mM $Mg(OAc)_2$, 0.1% (w/v) Nikkol, 5 mM ß-ME, 10 µg/µl cycloheximide, 250 mM sucrose) for 30 min on ice and transferred on 1.5 ml Talon metal affinity resin (Clontech) into the column. The resin was equilibrated with 5 ml 250 buffer before the addition of the ribosomes. The column with resin and resuspended ribosomes was agitated for 5 min to increase the interaction and binding of His-tagged nascent chains. The resin was washed with 10 ml 250 buffer, and 2 ml 500 buffer (250 buffer with 500 mM KOAc) to remove unspecific bound ribosomes. RNCs were eluted with 2.5 ml 100 mM imidazol pH 7.1 in 250 buffer and spun through the 400 µl high salt sucrose cushion for 45 min at 355000xg (TLA100.3 or TLA100.4 at 100000 rpm). The resulting pellet was slowly resuspended for 30 min in ca 50 µl G buffer (20 mM Tris.Cl pH 7.0, 50 mM KOAc, 10 mM $Mg(OAc)_2$, 1 mM DTT, 125 mM sucrose, 100 µg/ml cycloheximide, 0.05% (w/v) Nikkol, 0.5% (w/v) EDTA-free complete protease inhibitor pill [Boehringer] and 0.2 U/µl RNasin [Ambion]), shock-frozen and stored at -80°C. From 1.2 ml translation reaction 0.7 OD_{260} of RNCs (~15 pmol) were isolated.

2.2.4 Protein precipitation and SDS PAGE

Proteins were precipitated with 6% TCA and 0.0125% Na-deoxycholate and separated using SDS PAGE (Sodiumdodecylsulfate polyacrylamid gel electrophoresis) (Leammli (1970)) for approximately 1h at 150 V. 12% PA gels were used. The size of proteins was determined by comparison with broad range protein marker (P7702S, New England Biolabs) .

Protein staining was done with Coomassie Brilliant Blue R250, or Sypro Orange (1:5000) (Molecular Probes).

2.2.5 Western Blot analysis

To check the enrichment of translating ribosomes Western blot analysis was performed. Proteins were transferred onto a nitrocellulose membrane with a semi-dry blotting procedure in transfer buffer (20% MeOH, 48 mM Tris, 39 mM Gly), 0.037% SDS) for 45 min at 1 mA/cm^2 (50 mA). The nitrocellulose membrane was incubated first with fat free milk (5% w/v) for 30 min to prevent unspecific antibody interaction. As primary antibody, for the detection of the HA-tag, monoclonal anti-HA.11 16B12 from mouse (Babco) was used in dilution 1:500 in 5% w/v milk. As secondary antibody rabbit anti-mouse IgG-POD (DIANOVA) was used at a dilution of 1:5000 in 5% w/v milk. For the chemiluminescence reaction, the nitrocellulose membrane was incubated for 1 min

with ECL (100mM Tris pH 8.5, 1.25 mM aminophtalhydrazide (Luminol, Fluka), 0.2 mM Coumarinacid, 0.01% H_2O_2). Signals were detected with Kodak Biomax MR film.

2.3 Reconstitution of SRP-RNC complex

2.3.1 Reconstitution and sucrose gradient

RNC-SRP complexes were reconstituted by incubating 1.5 pmol mammalian SRP (isolated according to [86] and further purified by sucrose density gradient centrifugation[87]) and 0.5 pmol RNCs. Prior to the incubation the KOAc concentration of RNC buffer (G buffer) and SRP buffer was increased to 350 mM by mixing with K500 buffer (25 mM HEPES (pH 7.5), 500 mM KOAc, 5 mM DTT, 5 mM Mg(OAc)2, 100 mM sucrose, 0.02% Nikkol, 100 µg/ml cycloheximide, and 1% of EDTA-free complete protease inhibitor pill). After mixing, buffer conditions were adjusted to 25 mM HEPES (pH 7.5), 150 mM KOAc, 5 mM DTT, 5 mM Mg(OAc)2, 100 mM sucrose, 0.02% Nikkol, 100 µg/ml cycloheximide, and 1% of EDTA-free complete protease inhibitor pill (with K0 buffer which is equal to the K500 except that it lacks KOAc). After 15 min of incubation at RT, the reaction was brought back to 500 mM KOAc (with K1 buffer which is equal to the K500 except that KOAc concentration is 1 M), and spun through 10%-40% high salt sucrose cushion for 80 min in SW60 (Beckmann) at 55k (310000xg) (buffer conditions as for incubation except 500 mM KOAc) and analyzed by SDS-PAGE. Alternatively, instead of applying the complex onto the 10%-40% sucrose gradient, it was spun through 400 □l of 1 M sucrose cushion in a TLA100.2 rotor for 45 min at 100k (355000xg). SR-SRP-RNC complexes were reconstituted by incubating 3 pmol mammalian SRP with 5 pmol SR (from Irmgard Sinning, Biochemie-Zentrum Heidelberg) and 0.5 pmol RNCs. Buffer conditions were identical to SRP-RNC reconstitution with addition of SR and 200 nmol GMP-PNP after SRP-RNC complex formation. After 15 minutes of additional incubation with SR, the complex was analyzed in the same way as the SRP-RNC complex.

2.3.2 Grid preparation

For cryo-EM 1.8 pmol of SRP (1.5 µl of 1.25 µM SRP) were adjusted to ca 400 mM KOAc with K500 buffer (3 µl) and 0.5pmol of RNCs (7 µl of 6OD/ml) to ca 330 mM KOAc with K1 buffer (3 µl). Both components were mixed (14 µl) and salt concentration was reduced to 180 mM by adding the same amount of K0 buffer resulting in a total volume of 28 µl under the described conditions.

2.4 Electron microscopy

Samples were applied to carbon coated holey grids as described [88]. Micrographs of the SRP-RNC complex were recorded under low-dose conditions on a Tecnai F30 field emission gun electron microscope in Albany (USA) at 300 kV and on a Tecnai F20 at 160 kV in a defocus range between 1.0 µm and 4.5 µm. The micrographs were scanned on a Heidelberg drum scanner resulting in a

pixel size of 1.63 Å on the object scale. SR-SRP-RNC micrographs were recorded on a Tecnai F30 field emission gun electron microscope in Berlin at 300 kV and scanned at a pixel size of 1.21 Å on the object scale.

2.5 Image processing

Power spectra and defocus determination

The data were analyzed with the SPIDER software package [89]. Firstly, important parameters were saved in the document params.rib (using the script p_makeparams.srp). The structure of the document is described below:

key	name	values or units	values in SRP-RNC project
1	zip flag	0 : do not unzip 1 : needs to be unzipped	0
2	file format	0 : SPIDER 1 : HiScan tif 2 : Perkin Elmer 3 : ZI scanner	1
3	width	(of micrograph, in pixels)	
4	height	(of micrograph, in pixels)	
5	pixel size	(in Angstroms)	1.63
6	electron energy	(in keV)	300
7	spherical aberration	(mm)	2.0
8	source size	(1/A)	
9	defocus spread	(A)	
10	astigmatism	(A)	
11	azimuth	(degrees)	
12	amplitude contrast ratio	(0..1)	
13	Gaussian envelope halfwidth	(1/A)	
14	(reserved)	(-)	
15	(reserved)	(-)	
16	(reserved)	(-)	
17	window size	(pixels)	276
18	actual size	(pixels)	200
19	interpolation/decimation factor	(1…)	2

The entries 1-6, 17 and 18 are entered interactively while others have standard values or can be changed by editing the params.rib document. If the interpolation/decimation factor is an integer number, decimation will be used. The decimation will sum values of two neighbouring pixels

resulting in an increased the signal to noise ratio, which is the preferred way to reduce the size of images. The document micnum.rib containing the list of micrographs used for processing was created (using the SPIDER command doc create).

For all scanned images (micrographs) the matching contrast transfer function (CTF) and defocus value were determined with the program ctffind3 [90] (using scripts p_ctffind3.srp, p_convert1.srp, ctffind.sh, p_readmrc.py). The script p_ctffind3.srp prepares an image for ctf determination and it converts it into the mrc file format which can be used by the software. Ctffind.sh is executed by the script p_ctffind3.srp and it determines defocus values of micrographs while python script p_readmrc.py converts ctffind output file into the spider document file format. The defocus values for each micrograph were saved in defocus.rib document.

Ctffind3 creates the power spectrum images of micrographs with estimated model on the left and the real data on the right. Power spectra were visually inspected in Web (part of SPIDER software package) and only micrographs with acceptable power spectra (without or with very low drift and astigmatism), and images containing information in the frequency range below 15 Å were selected and used for further processing. Unwanted micrographs were removed from micnum.rib document and the document key was renumbered (using the SPIDER command doc ren). Altogether 150 micrographs were selected, 100 from the F30 and 50 from the F20 microscope, and used for further processing.

2.5.1 Particle picking

Since only particles over a thin layer of carbon film contain proper information, a mask for the hole on the grid was created. For easier handling the images were decimated 20-fold (p_decimate.srp) and 3 coordinates of the circle of the hole were determined visually in Web (using the command pixel) and saved into a document file. These coordinates were used to create a matching circular mask (p_3coordcircle.srp) for every individual hole.

Each micrograph contains several hundreds or even thousands of single ribosomes which have to be isolated. Particles were automatically picked from micrographs (p_pickCCM.srp, p_pickparticles.srp, p_convert1.srp) by a local fast correlation method where local cross-correlations are calculated with Fourier methods according to Alan Roseman [91]. This procedure needs a reference 3D volume similar to particles that should be searched, and generates one or more projections as template images for the search. Only one projection image was used as a template for these datasets. The procedure sorts particles dependent on the cross correlation with best fitting particles showing up first. This method reduced the time for visual inspection of the particles since low quality particles usually end up clustered together either at the top of the list (contamination with high contrast) or at the end (high noise).

Automatically picked particles were visually inspected in Web and good particles were selected. Prior to the visual inspection particles were low pass filtered depending on defocus value (p_filt.srp). Bad particles were removed from the dataset and good particles were renumbered

(p_copygood.srp). A total of 35488 particles were selected as good and used later for the reconstruction.

Selected micrographs were sorted according to the defocus value and a defocus group document defgrp.rib was created (p_makedefgrpfile.srp). Micrographs with similar defocus values were assigned to same defocus group (third column in defgrp.rib) with an average defocus not more than 250 Å distant from defocus values of the single micrographs. Micrographs from two microscopes were kept separately. Altogether 51 defocus groups were created, 33 for F30 dataset and 18 for F20 dataset.

2.5.2 Alignment

In the first alignment step particles were aligned (p_alidef.srp) to projections of the existing reference of the Sec61-80S ribosome complex from yeast. For each micrograph the reference volume was distorted with corresponding CTF function which depends on the defocus value of the micrograph. Initial alignment was done at an angular accuracy of 15 degrees which generates 83 projections. Shifts in x and y directions were as large as possible to ensure proper positioning of particles. To speed up the alignment particles were decimated by a factor of 2. The output document of the alignment includes for each particle the best fitting projection, and the shift and rotation parameters necessary to apply in order to match the projection.

2.5.3 3D-reconstruction

Rotation parameters and shifts were then used to create the new set of particles used for 3D-reconstruction (p_spinnem2.srp, p_rotate.srp, p_angles.srp). Two percent of particles with lowest cross-correlation coefficients were removed (p_howmanyvo2.srp) from the dataset. Particles were backprojected using parameters from the alignment (bp32f.srp). For each defocus group three volumes were created; one was backprojected with all particles and two additional ones were backprojected with two independent half's of all particles.

All odd and all even volumes were CTF corrected and added to create two volumes each containing half of the particles. These two volumes were then compared and the Fourier shell correlation, which is used for resolution determination, was calculated. The cut-off in the Fourier shell correlation curve used for resolution determination was 0.5. Volumes created with all particles in each defocus group were ctf corrected and summed up resulting in the final volume. This volume was filtered to the resolution and used as an initial volume in the refinement procedure.

2.5.4 Refinement

In the refinement particles are iteratively aligned to new references created by those particles (ref_sortref.srp). Before the refinement, stack files containing aligned particles have to be created for each micrograph. Stack files have to be interpolated or decimated to the desired pixel size if necessary. Decimation factor of 2 was used giving a pixel size of 3.26 Å on the object scale. Prior

to the refinement, transformation files have to be created (p_maketrans.srp). Transformation files contain shifts and rotation for each particle which have to be applied to particles to fit the reference projection. To avoid subsequent interpolation, after each refinement round original particles are rotated and shifted using transformation files.

In first round of refinement particles were aligned to the volume created in the first reconstruction with angular accuracy of 2 degrees without angular restriction. This procedure offers all possible references to each particle, however, in cost of the speed. In the next rounds particles were compared only with projections inside defined angular restriction and shifts were allowed to position them even more accurate. Angular restriction and angular accuracy were slowly reduced in following rounds allowing better alignment of particles.

The density of SRP was visible at lower contour levels compared to the density of the ribosome showing lower occupancy of the ligand. To increase the occupancy computationally, the particles were iteratively sorted into two subsets, one containing the ligand and one without. For the initiation of the sorting a volume without SRP was manually created by masking away the density of SRP using a binary mask. Both volumes were offered for alignment to the particles resulting in two different cross correlation coefficients for each particle. The cross correlation coefficients were compared and, dependent on the best match, the particles were sorted into two subsets and backprojected separately. This procedure was repeated iteratively until particles stabilized in each subset. At the end, two subsets of particles were created, one with SRP containing 25397 particles and one lacking SRP containing 10097 particles. Since the sorting was not perfect due to the high level of noise, the SRP containing volume still contained ribosomes without SRP. Nevertheless, the SRP occupancy was significantly enriched.

After the final alignment particles were backprojected with the procedure bprp.srp which is using a slower real space backprojection algorithm resulting in a better signal to noise ratio, and in that way better resolution.

The final CTF-corrected reconstruction was at a resolution of 12.0 Å (7.7 Å) based on the Fourier shell correlation with a cut off value of 0.5 (3σ). This map was used for further interpretation and the model building.

2.6 Building the SRP model

Firstly, the final volume was adjusted in size, position and orientation to fit the yeast Sec61 volume which allowed usage of the existing models for the yeast ribosome. Orientation search was done in a first step manually to find an approximate orientation and then fine-tuned using SPIDER command OR 3Q. After the volume rotation, size and position were adjusted with the script vol_resize.srp which calculates the cross correlation between the volumes and searches for the highest peak.

For the modelling, the programme package O was used[92]. Since yeast and wheat germ ribosomes showed an extremely high degree of similarity, the molecular model of the yeast ribosome was used as a model for the ribosome (1K5X, 1K5Y, 1K5Z).

Several crystal structures of SRP components were used to make a model of mammalian SRP. First, a large fragment of mammalian S-domain containing 7SL RNA helix 6,7, 8, part of helix 5, SRP19 and the SRP54 M-domain [46] (1MFQ) was docked. The M-domain from this crystal structure was replaced by a different model [93] using the RNA binding moiety for alignment. This model, derived from site-directed mutagenesis, was a modification of the M-domain from the S-domain crystal structure and was fitting better into the density. The structure of a prokaryotic SRP54 NG-domain [94] (1JPJ) was docked into density present near the M-domain. A short α-helical peptide fragment was docked as a signal sequence in the empty density belonging to M-domain at a place predicted to bind a signal sequence. The X-ray structure of the mammalian Alu 5'RNP [40] (1E8O) was docked in intersubunit space and, for the missing part of 7SL RNA, three fragments from a model provided by the SRP-database [95] were used.

Densities for 60S, 40S, tRNA and SRP were isolated using binary masks. Amplitude correction for the final volume was done by Fourier filtering using B-factors. A higher B-factor was applied to the ribosomal density (150) then to the SRP density (100). For surface representation a lower contour level of the SRP density was applied. This reflects that the SRP density is underrepresented due to incomplete removal of SRP-free ribosomal particles from the final particle subset.

2.7 High resolution structure of SRP-RNC complex

To increase the resolution of the structure more images of SRP-RNC complex were collected on a Tecnai F30 microscope resulting in additional 25000 particles. Altogether 50000 particles were used for the high resolution project. The data from Tecnai F20 microscope were not used due to lower quality in higher frequencies. As the pixel size severely limits the resolution when 0.5 cut-off in Fourier shell correlation curve reaches spatial frequency of approximately 0.25 (describing features defined by 4 pixels), the high resolution project required smaller pixel size of the data. The pixel size was changed as the resolution was increasing, from 3.26 Å/pixel (decimation factor 2) used at the beginning, to 2.44 Å/pixel (interpolation factor 1.5) and finally to 2.04 Å/pixel (interpolation factor 1.24).

Because of the envelope function of the electron microscope higher frequencies are underrepresented and their contribution to cross-correlation coefficients used in alignment procedures is severely impaired. To reach higher resolution, it was necessary to increase the weight of higher frequencies by increasing the amplitude. Amplitude correction was done by Fourier filtering using B-factors and amplitude corrected volumes were subsequently used as references in the refinement procedures. B-factor values were varying between 60 and 140. To be used in the

Fourier filter these values have to be divided by the square of the pixel size. Amplitude correction severely improved the resolution of the density.

A modified sorting procedure has been used to generate two subsets of particles. As sorting criteria the presence of the ligand and also the contribution of the particle in the high frequency region were used. Two subsets of particles were created, the first containing SRP and particles with highest correlation in high frequencies, and the second containing ribosomes without the ligand and particles with dominant low frequencies or weakly aligned high frequencies. These particles did not contribute to the signal in high frequencies, however, they increased the noise. Therefore, their removal resulted in increased resolution. Altogether, approximately 20000 particles, which were used for the final reconstruction, sorted to the positive volume leaving 30000 particles in the negative volume.

To obtain high frequency information (significantly below 10 Å) the contrast transfer function correction has to be done as precise as possible. In first steps, the contrast transfer function was determined from micrographs based mainly on the signal from the carbon film which results in a shift of the defocus. To correct that, the defocus of each micrograph was determined again from volumes backprojected from particles from each micrograph. The volumes offer a better signal to noise ratio of the object of interest itself and in that way, a more precise defocus determination.

The final CTF-corrected reconstruction is at an overall resolution of 9.5 Å (6.9 Å) based on the Fourier shell correlation with a cut-off value of 0.5 (3σ). The resolution of the ribosome is at 8.8 Å with SRP density being at lower resolution due to lower occupancy and possibly lower rigidity.

2.7.1 L30 localization and the model

The high-resolution structure of the ribosome has α-helical secondary structure clearly resolved allowing the localization of the eukaryotic ribosomal protein L30e. The fold of L30e could be visually identified in the cryo-EM map and the crystal structure from *Thermococcus celer* could be docked. To confirm the localization the signature search procedure was used (sigsearch.srp) [96]. In the first step search was done at 15 degrees allowing all possible orientations of L30e to roughly be localized in the map. In the second step the search was done at 2 degrees with restricted L30e orientation to fine tune the fit. When L30e was localized, the crystal structure was replaced with the wheat germ homology model. As the template for homology modelling the crystal structure of yeast L30e in complex with maltose-binding protein was used (1NMU, chain D) [97]. The homology model was manually docked using the program package O with further manual adjustment of poorly fitting regions. Firstly, a flexible region between residues 70 and 86 was adjusted to fit into the density. The main chain was manually placed into the corresponding density with side chains positioned in their most common orientation from the O rotamer database. Both main and side chains were refined in O to follow stereochemical constraints. The N- and C-terminal helices were slightly shifted towards the flexible region. The model was completed by positioning missing residues of the N- and the C-terminus in the corresponding density. Due to the limited resolution of

the map, these N- and C-terminal residues, the loops connecting helix 4 of L30e and all side chains could not be positioned precisely in an unambiguous manner.

2.8 Structure of SR-SRP-RNC complex

The SR-SRP-RNC dataset was recorded at a Tecnai F30 field emission gun electron microscope at 300 kV in a defocus range between 0.9 μm and 3.2 μm, and scanned on a Heidelberg drum scanner resulting in a pixel size of 1.22 Å on the object scale. Altogether 116 micrographs were selected and used for processing resulting in a total of 73000 particles. The processing was done in a very similar way as the processing of the high resolution structure of the SRP-RNC complex. Sorting according to the presence of ligands resulted in two datasets, one containing SRP and SR (55000 particles) and one without them (18000).
The final CTF-corrected reconstruction is at an overall resolution of 8.8 Å (6.3 Å) based on the Fourier shell correlation with a cut-off value of 0.5 (3σ).

3 Results

3.1 Ribosome nascent chain complex purification and reconstitution of SRP-RNC complex

Since formation of a stable complex was a prerequisite for this study, wheat germ RNCs and canine SRP were used for reconstitution of the targeting complex. This well characterized combination, which led to the discovery of SRP, displays strong elongation arrest activity [15]. Assuming that this activity is a result of equally stable binding of the S-domain and the Alu-domain to the ribosome, this heterologous complex was considered as the most suitable candidate for structure determination.

First programmed ribosomes carrying a functional signal sequence (RNCs) were isolated from an *in vitro* translation reaction as described in materials and methods section. For the translation a wheat germ in vitro system was used (Ambion), with mRNA encoding for first 90 amino acids of the type-II membrane protein dipeptidylpeptidase B (DPAP-B) from yeast, containing a signal anchor sequence and, in addition, an HA/His tag. Since the mRNA did not have a stop codon translating ribosomes were stalled at the end of the mRNA with the peptidyl-tRNA in the P-site. These ribosomes were affinity-purified by metal affinity chromatography. The programmed ribosomes were eluted under native conditions using imidazol. The enrichment of ribosome nascent chain complexes is shown in fig. 11a. When comparing the specific signal before purification (R) and after purification (E) it is apparent that a several-fold stronger nascent-chain dependent signal with lower amounts of ribosomes indicates at least a 5-fold enrichment. If in the translation system, conservatively estimated, only 20% of the ribosomes were programmed and stably stalled, more than 95% of the ribosomes in the final fraction can be expected to carry a nascent chain.

Stalled RNCs were used for the reconstitution with excess amounts of purified canine SRP. To ensure specific, i.e. signal sequence dependent complex formation, sucrose density gradient centrifugation was performed under high salt conditions (500 mM KOAc) [98], which confirmed high affinity binding of SRP to RNCs with an estimated occupancy varying between 50-90%.

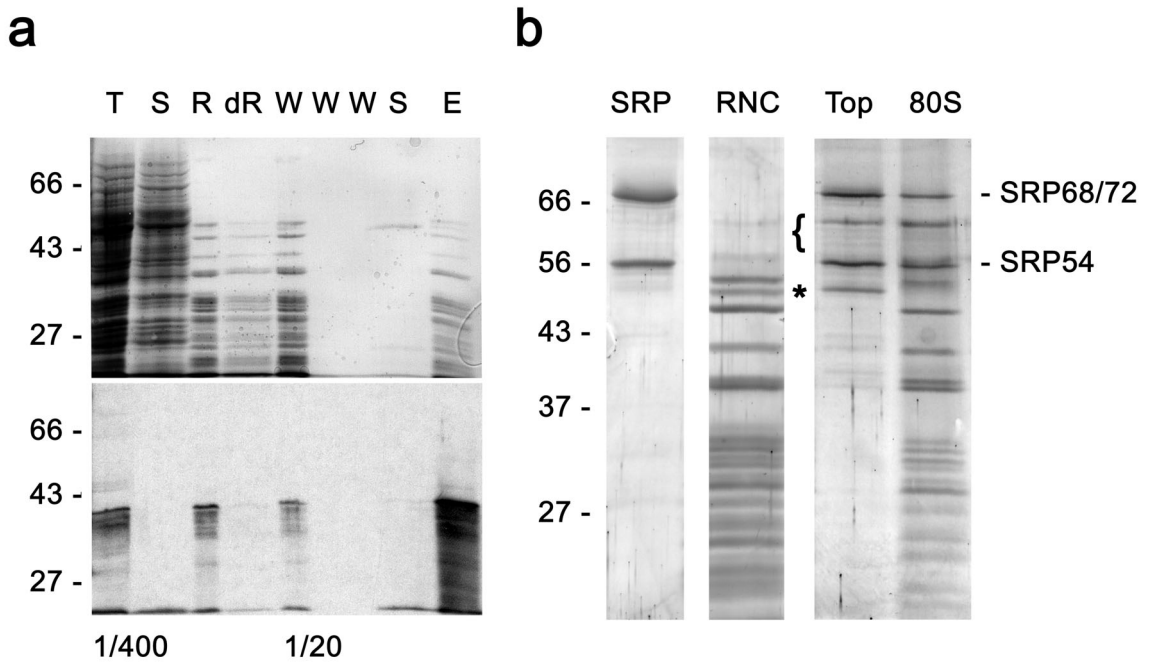

Figure 11: Purification of RNCs and reconstitution of the RNC-SRP complex. a, A truncated mRNA coding for the first 90 amino acids of dipeptidylpeptidase B with His-tag was translated in a wheat germ cell-free system and RNCs purified as described in the Methods section. Aliquots of fractions were subjected to SDS-PAGE, blotted onto nitrocellulose and amido black stained (top) and probed using a monoclonal anti-HA antibody (bottom). T, total; S, supernatant; R, crude ribosomes; dR, depleted crude ribosomes after column incubation; W, washes; S, supernatant after elution; E, pellet after elution using imidazol. Note the enrichment of DP90 RNCs and the characteristic pattern of ribosomal proteins in the final fraction (E). b, Purified DP90 RNCs (RNC) were reconstituted with excess SRP (SRP) and, subjected to sucrose density centrifugation at 500 mM KOAc, fractionated and analyzed by SDS-PAGE and Sypro-Orange stain. Brackets indicate contaminating proteins in the gradient. The asterisk marks RNase inhibitor, which partially copurifies with RNCs, but is not present in the reconstituted RNC-SRP complex (compare Top with 80S). High salt resistant RNC-SRP complexes migrate in the 80S fraction indicating signal sequence-dependent SRP binding to RNCs.

3.2 Structure of the signal recognition particle interacting with the elongation arrested ribosome

Cryo-EM and three-dimensional (3D) reconstruction of the targeting complex revealed the typical appearance of an 80S ribosome at 12 Å resolution (7.7 Å according to 3σ criterion, see fig. 12, 13) with two additional densities (fig. 12): firstly, a tRNA is visible in the P-site in the ribosomal intersubunit space. Secondly, a large elongate mass representing SRP stretches from the peptide exit site of the 60S ribosomal subunit (S-domain) into the intersubunit space (Alu-domain), forming a total of 6 connections (C1-C6) with the ribosome (fig. 12, 14).

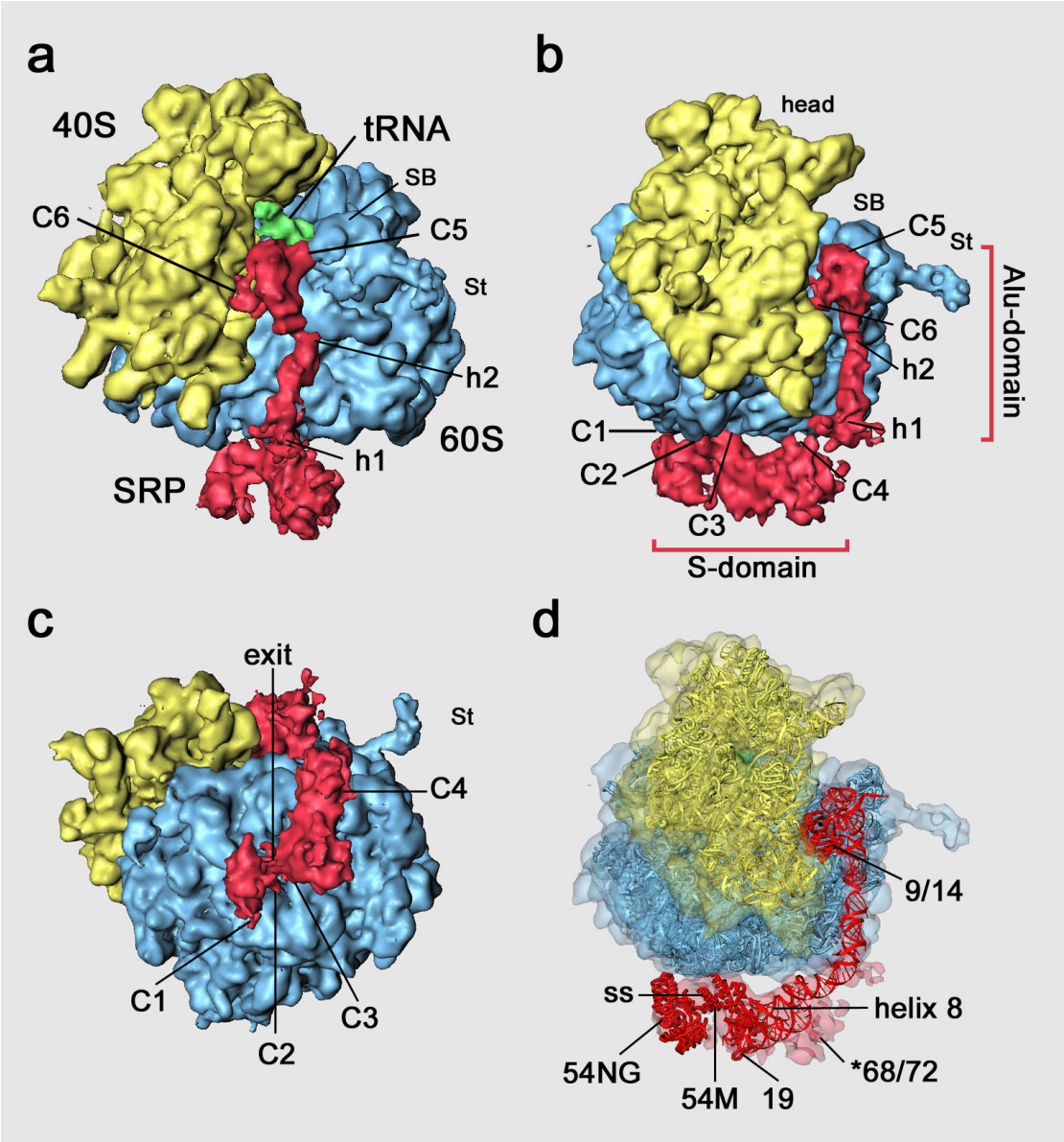

Figure 12: Cryo-EM map of mammalian SRP bound to 80S RNC at 12.0 Å. Ribosomal and SRP densities are shown at different contour levels and amplitude correction was done with different B factors. The lower contour level necessary for the SRP density is a result of lower occupancy of SRP as ligand and uncompleted removal from the dataset of RNCs without SRP during sorting. Accordingly, the lower B factor used for amplitude correction of SRP density is also due to lower occupancy of SRP and the lower overall resolution of the SRP density. a, The RNC-SRP map is shown with the separated colour-coded densities. Yellow, 40S small ribosomal subunit; blue, 60S large ribosomal subunit; green, P site tRNA; red, SRP. C1-C6 assigned positions of RNC-SRP connections (see also table 1); h1 and h2 are hinges of the 7S RNA backbone of SRP; St, stalk; SB, stalk base. b, As a but rotated by 70° to the right. c, As a but rotated upward by 90°. d, Same orientation as b but with molecular models for SRP and the 80S RNC in transparent densities.

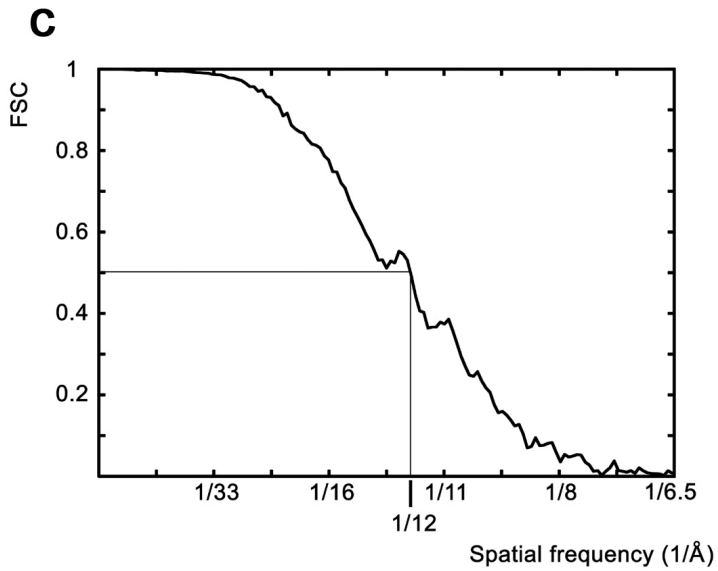

Figure 13: Resolution curve: Fourier shell correlation (FSC) curve for the cryo-EM map of the RNC-SRP complex. FSC = 0.5 indicates 12.0 Å resolution. Some structural information extends to 7.7 Å according to the more lenient 3σ criterion.

The tRNA density reflects the presence of the nascent peptidyl-tRNA containing the signal sequence, which is stalled at the 3'-end of the truncated mRNA and stabilized by cycloheximide (purification described in Methods section). Sorting of the dataset according to the presence of SRP density resulted in a subset of ~70% of particles, in agreement with the occupancy estimated by SDS-PAGE, which were used in the final reconstruction. Sorting of the dataset according to the tRNA presence removed ~1-2% of particles from the dataset showing that the purification of programmed ribosomes was highly efficient.

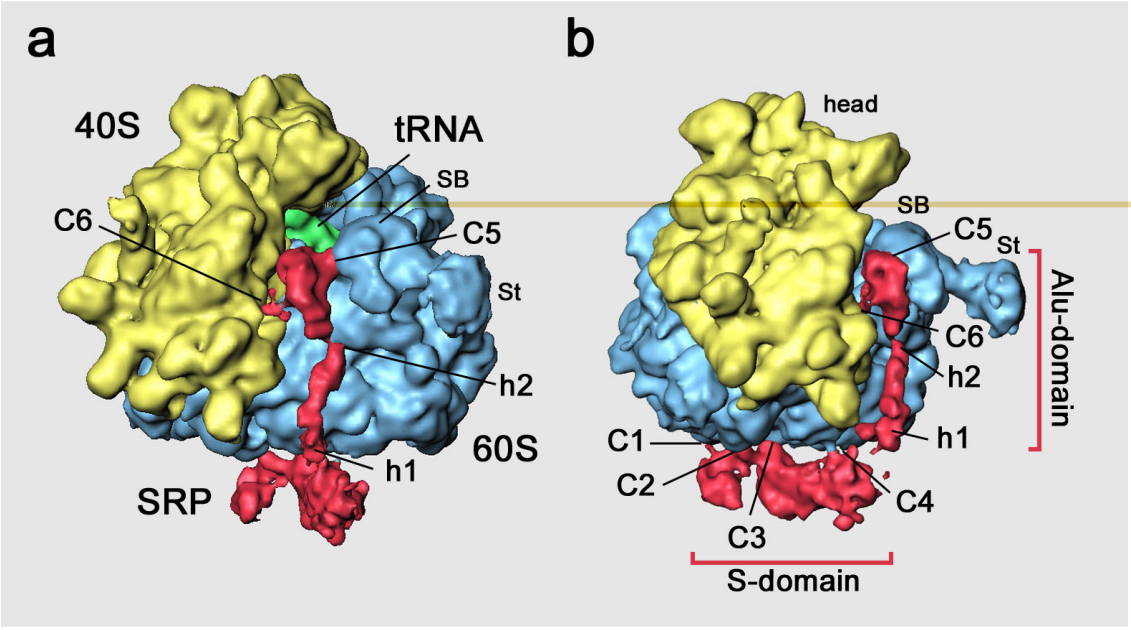

Figure 14: Cryo-EM map of the SRP-RNC complex. a, RNC-SRP map shown with separated colour-coded densities, all at the same contour level and before application of Fourier filtering using B-factors. Colour coding and labels as in fig. 12. b, As a but rotated by 70°. Notably, the dynamic expansion segment 27 (ES27) is not visible. Noise between the S-domain density and the ES27 position near L1 (visible only at very low contour levels) indicates that ES27 has no preferred orientation in this complex.

In order to allow interpretation on a molecular level, crystal structures and molecular models were docked into the electron densities. In the case of the ribosome, the remarkable similarity between the wheat germ RNC and yeast RNC [99] (see fig. 18 and fig. 27) allowed the use of a molecular model generated earlier [100]. Therefore, here was used the yeast nomenclature for the molecular description of ribosomal components (family names in parenthesis). In the case of the SRP, recently solved X-ray structures of SRP fragments were docked into the density as rigid bodies (see Methods).

SRP shows a bent conformation with one of two hinges apparently facilitating a major kink (hinge 1) separating the S- and Alu-domains. Hinge 1 separates the 160 Å long S-domain of SRP near the peptide exit site from a RNA linker connecting Alu-domain in a region close to the subunit interface (spanning a length totalling 120 Å). The RNA at hinge 1 represents a large loop around nucleotides 100/250 and forms an angle of almost 90° (fig. 12b, 15). Hinge 2 is located in a region corresponding to a small loop formed by nucleotides 70 and 275 of 7SL RNA. This hinge facilitates a bend (~ 30°), which leads to an orientation of the 5' Alu-RNP that is perfect for its entry into the intersubunit space (fig. 12a, 16b).

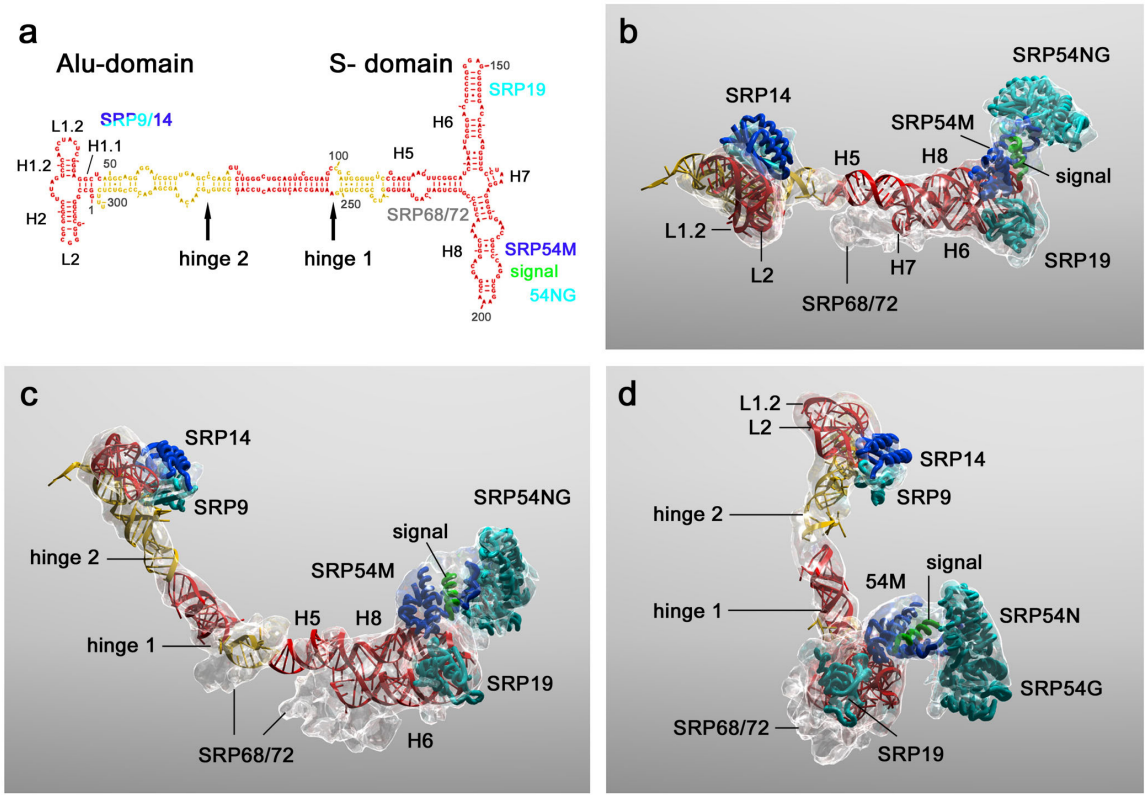

Figure 15: Molecular model of SRP. a, Secondary structure of the SRP RNA with protein binding sites and hinges indicated. H1-H8 denote the RNA helices of SRP, following the nomenclature of Weichenrieder et al[40]. In the case of the Alu-domain. Cyan, blue and grey, SRP proteins; red and yellow, 7S RNA; green, signal sequence. b, Molecular model of SRP with density transparent and colour coding as in a. Top view showing SRP as seen from the ribosome. c, As b but rotated upwards. d, As c but rotated left.

The structure of a large fragment of the mammalian S-domain containing 7SL RNA helices 6-8 and part of helix 5 as well as the SRP19 protein and the SRP54 M-domain [46] was docked into the density identified as the S-domain. The original SRP54 M-domain was replaced with another model [93] differing only in the position of helix 1 and the finger loop, since this model was fitting better into the density. As a signal sequence, an alpha-helical peptide fragment of 16 amino acids was positioned into the corresponding density near the exit site which was not occupied by the crystal structure. As a result, the signal sequence can contact the hydrophobic groove of the SRP54 M-domain and the phosphate backbone of SRP helix 8 RNA with its positively charged N-terminal part [11]. The conserved structure of a prokaryotic SRP54 NG-domain from *T. aquaticus* bound to the nonhydrolisable GTP analog GMPPNP [94] was docked next. Interestingly, the NG-domain is positioned such that a gap of ~20 Å is separating it from helix 8 of 7S RNA, only connected by the M-domain. In this position, a part of the NG-domain is in too close proximity to the finger loop of the M-domain indicating a more compact conformation of the loop in the case of signal sequence binding. In the crystal structure of M-domain [46, 93] the loop is wide open because of high detergent concentrations apparently destabilizing hydrophobic interactions. In support of this model a very recent crystal structure of an archaeal SRP54-RNA complex revealed a similar overall arrangement of M- and NG-domains [53] with the finger loop closed. SRP in the cryo-EM structure is bound to a signal sequence and, therefore, the loop can be expected in the open conformation covering the bound signal sequence, but not extensively open as in the structure of SRP54 M-domain by Kuglstatter et al.

Extra density in the S-domain was interpreted as the SRP68/72 dimer of a hitherto unknown structure. It is located mainly at the junction of helices 5-8; however, additional density is present at the hinge 1 region of helix 5 (fig. 15c) and it belongs most likely to SRP68/72 dimer. This is in accordance with foot printing experiments showing protection of all of these regions of 7S RNA (including nucleotides 100/250) [49]. The fragmented mass may be an indication for a tertiary structure containing thin, extended ‘tentacle’ regions as observed for some ribosomal proteins such as L19e or L22 [101]. In the described position, SRP68/72 can serve as a brace between the core of the S-domain and the dynamic hinge 1, thereby functionally connecting Alu- and S-domain.

The X-ray structure of the mammalian SRP9/14 dimer bound to the 5’ part of the Alu-RNA[40] fits perfectly into the density in the intersubunit space (fig. 16). This model matches the conformation suggested before [40], in which the 5’-RNP, comprising the SRP9/14 dimer and the first 48 nucleotides of the RNA, folds back onto the 3’RNA stem of the Alu-domain. Thus, this back-folding appears indeed to be a necessary assembly step of the Alu-domain.

In a final step three fragments from a model provided by the SRP-database [95] were used as a ruler to corroborate that the missing part of 7SL RNA can span the distance between the docked Alu- and S-domain fragments.

Taken together, density could be assigned to all known components of the mammalian SRP, consistent with their size and structure, thus, leading to a first molecular model of SRP in the functional context of a ribosomal targeting complex.

An overview of the complete model in the context of the ribosome is illustrated in fig. 12d and fig. 16a-b. The docked fragments easily span the distance between the peptide exit site and the elongation factor binding site. The three connections of the S-domain with the ribosome, found in the immediate vicinity of the peptide exit site, are contributed exclusively by the SRP54 protein. A fourth connection is contributed by 7S RNA and the SRP68/72 dimer. The Alu-domain bridges, in a tight fit, the ~65 Å distance between the large and small ribosomal subunits (fig. 16b) where it interacts with both small and large ribosomal subunit. An empty space in the intersubunit cavity, corresponding to the unoccupied A-site is indicating that the Alu-domain would not interfere with a tRNA bound in this position (fig. 16a-b).

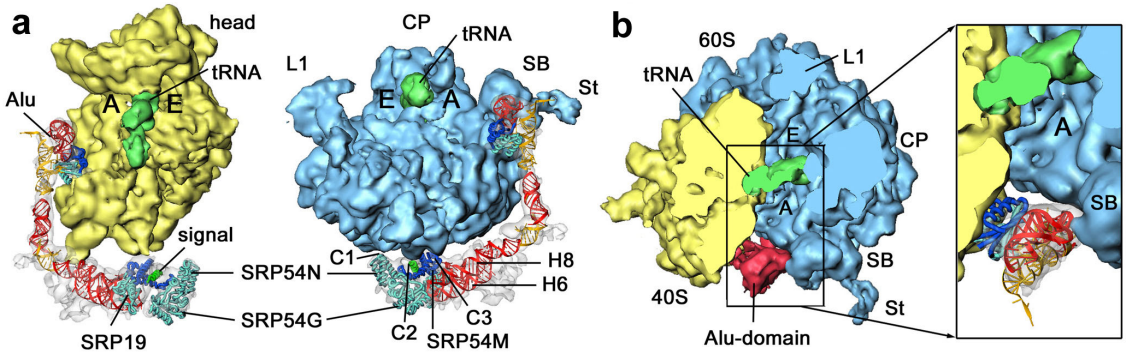

Figure 16: Molecular model of SRP and the ribosome. A, SRP with isolated 40S and 60S ribosomal subunits exposing P-site tRNA (green) shown from the 60S and the 40S side, respectively; A and E, position of A- and E-sites; Alu, Alu-domain; head, head of 40S subunit; L1, L1 protuberance; CP, central protuberance. Other labels as in a. B, Cut top view showing the Alu-domain in the intersubunit space, with labels as in e. Same view magnified, with molecular model of Alu-domain colour coded as in fig. 15.

3.2.1 Environment and function of the Alu-domain

The two connections between the Alu-domain and the ribosome are contributed exclusively by the 5'-RNP comprising the first 48 nucleotides of SRP RNA and the SRP9/14 heterodimer (fig. 17). In connection 5, the 5'RNA of SRP is interacting with both RNA and protein of the large ribosomal subunit. The loops L1.2 and L2 as well as the short helix 2 of 7S RNA contact the large ribosomal subunit via the so-called stalk base and, probably, the universally conserved α-sarcin-ricin loop (SRL). The participating components of the stalk base are the N-terminal part of rpL12 (L11p) and the tip of helix 43 of 25S ribosomal RNA (fig. 17b).

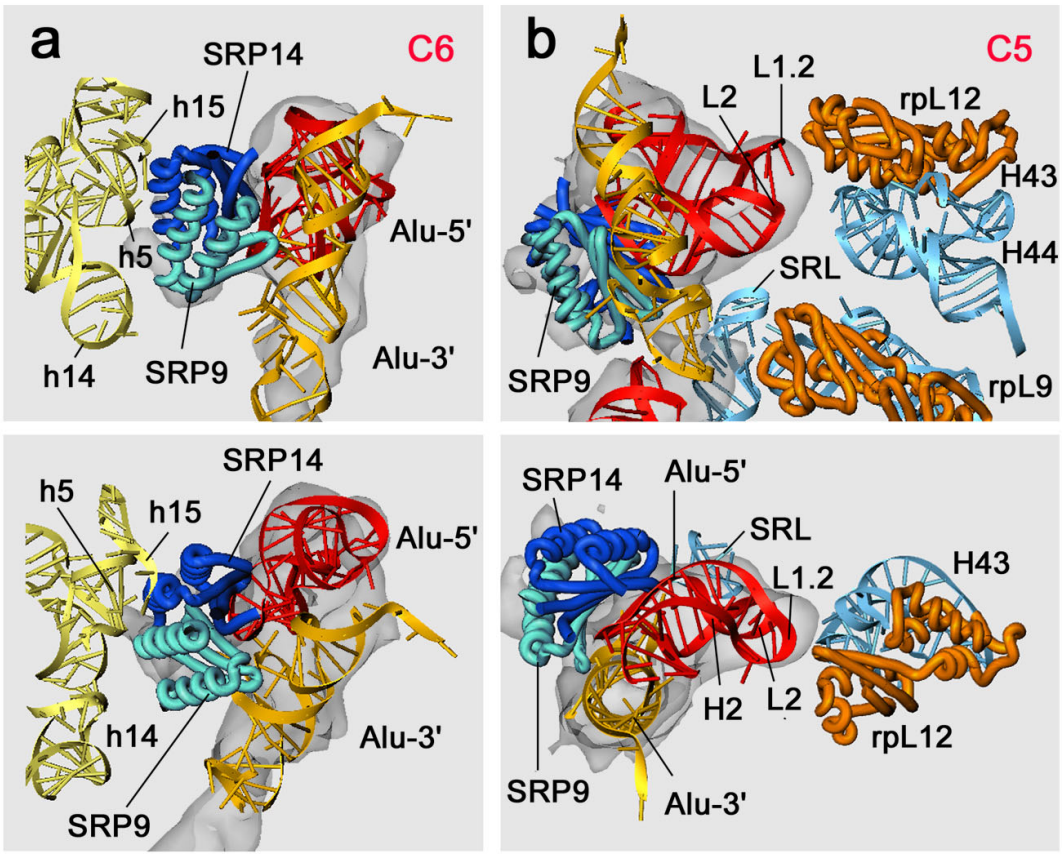

Figure 17: SRP Alu-domain interaction with 80S ribosome. a, SRP density with models showing connection 6 between SRP9/14 and ribosomal 18S RNA (helix 5, 15 and 14) in an orientation similar to fig. 12b. Colour code as in fig. 15; pale yellow, 18S ribosomal RNA; light blue, 25S RNA; orange, 60S proteins. Bottom: as top view but tilted toward the viewer. b, Connection 5 between SRP Alu-RNA (loop 1.2 and helix 2) and the GAC of the 60S ribosomal subunit (rpL12, helix 43 and SRL, sarcin-ricin-loop). Bottom: as top view but tilted toward the viewer.

In connection 6 (fig. 17a), the only contact of SRP with the small ribosomal subunit is established through the SRP9/14 dimer and ribosomal 18S RNA. Mainly the SRP14 surface participates in contacts with helices 5 and 15 of 18S RNA. SRP9 is in contact with the same helices and, in addition, is close to helix 14. According to biochemical data [102] deletion of the C-terminus of SRP14 abolishes elongation arrest. This functionally essential region and a large loop between the ß2- and ß3-strand of SRP14 are not resolved in the X-ray structure [40], therefore, at the given resolution it is not possible to draw any conclusions regarding their participation in ribosomal contacts.

3.2.2 Environment and function of the S-domain

The S-domain makes altogether four connections with the large ribosomal subunit. The first connection between S-domain and the large ribosomal subunit is formed by the tip of the SRP54 N-domain (fig. 18a). Two loops connecting helices 1 and 2, and helices 3 and 4, which build the four-helix bundle, come into close proximity with rpL25 and rpL35 (corresponding to L23a/L35 in wheat germ and L23p/L29p in *E. coli*). This contact site is in agreement with previous cross-linking

experiments identifying the same proteins as the main proteinaceous ribosomal constituents in immediate vicinity to SRP54 [13]. In similar experiments, the same region of the bacterial SRP54 N-domain has been found in a position adjacent to L23p [103], suggesting that this interaction is evolutionary conserved. In addition to SRP, signal sequences [104] and the chaperone trigger factor [105, 106] have been shown to bind to L23p, and the protein-conducting channel (PCC) of the ER (the Sec61 complex) to rpL25/rpL35 [99] (fig. 19c). Thus, the rpL25/35 (L23p/29p) proteins constitute a promiscuous binding site of the ribosome, which facilitates the interaction with multiple factors involved in the different aspects of cotranslational processing (fig. 19c).

The second connection is formed by the N-terminal part of the SRP54 M-domain contacting the helix 59 (expansion segment 24, ES24) of 25S ribosomal RNA (fig. 18b). As in the case of the first connection involving rpL25/35, this contact site of SRP is shared with the Sec61 complex [99]. The signal sequence is also closest to this connection when bound to SRP in the suggested position.

The third connection engages the C-terminal region of the M-domain, in particular the 7S RNA-binding part of it, which, again like the Sec61 complex, interacts with helix 24 of the 25S ribosomal RNA (fig. 18b). The interaction is established between helix 3 of the SRP M-domain and the tip of helix 24. The M-domain of mammalian SRP54 contains an additional region of about 60 residues at the C-terminus, which is present as density in the EM structure but not present in any of the current high resolution crystal structures. The helix 5 and the C-terminal part of the M-domain may play also a role in this connection. However, in contrast to the Sec61 complex, which contacts the stem of this helix, the SRP binding site is shifted toward the tip of rRNA helix 24.

The exclusive involvement of ribosomal RNA in the connections 2 and 3 is in agreement with the observation that rpL25/35 (L23p/29p) are the only ribosomal proteins cross-linked to SRP54.

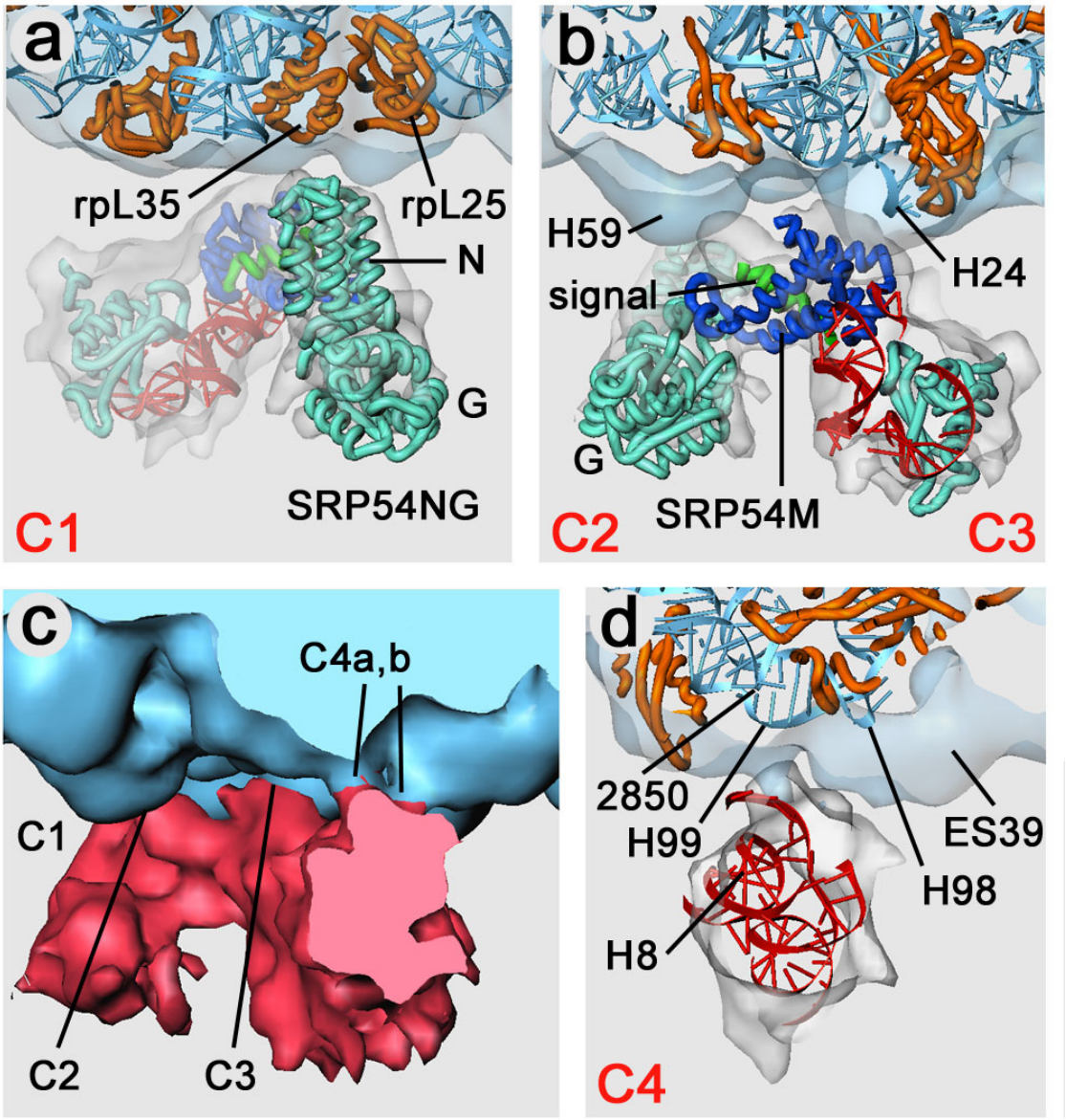

Figure 18: SRP S-domain interaction with 80S ribosome. a, Density with molecular models docked and cut to show connection 1 (C1) between SRP54NG and rpL25/rpL35. SRP colour code as in fig. 15; light blue, 60S ribosomal density and 25S RNA; orange, 60S proteins. b, Connections 2 and 3 (C2, C3) between SRP54M and ribosomal H59 and H24, respectively. c, Density in orientation as b and d, cut to show connections C2 to C4. d, Connection 4 with helix 5 of SRP (and SRP68/72) contacting the 60S subunit. 2850, position of nucleotide 2850 in 25S ribosomal RNA model; H99 and H98, 25S RNA helices; ES39, expansion segment 39.

Table 1: Contacts between mammalian SRP and the 80S ribosome

Contact	Type[a]	SRP	RNA/protein position	80S Ribosome[b]	RNA/protein position[c]
		S-domain		60S subunit	
C1	p-p	54NG	60-75 15-26	rpL25(L23) rpL35(L29)	130-35 16-27
C2	p/R-p p-R	54M/H8 54M	N-term of M	signal sequence H59[ES24]	 1627-34[d]
C3	p-R	54M	388-99	H24	490-95
C4	R-R/p p-R/p	H5 68/72	218-28,121-27	H99, 100/101, rpL16 H98/ES39, rpL16	2907-10, 2849-51
		Alu-domain		60S subunit	
C5	R-p R-R R-R	L1.2 L2 H2	35-36 13 09-19	rpL12(L11) H43 H95[SRL]	65-69 1171 2696-99
				40S subunit	
C6	p-R p-R p-R	14 9 9	74-89 57-75 55-60	h5, h15 h5, h15 h14	55-58, 356-59; 368 55-58, 368 341-44

[a]) R and p correspond to RNA (R) and protein (p) involved in contacts
[b]) Yeast nomenclature is used with family name in parenthesis
[c]) Positions correspond to model based on yeast 80S ribosome[100]
[d]) Positions correspond to yeast 25S RNA secondary structure (http://www.rna.icmb.utexas.edu)

The fourth connection is the only one involving the 7S RNA of the S-domain. It appears to be split into two entities, one of which (4a) is very close to RNA helix 5 of SRP. However, it is likely that SRP68/72 is involved in this connection (4b) as well, since there is additional density around RNA helix 5 and connection 4. The second connection (4b) is located right next to a ribosomal density that has been identified as expansion segment 39 (ES39) [100], formed by an extension of helix 98 of 25S RNA. This interaction would be then characteristic only for eukaryotic ribosomes, since ES39 is not present in eubacteria and archaea. In addition, rpL16 (L13p) projects a loop into the vicinity of connection 4. The closest ribosomal structures found for connection 4a are RNA helix 99 and a small loop at the junction between helices 100 and 101 of 25S RNA. The corresponding region in the *E. coli* ribosome, around nucleotide 2828 of 23S RNA (nucleotide 2850 in our model), has been found in vicinity of bacterial SRP 4.5 S RNA by cross-linking [107], again, suggesting a conserved mode of interaction.

Thus, considering the previously mentioned localization of SRP54, the core of the eukaryotic S-domain, including SRP54 and helices 8 and 5, appears to be positioned on the ribosome in a similar overall orientation as its counterpart in prokaryotes.

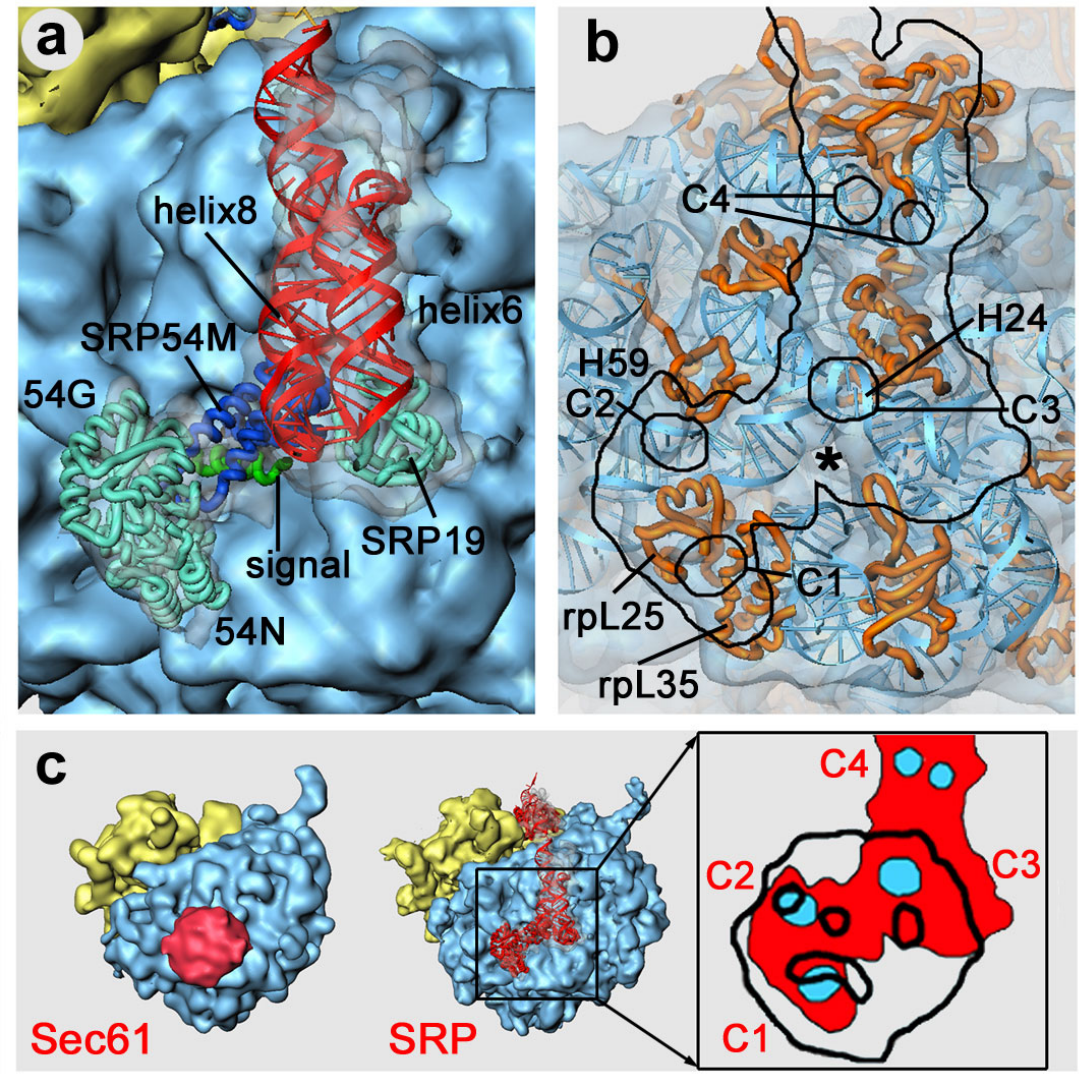

Figure 19: SRP S-domain interaction with the 80S ribosome. a, Model of S-domain covering peptide exit site of 60S subunit. SRP colour code as in fig. 15; light blue, 60S ribosomal subunit, yellow, 40S ribosomal subunit. b, As e with transparent ribosomal density and contour of SRP density to show locations of connections. Asterisk denotes peptide tunnel exit. c, Comparison of 80S RNC-Sec61 complex from Yeast with 80S RNC-SRP complex in same orientation. The magnified area is shown with contour of SRP (red) and Sec61 (black line) and their partially overlapping contact sites, SRP (blue), Sec61 (black line).

3.2.3 Functional states of SRP54

The most conserved part of SRP is the core of S-domain consisting of protein SRP54 (Ffh for Fifty-four-homolog in bacteria) bound to helix 8 (domain IV in bacteria) of SRP RNA [4, 26]. Structures of individual domains of SRP54 from various species are known since several years, but not their relative orientation [47]. Only recently, the spatial arrangement of these domains in two different functional states of SRP, in the free state (before binding to the ribosome or SR) and in the ribosome-bound state, became available from X-ray [53] and cryo-electron microscopy (cyro-EM) data, respectively (fig. 20). The X-ray structure of SRP54 of the Crenarchaea *Sulfolobus*

solfataricus was obtained with and without SRP RNA helix 8, resulting in very similar domain arrangement. Check for repetition and adjust (you cannot quote yourself!) Although the crystal packing might have influenced the conformation, it is very likely that the overall domain arrangement indeed represents the conformation of SRP54 in the free state since these structures were obtained in different crystal forms with different crystal packing. At the same time, the differences between them reflect the intrinsic flexibility of SRP core in free state. A cryo-EM structure shows the complete mammalian SRP after binding to the RNC and represents the ribosome-bound state of SRP. Here, the SRP core is part of the active targeting complex after binding both the signal sequence and the large subunit of the ribosome near the peptide exit tunnel. Although the resolution of the cryo-EM map is limited to 12 Å, the accuracy of interpretation can exceed that resolution several fold by docking of molecular models. The comparison of these two structures allows identifying large dynamic changes of SRP core between the free state and the ribosome-bound state during step I of SRP cycle. In addition, X-ray structures of the interacting NG-domains of bacterial SRP and SR provide a glimpse at the docking step (step II) at the target membrane [77, 78]. It turns out, that extensive conformational changes within the SRP core take place between the functional states, in particular between the free and the ribosome-bound state.

The X-ray structure of the free SRP core [53] reveals SRP54 as an L-shaped molecule, with SRP54NG as the longer arm of the L which aligns parallel with helix 8 of the SRP RNA (free state) (fig. 20a). Although SRP54NG does not directly contact the RNA, biochemical data [108] and differences within the SRP54 structures with and without RNA indicate that such an interaction is likely to exist. SRP54NG and SRP54M are connected by a flexible linker region that has not been observed in other earlier SRP54 structures. The linker region consists of a conserved 'LGMGD' sequence fingerprint in a loop preceding a long linker helix followed by another loop of variable size. SRP54M itself can be divided into a flexible N-terminal and a rigid C-terminal part. The C-terminal part (MC) binds to helix 8 of SRP RNA as a rigid body and provides a stable platform for the hydrophobic groove which is proposed to bind the signal sequence. The flexible N-terminal part (MN) includes a proline-kinked helix (αM1 and αM1b) followed by the finger loop which in the absence of a signal sequence shields the hydrophobic groove from the aqueous solvent. The comparison with the SRP54M structure from *Thermus aquaticus* [1] allowed to assign several hinge points in SRP54MN which would be sufficient for anchoring to SRP54MC and for adjusting the hydrophobic groove in order to accommodate the signal sequence [53].

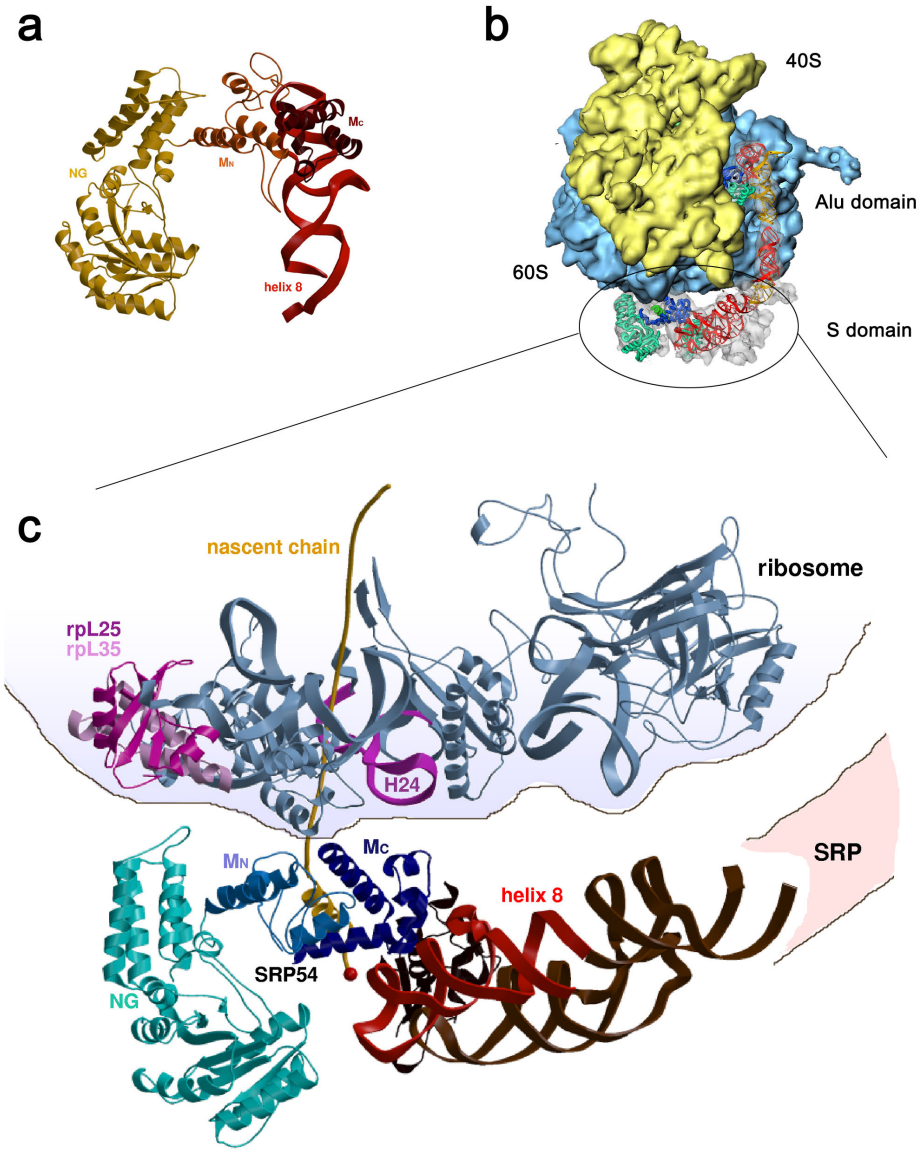

Figure 20: Structures of the SRP core in the free and ribosome-bound state. (a) The SRP core in the free state as derived from the X-ray structure [53]. The colour code is: RNA (red ribbon), SRP54NG (yellow), SRP54MN (orange), SRP54MC (dark red). (b) Cryo-EM structure of the mammalian SRP bound to the signal sequence carrying 80S ribosome. The SRP core as part of the S-domain is positioned near the tunnel exit of the large ribosomal subunit. The small 40S and large 60S ribosomal subunits are yellow and light blue, respectively. The SRP density is shown transparent with docked molecular models. Colours of labelled elements are: SRP54NG (turquoise), signal sequence (green), SRP54M (dark blue), RNA helix 8 (red). (c) Close-up view along the membrane surface of the SRP-RNC complex using molecular models. Ribosomal parts around the polypeptide exit tunnel are given in light blue with the exception of the two proteins rpL25 and rpL35 (dark purple and light purple, yeast nomenclature corresponding to L23p/L29p families) contacting SRP54N, and rRNA helix H24 (purple) contacting SRP54M. The nascent chain (yellow) is modelled in the polypeptide exit channel and into the hydrophobic groove of SRP54M which directly resides upon the exit site. The positively charged N-terminus of the signal sequence (red sphere) is in close proximity to the negatively charged SRP RNA next to the tip of helix 8 as predicted previously [11]. Figures have been prepared with programs Iris Explorer, BOBSCRIPT [109] and Raster3D[110] by Klemens Wild.

Compared to the described free state of SRP, the cryo-EM structure of SRP bound to an active 80S ribosome reveals a strikingly different conformation of the SRP core, referred to as open conformation (fig. 20b-c, 21, 22). The conformational transition of SRP core is shown schematically in fig. 21. The SRP core is positioned directly at the tunnel exit site of the large ribosomal subunit and the dynamics within SRP54 upon binding the signal sequence on the ribosome indeed reflect the dynamic potential as inferred by the X-ray structures [53]. Moreover, the observed structural changes are immense and came as a surprise even with the knowledge of the intrinsic flexibility of SRP54. The superposition of the SRP core from both X-ray and EM data is shown in fig. 22. On the ribosome, SRP54NG is rotated by 50° and shifted about 50 Å away from the aligned position with RNA helix 8 and is found at the very tip of the SRP core instead (fig. 21, 22a-b). The two distal loops of SRP54N interact with the two ribosomal proteins rpL25 and rpL35 (corresponding to L23a/L35 in wheat germ and L23p/L29p in *E. coli*) in agreement with previous cross-link data [13, 103, 106] (fig. 20c). As the rest of SRP is fixed on the ribosome, the linker region has to accommodate the large conformational changes. One rigid anchor point between the resting and the moving part could be assigned by comparing different X-ray structures of SRP54M [53]. It localizes to the end of the linker region at the N-terminus of helix αM1 of SRP54M and corresponds very likely to a conserved leucine residue (L329 in Sulfolobus solfataricus) which is deeply buried in the hydrophobic core of SRP54M [53]. The significance of this residue is underlined by the finding that its mutation abolishes signal sequence binding [93]. Although it is not resolved at the present resolution, in the open conformation of SRP54 the signal sequence can be accommodated in the hydrophobic groove in an orientation, which positions one end of the signal sequence near the backbone of the SRP RNA helix 8 as proposed earlier [11]. Direct participation of the SRP54NG domain in signal sequence interaction as suggested before [111] appears unlikely in this position.

3.2.3.1 A flexible domain linkage between SRP54M and SRP54NG

When further comparing SRP54 in the free and the signal sequence-bound state on the ribosome, it is apparent that especially two regions forming hydrophobic contacts within SRP54 are of particular significance for its dynamic behaviour: (i) in the free state a peripheral loop of SRP54N establishes a contact with αM1b of SRP54M. This is the only direct contact between SRP54N and the signal sequence binding part of the M-domain. It contributes to the stabilization of the compact conformation in the free state and is lost in the ribosome-bound state of SRP54; (ii) the linker region connecting the SRP54NG and M-domains maintains a contact to helix αM1 in both, the free and the ribosome-bound state, and undergoes the largest conformational change between the two states. The linker region consists of three parts: the conserved 'LGMGD' sequence fingerprint in a loop connecting the G-domain with the linker, an 18 residue long linker helix (termed αML) and a loop of variable size up to the conserved leucine residue. The first loop (with two conserved glycines in the 'LGMGD' motif permitting rotational freedom) has to change its conformation upon

ribosome binding while the linker helix αML seems to persist as a rigid body. The linker helix αML seems to persist as a rigid body although its relative orientation changes dramatically (almost 90°) with respect to both SRP54NG and SRP54M (fig. 20, 21b). In the EM density an empty tube, not accounting for any other parts of the separated domains, very likely represents this helix indeed spanning the distance from SRP54NG to SRP54M. The linker helix mainly interacts via hydrophobic interactions with helix αM1 and has already previously been implied to form a kind of greasy slide upon which the interface can be smoothly adjusted [53].

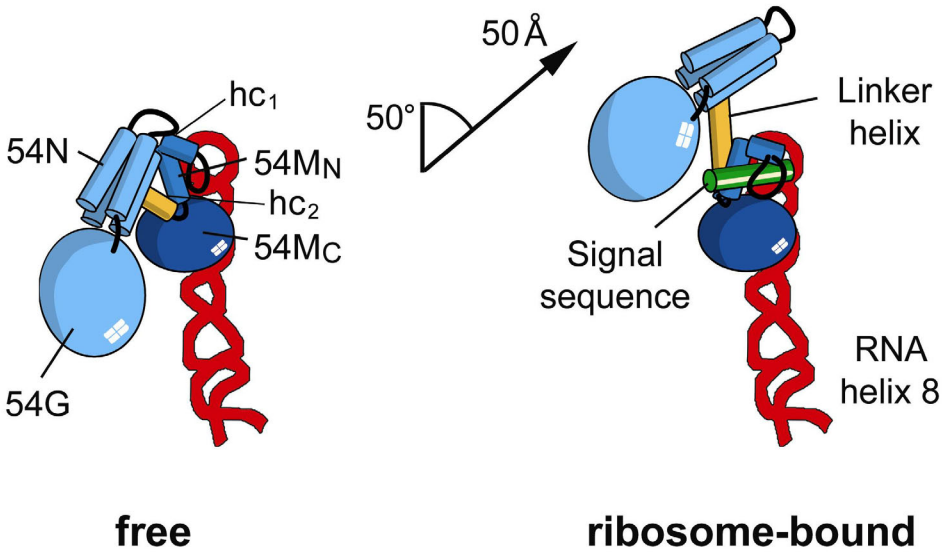

Figure 21: Dynamics of the SRP core. Schematic view of the dynamic behaviour of the SRP core (RNA helix 8 and the SRP54 subunit) when switching from the free state (derived from the X-ray structure [53]) to the ribosome-bound state (derived from the cryo-EM structure). The ribosome engagement causes a 50° rotation and a 50 Å shift of the SRP54NG domain as indicated. The linker helix (orange), which connects the SRP54NG with the SRP54M domain, rotates almost 90°. The signal sequence is positioned in the hydrophobic groove of SRP54MN which directly resides upon the exit site and adjusts accordingly: helix αM1a moves towards the groove and helix αM1b and the finger loop are shifted out of the groove and form a lid over the helical signal sequence. The positively charged N-terminus of the signal sequence is in close proximity to the negatively charged SRP RNA next to the tip of helix 8 as predicted previously [11]. The colour code is the same as in fig. 20, except that the linker helix is shown in orange (RNA, red ribbon; SRP54NG, turquoise; SRP54MN, blue; SRP54MC, dark blue; signal sequence, green; linker helix, orange).

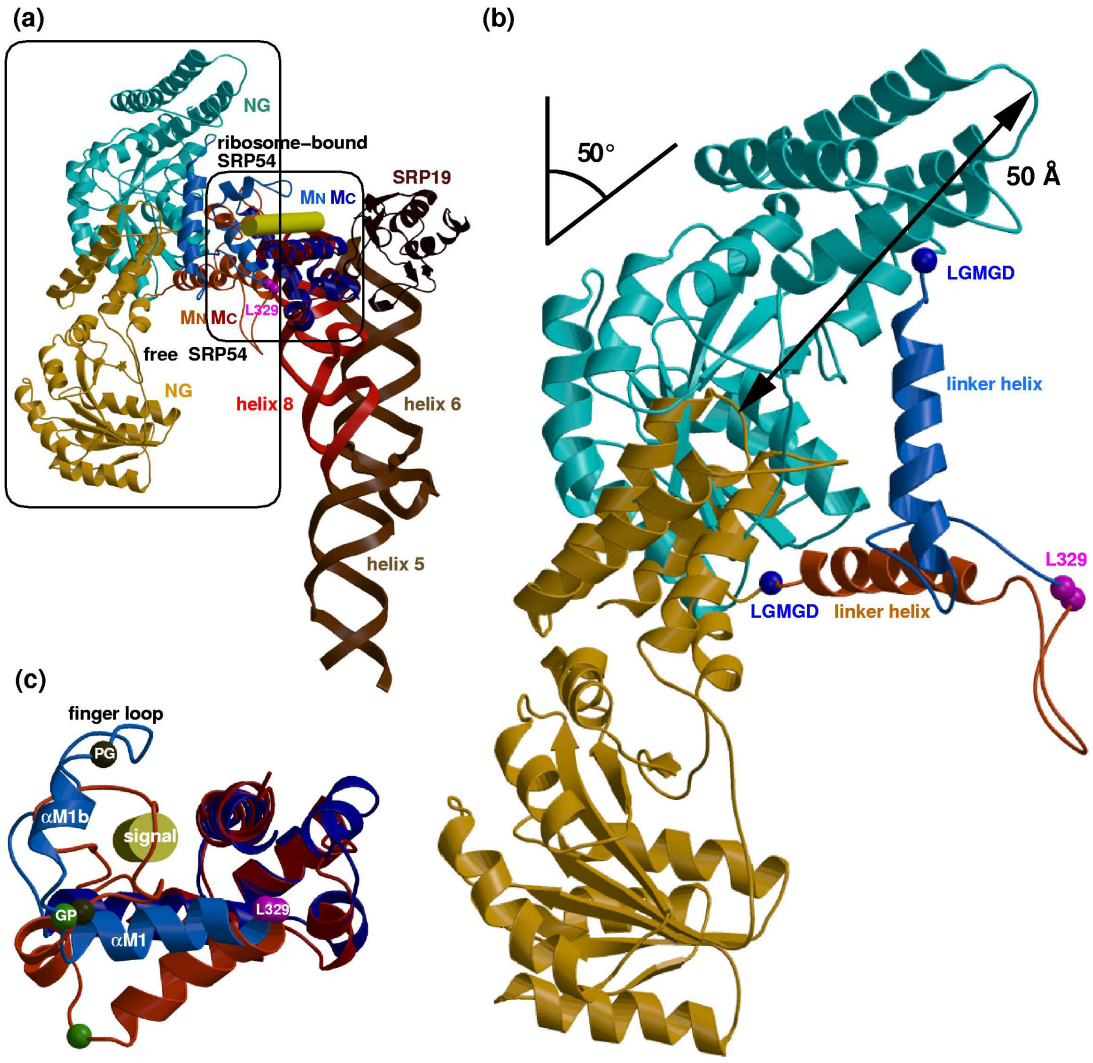

Figure 22: Dynamics of the SRP core with secondary structure. (a) Superposition of the free and the ribosome-bound SRP core. The superposition is based on the rigid parts present in both structures (SRP54M_C, and SRP RNA helix 8). The conformation of the free SRP54 as derived from the X-ray structure is shown in red colours, the ribosome-bound SRP54 placed in the cryo-EM data is depicted in blue colours. A putative signal sequence (helix represented as yellow cylinder) is modelled in the hydrophobic groove of SRP54M. The position of the fixed anchor point leucine (L329 in Sulfolobus solfataricus) between the MN and MC domain is given as a magenta sphere. (b) Movement of SRP54NG. The NG domain and the linker region are shown up to L329. The ribosome engagement causes a 50° rotation and a 50 Å shift as indicated. The linker region is highlighted: the conserved 'LGMGD' motif is given as a blue sphere. The linker helix (αML) rotates almost 90°. A flexible loop connects the linker to the anchoring leucine of SRP54M. The correct conformations of the two loops flanking αML remain elusive. (c) Conformational changes in SRP54M during signal sequence binding. The M domains are shown from the anchoring leucine to the C-terminal helix αM5. The model for SRP54M with bound signal sequence is based on a comparison of the M domain with a closed hydrophobic groove as seen in the free SRP54 [53] with an open structure [1] adjusted at several hinge points [53] (coloured spheres) to fit the EM data. Labelling is for SRP54MN with bound signal sequence only. Helix αM1 rotates towards the groove and helix αM1b and the finger loop are shifted out of the groove and form a lid over the helical signal sequence. Figure has been prepared by Klemens Wild.

Helix αM1 seems to undergo a rotation around the already mentioned conserved leucine residue and is part of the signal sequence binding groove (fig. 22c). This allows for the accommodation of a signal sequence in the orientation mentioned before, which positions one end of the signal sequence

near the backbone of the SRP RNA helix 8 as proposed earlier [11]. Signal sequence accommodation is facilitated by adjusting the subsequent helix αM1b and the following finger loop. In agreement with the previously proposed model [53] the adjustments necessary to fit the EM data involve a conserved GP/PG tandem motif flanking helix αM1b and the N-terminus of helix αM2, which marks the start of the rigid C-terminal half of SRP54M. Similar to the 'LGMGD' loop, also the second loop, which connects the linker helix αML with SRP54MN, has to change its conformation in order to bring the linker helix in the correct position. This loop may also be involved in signal sequence binding as it is very close to the hydrophobic groove and often contains methionine residues. The linker region ends with a deeply buried conserved leucine residue (L329 in *Sulfolobus solfataricus*) serving as a rigid anchor point at the N-terminus of helix αM1 of SRP54M [53].

When the N-domain interaction with SRP54M is lost in the ribosome-bound state, the linker region appears to provide the only physical link between the signal sequence-binding domain (SRP54M) and the GTPase domain (SRP54NG). Therefore, one can easily imagine that the change in the position of the N domain or a conformational change of the linker region is transmitted to the signal sequence binding groove and *vice versa*.

3.3 Structure of the signal recognition particle receptor interacting with the SRP-RNC complex

Following the protein targeting cycle the SRP-RNC complex docks in the next step to the membrane-bound SRP receptor (SR) in GTP dependent manner. Comparing of cryo-EM structures of RNCs in complex with the translocon [99] and SRP reveals that both, SRP and the translocon, bind at the tunnel exit of the ribosome in a mutually exclusive way. Therefore, the question remains how the transfer of the signal sequence and the entire RNC from SRP to the translocon is facilitated. Hence, our aim was to determine the structure of a SR-SRP-RNC complex.

3.3.1 Reconstitution of SR-SRP-RNC complex

The SR-SRP-RNC complex was reconstituted *in vitro* in an analogous way to the reconstitution of the SRP-RNC complex. Stalled RNCs were used for the reconstitution with excess amounts of purified canine SRP and human SR. Sucrose density gradient centrifugation under high salt conditions (500 mM KOAc) confirmed specific and high affinity binding of SRP and SR to RNCs with an estimated occupancy between 70-80% (fig. 23). Since the SRP-SR interaction is GTP dependent, in the reconstitution reaction GMP-PNP was used, a nonhydrolisable analogue of GTP. In the absence of GTP analogues no stabile SRP-SR interaction was observed.

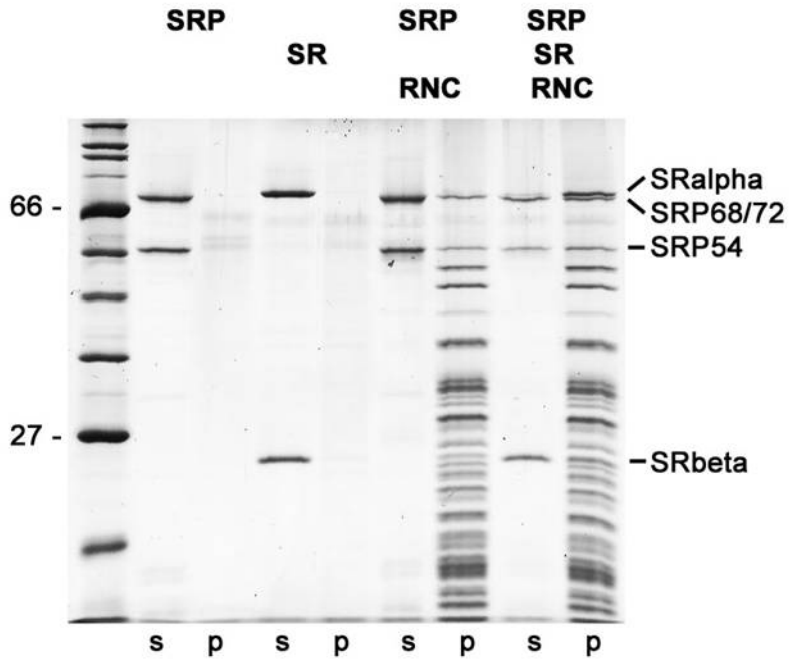

Figure 23: Purified DP90 RNCs were reconstituted with an excess of SR and SRP, subjected to sucrose density gradient centrifugation in the presence of 500 mM KOAc, fractionated and analyzed by SDS-PAGE and Sypro-Orange staining. SR-SRP-RNC complexes migrate in the 80S fraction indicating SR and SRP binding to RNCs. S, supernatant; p, pellet.

3.3.2 Cryo-EM map of SR-SRP-RNC complex

The preliminary cryo-EM map shows the typical appearance of an 80S ribosome at 9.1/6.6 A (0.5/3σ cut-off of FSC curve) with additional density, stretching from the peptide exit site to the intersubunit space, similar to the SRP density observed before (fig. 24). The part of the density, previously described as Alu-domain, appears at higher contour levels and is better resolved than the density around peptide tunnel exit site consisting of SRP S-domain and SR. This is most likely due to higher rigidity of Alu-domain which does not go through conformational changes after the interaction of SRP-RNC complex with SR. The Alu-domain resolution, which is close to that of the ribosome, is indicating high occupancy of the ligands in the final reconstruction. For this, a subset of 75% of the particles was used as a result of sorting according to the presence of ligands. The differences in the appearance of S-domain and Alu-domain densities, which is accompanied by a lower resolution, might reflect the higher flexibility of the S-domain in the newly formed complex after SR interaction.

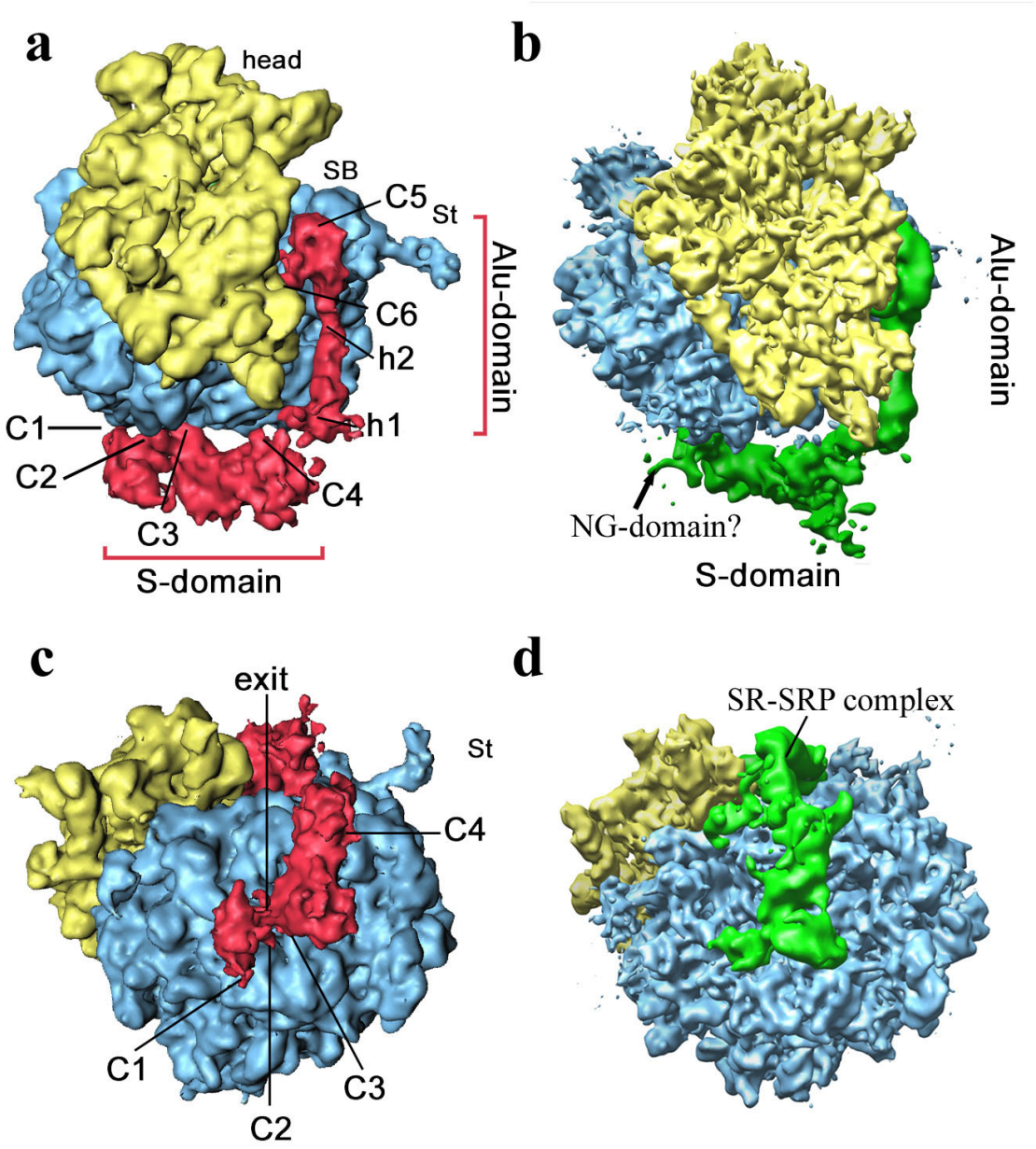

Figure 24: Cryo-EM maps of mammalian SRP bound to 80S RNC at 12 Å and mammalian SR and SRP bound to 80S RNC at 9.1 Å. Ribosomal and SRP/SR densities are shown at different contour levels and amplitude correction using B-factors was applied only to the ribosome. a, RNC-SRP map showing the separated colour-coded densities. Yellow, 40S small ribosomal subunit; blue, 60S large ribosomal subunit; green, P site tRNA; red, SRP. C1-C6 assigned positions of RNC-SRP connections (see also table 1); h1 and h2 are hinges of the 7S RNA backbone of SRP; St, stalk; SB, stalk base. b, SR-SRP-RNC map with separated colour coded densities. Green SR-SRP complex. The arrow is indicating delocalized NG domain. c, As a but rotated upward by 90°. d, As b but rotated upward by 90°.

The comparison of the electron density of SR-SRP-RNC complex with the density of SRP-RNC complex reveals several differences in the S-domain region of SRP. First, the S-domain of SRP is rearranged on the 60S subunit by shifting and tilting as seen in fig. 25. As a result of the shift SRP-SR complex moves slightly away from the peptide exit site and at the same time, as a consequence of the tilt, it comes closer to the ribosome, especially the protein SRP19 as seen in fig. 25b. This

rearrangement could be necessary for the interaction with translocon in the next step of protein targeting.

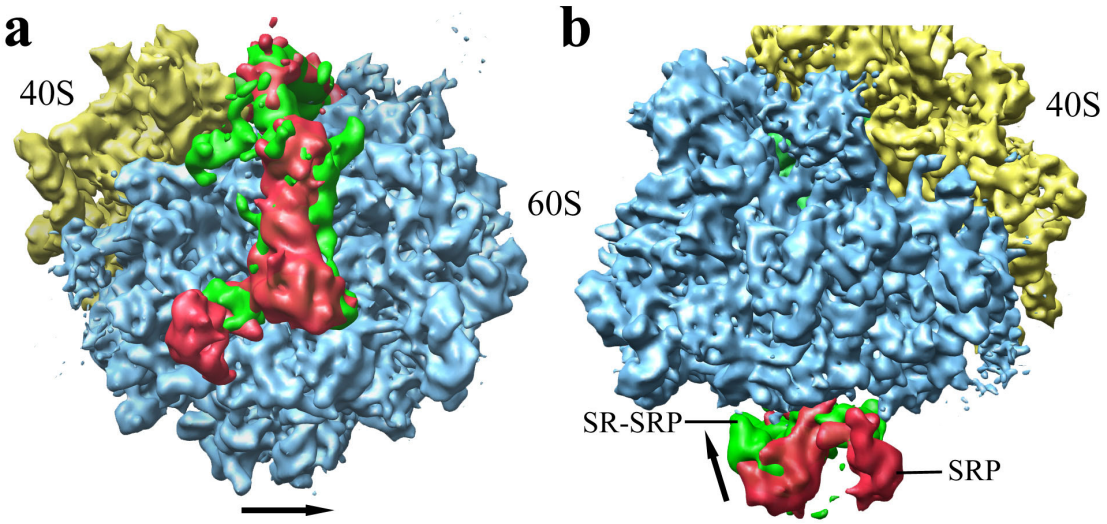

Figure 25: Cryo-EM map of mammalian SR-SRP-RNC complex at 9.1 Å superimposed with SRP density from SRP-RNC complex. Densities are colour coded as in figure 24. a, Peptide exit site view of the ribosome. The arrow is indicating shift of SR-SRP complex to the right related with SRP. b, View from the back of large subunit. The arrow is indicating a tilt of SR-SRP complex towards the ribosome.

The second main difference between the two densities is the apparent delocalization of both NG-domains. The density for these two components is not visible and it can be seen only as a very weak undefined mass at low contour levels (fig. 24b). Upon SRP-RNC complex interaction with SR in presence of GTP, the SRP54 NG-domain forms together with the SRα NG-domain a heterodimeric complex. Delocalization of these two domains dissociates SRP from binding site C1 which involves ribosomal proteins L23e and L35. These two proteins provide also the binding site for the translocon and, therefore, clearing of the binding site C1 allows spatial access of the translocon.

The third clear difference compared to the SRP structure is extra density visible as part of S domain around the previously described connection C4 and the RNA kink. This density is present on both sides of SRP RNA and it can be identified as SRα and SRβ. SRα consists of three domains, two of which are visible in the cryo-EM electron density, while the third, NG-domain, is disordered. The density for SRX1-domain, the N-terminal domain of SRα, is well resolved and allows unambiguous docking of the crystal structure [81] (fig. 26). The positively charged SRX2-domain, a long linker domain, stretches parallel along the SRP RNA and connects SRX1-domain with the SRNG-domain as seen in fig. 26. The docking of the SRα results in steric clashes of SRβ with other structures when in complex with SRα as in the crystal strucuture. This leads to the assumption that SRβ may dissociate from SRα and bind to the SRP and the ribosome at different location. The additional density which is not present in the SRP-RNC complex can be actually identified as SRβ and preliminary model can be built.

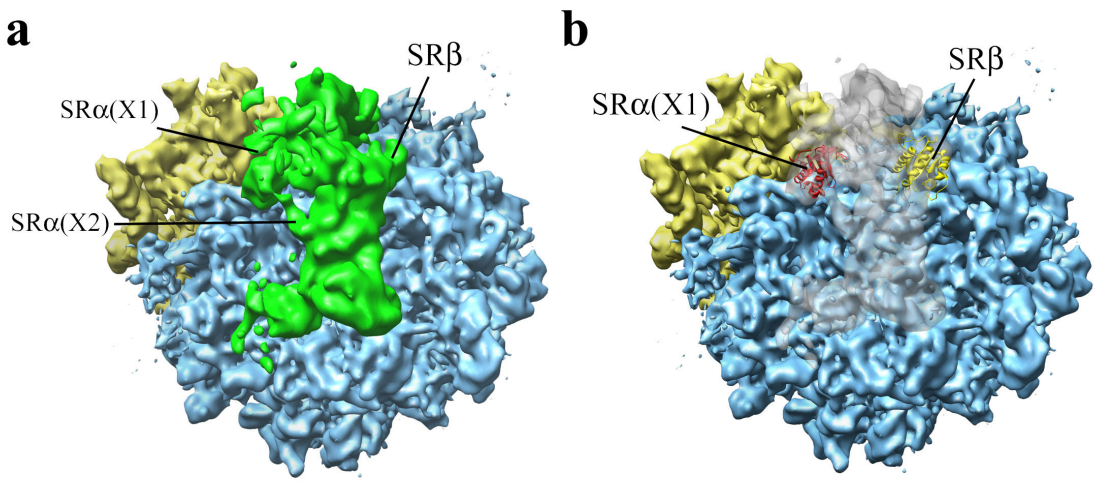

Figure 26: Cryo-EM map of mammalian SR-SRP-RNC complex at 9.1 Å. Peptide exit site view of the ribosome. Densities are colour coded as in figure 23. a, SR-SRP complex density with pointed out densities belonging to SR. SRa(X1), X1 domain of SRa, SRa(X2), X2 domain of SRa. b, Transparent density of SR-SRP complex with preliminary models for SRb (yellow) and X1 domain of SRa (red).

3.4 High resolution structure of the ribosome and localization of L30e

The present cryo-EM map of the SRP-RNC complex with its resolution limited to approximately 12 Å leaves several interesting questions unresolved. How does SRP54 bind the signal sequence and how does that correlate with GTP binding to the SRP54 NG-domain? How does the interaction between N- and G-domain change the GTP affinity of the G-domain? To get more insights into these problems, a 3D reconstruction of the SRP-RNC complex at higher resolution was aimed at. Although the resolution of the map improved to 9Å with alpha-helical secondary structure resolved in the ribosomal density, the density of the SRP is not at a sufficiently high resolution yet. Since the resolution of the ribosomal density allows fold recognition, the eukaryotic ribosomal protein L30e was located in the 60S ribosomal subunit.

L30e binds to the transcript of its own gene to inhibit splicing to mature mRNA [112, 113] and to reduce translation [114]. This prevents accumulation of L30e in excess of amounts needed to assemble ribosomes [115]. Like other ribosomal proteins, L30e has been highly conserved through evolution. Yeast L30e is 63% identical to wheat germ (and mammalian) and 33% identical to archaeal L30e. All these L30e proteins have a highly conserved structure lacking major insertions or deletions most likely due to requirements of its interaction with ribosomal RNA and proteins. The functional conservation allows archaeal L30e to bind to the RPL30 transcript of yeast resulting in inhibition of splicing [116].

Recently, several crystal and NMR structures of yeast and archaeal L30e have been solved, however, leaving open the localization of L30e on the ribosome. Based on its interaction with its own mRNA, there have been several attempts to assign the RNA region for L30e binding to the

ribosome. As one candidate site of interaction the 25S RNA, region 830-862 (helix 34) was identified [116] in *S. cerevisiae* on the basis of strong binding of L30e to this helix when isolated. As another candidate, helix 38 of ribosomal 25S RNA was identified as the likely binding site for L30e by satisfying the consensus requirements for RNA kink turns [117]. This characteristic structure is required to bind L30e and, in the case of the large ribosomal subunit of *H. marismorturi* which lacks L30e, no interaction of this region with any other ribosomal protein has been observed [117]. Thus, the questions remain where L30e is located in the ribosome and what is its essential function there?

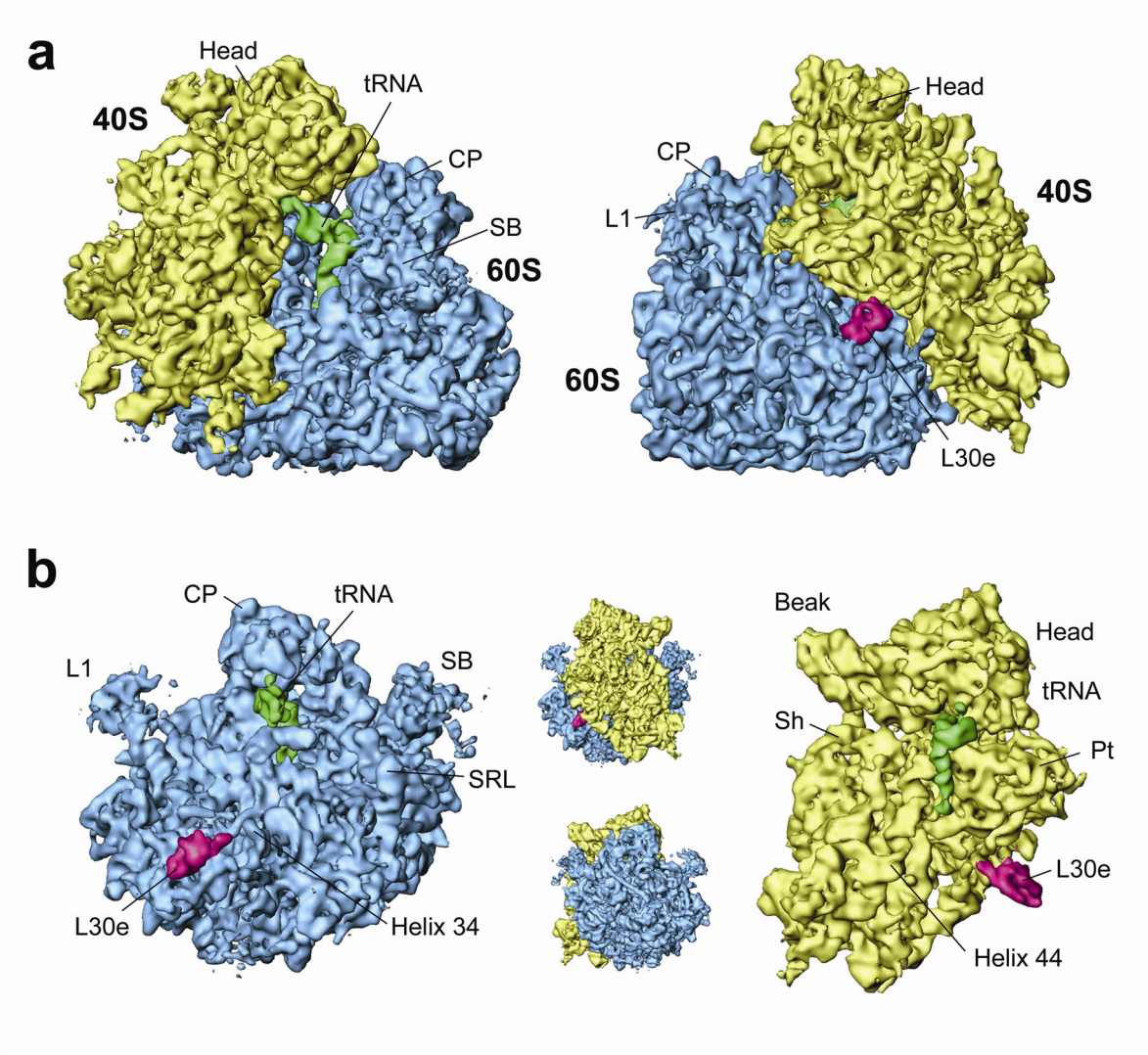

Figure 27: Localization of L30e in a 9.5 Å cryo-EM map of the 80S ribosome. a, Cryo-EM density of the wheat germ 80S ribosome. The separated ribosomal subunits, tRNA and L30e are colour-coded. Yellow, 40S ribosomal subunit; blue, 60S subunit; green, P-site tRNA; magenta, L30e; landmarks: SB, stalk base; CP, central protuberance. b, As a but rotated by 150° to the right. c, L30e as part of isolated 60S subunit density. SRL, sarcin ricine loop. Top insert indicates the orientation of the subunit. d, L30e shown with isolated 40S subunit density. Sh, shoulder; Pt, platform. Bottom insert indicates the orientation of the subunit

With the high resolution cryo-EM map of the 80S wheat germ ribosome it is now possible to determine the localization of L30e based on its characteristic tertiary fold. The map shows the

ribosome at 9.5/6.9 Å resolution (0.5/3sigma cutoff in FSC curve) with α-helical secondary structure of proteins clearly resolved (fig. 27a). This map was generated by improving the resolution of a previous SRP-RNC complex map through extension of the dataset to 52,000 particles and using the best 21,000 particles for a final 3D reconstruction. The ribosome is in the posttranslational state with peptidyl-tRNA bound in the P-site. Since helix 34 of 25S RNA was predicted as one of the binding sites [116] it was localized in the map and the L30e fold was recognized in its vicinity. This localization was then confirmed with the signature search [96] determining L30e's position in the 60S subunit participating in the interface between large and small ribosomal subunit (fig. 27b-d). The yeast crystal structure was used for the search of L30e (1NMU chain D) [97]. The same crystal structure was also used for homology modeling of the wheat germ L30e (3D-JIGSAW) [118]. When comparing the electron density with the model or the crystal structure it is apparent that different conformations of the region between residues 70 and 86 of L30e exist. On the ribosome, the helix 4 in this region is flipped down which allows contacts of L30e with different ribosomal proteins and RNA. The same region of L30e is already known as highly flexible from different crystal and NMR structures of isolated L30e in which it adopts different conformations [97]. Another difference between the conformation of L30e in the ribosome and in isolation is a minor shift of the two helices next to the N- and the C-terminus towards helix 4 (fig. 28a-d). The homology model was adjusted accordingly in those two regions to fit the EM density (fig. 28c-d). It was completed by positioning missing residues of the N- and the C- terminus in corresponding density of the EM-map. Two residues of the C-terminus were added, where the density indicates an interaction with β-strand 3, and three residues of the N-terminus were added reaching over to the small ribosomal subunit (fig. 28c-d). Due to the limited resolution of the map, these N- and C-terminal residues as well as the loops connecting helix 4 of L30e could not be positioned precisely in an unambiguous manner. The wheat germ ribosomal proteins contacting L30e were homology modeled (3D-JIGSAW) and adjusted to the EM map. Ribosomal RNA in this region was adjusted to the EM map using the *H. haloarcula* (for 25S) and the *T. thermophilus* (for 18S) model used before for the yeast 80S ribosome [100].

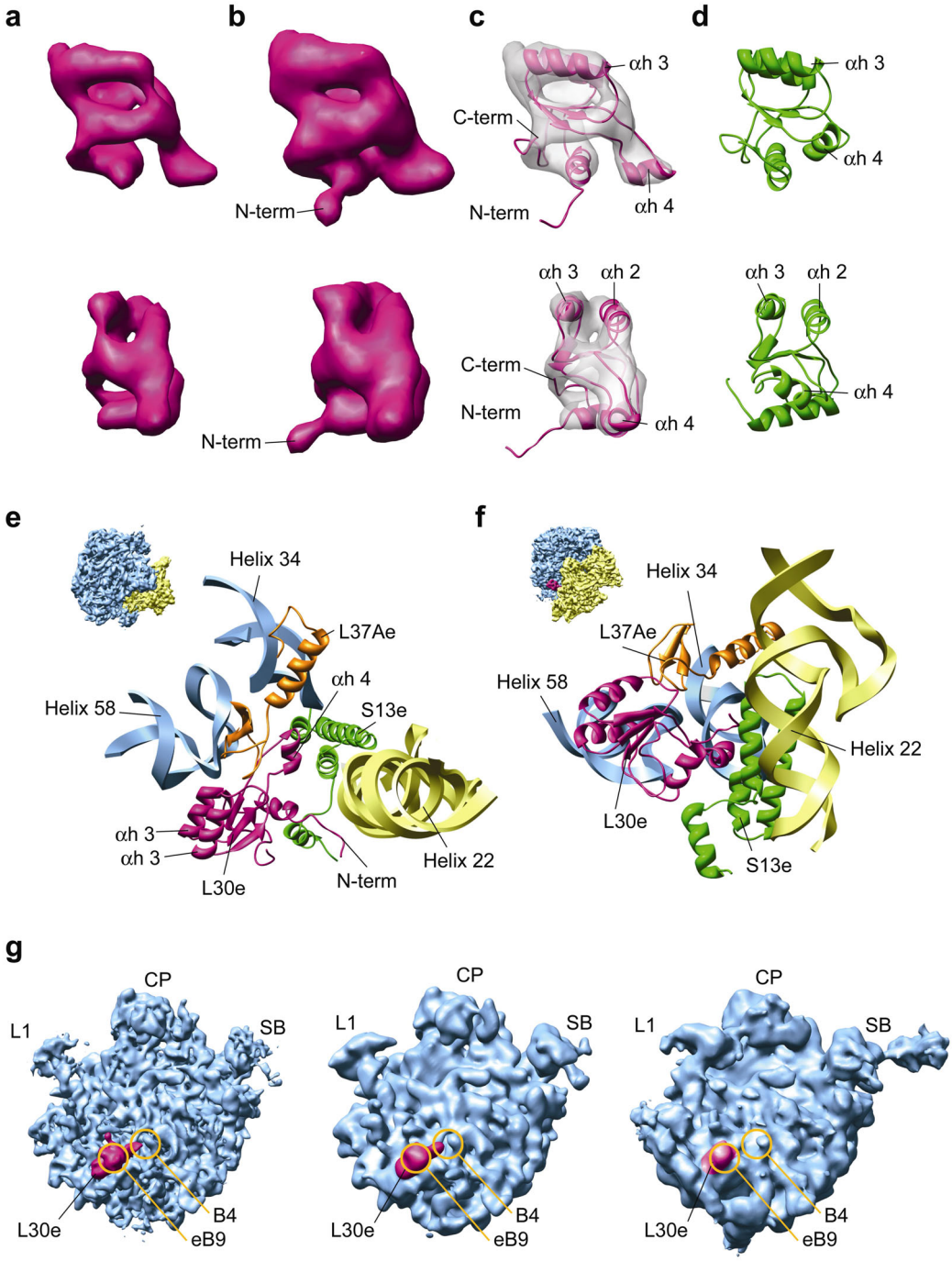

Figure 28: Molecular model of L30e and its ribosomal environment. a, Isolated L30e density (contour at ~2.5 sigma) in a "side" view (top) and rotated 90° to the left (bottom). b, As a but shown at lower contour level (~1 sigma). N-term, N-terminus. c, Adjusted homology model of wheat germ L30e shown with transparent EM density. C-term, C-terminus; αh 2-4, α-helix 2-4. d, Crystal structure 1NMU_D shown to illustrate conformational differences. Note the different position of the α-helix 4. e, Molecular environment of L30e in the ribosomal interface. Blue, 25S RNA; orange, L37Ae, magenta, L30e; yellow, 18S RNA; green, S13e. The inset indicates the orientation of the view. f, As e but rotated by 90° upwards. g, Comparison of L30e in a 80S ribosome in the post state and in the eEF2-bound state. The 60S subunit of the wheat germ 80S ribosome map (post state) is shown at 9.5 Å resolution (left) and filtered to 13 Å (center) together with the 60S subunit of the yeast 80S ribosome-eEF2 complex at 11.7 Å (right). Landmarks as in fig. 27. B4 and eB9 indicate the location of intersubunit bridges. Note the different location of the density for the helix 4 of L30e in EF2-ribosome complex.

Located in the ribosomal intersubunit space, L30e makes several connections to both, proteins and RNA, of both subunits. In the 60S subunit, L30e contacts two RNA helices (table 2). The largest and most important contact is formed between aa residues 24-28 and 86-88 of L30e and RNA helix 58 of 25S RNA (nt 1591, 1603-1605, *H. marismorturi* model). In addition, the tip of the helix 4 of L30e (aa 79-81) comes into close proximity to RNA helix 34 (nt806-808) and likely forms a second contact with 25S RNA (fig. 28e-f). Two more protein-protein contacts exist: the loop between β-strand 2 and α-helix 3 (aa 46–48) of L30e interacts with a loop of the ribosomal protein L37Ae (aa 41-43). Yet another contact of L30e in the 60S subunit involves a unknown ribosomal protein which is part of the previously described cluster II [100].

Interacting with the 40S subunit, L30e contacts one 18S RNA helix and one ribosomal protein (table 1). The N terminus of L30e contains 3 lysines (aa 1, 3 and 4) and interacts with the helix 22 of 18S RNA (661-662, *T. thermophilus* model) forming a relatively week connection visible only at lower contour levels (fig. 28e-f). The helix 4 of L30e forms two connections with two helices of the ribosomal protein S13. The tip of the helix 4 (aa 77-81) connects to the C terminal part of S13 (aa 143-145) which is also interacting with the helix 34 of 25S RNA of large ribosomal subunit. The residues 74-76 of the helix 4 interact with a second S13 helix involving aa residues 92-94. Finally, the N and C terminal part of L30 appear to form another weak contact to yet another helix of S13 (aa 77-79). Many of these residues are shown to be evolutionary conserved between archaeal and yeast L30e [117].

Although helix 34 and helix 38 of 25S RNA were predicted as the most likely ribosomal binding sites for L30e, ribosomal RNA helix 58 turns out to be the main binding site. The interaction with helix 34 is significantly weaker (tip of helix 4 of L30e) and it is possible only in this conformation of L30e (see below). In agreement with our findings L30e has been shown to bind to fragments of both helices (34 and 58) *in vitro* [116]. Moreover, RNA helix 58 indeed meets the conformational requirements suggested previously [117] and binds L30e via a RNA kink turn.

In the determined position L30e appears to be the only 60S constituent of the intersubunit bridge eB9 [99, 100] and may contribute also to the bridge B4 formed mainly by 25S RNA helix 34 on the 60S side. It has been shown previously that lack of L30e in *S. cerevisiae* leads to stalled initiation complexes suggesting a subunit joining defect [119]. A role of L30e in subunit joining or 80S stabilization could therefore be explained by its function in bridge formation. Interestingly, bridge eB9 formed by L30e is dynamic since it is present in the post translational state of the ribosome but absent in the eEF2-bound state [120]. Moreover, when comparing our present EM map in the post state with the map of the 80S ribosome-eEF2 complex at similar resolution, it is evident that the flexible region of L30e involving helix 4 adopts a different conformation in this functional state of the ribosome. Here, the contact to B4 is lost and the conformation of the flexible region is likely to be more similar to the conformation observed in the crystal structure(1NMU) [97]. Hence, it is possible that the conformation of the flexible region of L30e is related to the conformational states of the ribosome and that L30e plays a role in facilitating the ratchet movement of the 80S ribosome

during the translation cycle. Therefore, in contrast to the majority of ribosomal proteins which play a role in merely fine tuning the 3D structure of ribosomal RNA, L30e appears to have adopted a direct function in controlling large scale conformational changes of the ribosomal machinery.

4 Discussion

Since its discovery in the early 80ties research in the SRP field was focusing on the functional characterization of the SRP system. SRP turned out to be the central player in co-translational protein targeting: it interacts with hydrophobic signal sequences, pauses peptide elongation and targets the ribosome nascent chain complex (RNC) to the membrane in a GTP-dependent manner. There, SRP dissociates and the RNC binds to the protein-conducting channel, the translocon [4, 26].

It has been known for a long time that almost all SRPs (except in gram-negative bacteria) have two main domains: (i) the S domain, which mediates signal sequence binding and membrane docking, and (ii) the less well conserved Alu domain, which mediates pausing of the peptide elongation. Little was known about the structural arrangement of the complete SRP [121], [47], especially when bound to the active ribosome. How can SRP recognize a signal sequence and stop the elongation at the same time? The structure of mammalian SRP bound to an elongation-arrested 80S ribosome bearing a nascent polypeptide chain that contains a signal sequence can now provide some answers.

As seen in fig. 12, mammalian SRP is a large elongate mass stretching from the peptide exit site of the 60S ribosomal subunit (S-domain) into the intersubunit space (Alu-domain), forming a total of 6 connections (C1-C6) with the ribosome. Four connections are formed by S domain (C1-C4) and two (C5-C6) by Alu domain. SRP shows a bent conformation with one of two hinges apparently facilitating a major kink (hinge 1) separating the S- and Alu-domains. The kink is in agreement with a three domain structure of 260-280 Å length proposed for SRP in solution [121] as seen in early electron microscopy images. The RNA at hinge 1 represents a large loop around nucleotides 100/250 and forms an angle of almost 90° (fig. 12b, 15). This site coincides precisely with the cutting site for *micrococcus* nuclease [5], which separates SRP into S- and Alu-domain. The second hinge is located in a region close to Alu-domain and it facilitates a bend (~ 30°), which leads to an orientation of the 5'-Alu-RNP so that it fits into the intersubunit space (fig. 12a, 15f). These hinges probably provide the necessary plasticity for proper positioning of S- and Alu-domain on the ribosome.

When comparing the binding sites of SRP and the PCC [99, 122] it is evident that they both cannot bind to the ribosome at the same time [123] (fig. 19). Both PCC and SRP share connections C1 and C2, and connection to helix 24 (C3) is just slightly different; SRP interacts with the tip of the helix and PCC with the stem. Therefore, docking of the ribosome to the PCC requires first a rearrangement of the entire S-domain relative to the ribosome, which is triggered by the interaction of the SRP-RNC complex with SR [13]. This rearrangement may precede a state in which the binding sites for the PCC are accessible and the transfer of the signal sequence can take place.

4.1 Model of elongation arrest

The ribosomal components bound by the Alu-domain are well conserved in all ribosomes and comprise the elongation factor binding site [124]. It is intriguing that all the contact sites used by the SRP Alu-domain are used by eEF2 [125, 126] as well, allowing us to interpret the Alu domain ribosome interaction as elongation factor mimicry (fig. 29). A tRNA-like interaction, however, is taking place concomitantly: the RNA-RNA interaction between the loop L2 of the SRP 5'-RNP and helix 43 of the stalk base is reminiscent of the interaction of the tRNA T-loop with the same ribosomal helix in the context of the EF-Tu*tRNA*GTP ternary complex bound to the ribosome [127].

Binding of the Alu-domain in this position directly competes with elongation factors entering their binding site. Therefore, sufficiently high affinity of the Alu-domain for this site explains its elongation arrest activity. Variations of the Alu-domain affinity could explain different efficiencies observed in different systems [17, 128]. In the cryo-EM structure the Alu-domain is bound to a ribosome in the post-translocational conformation (POST state), as defined by the presence of the peptidyl-tRNA in the P site and an unoccupied A-site. Thus, it is possible that the POST state of the ribosome is the preferred conformation for SRP binding during the elongation cycle [129].

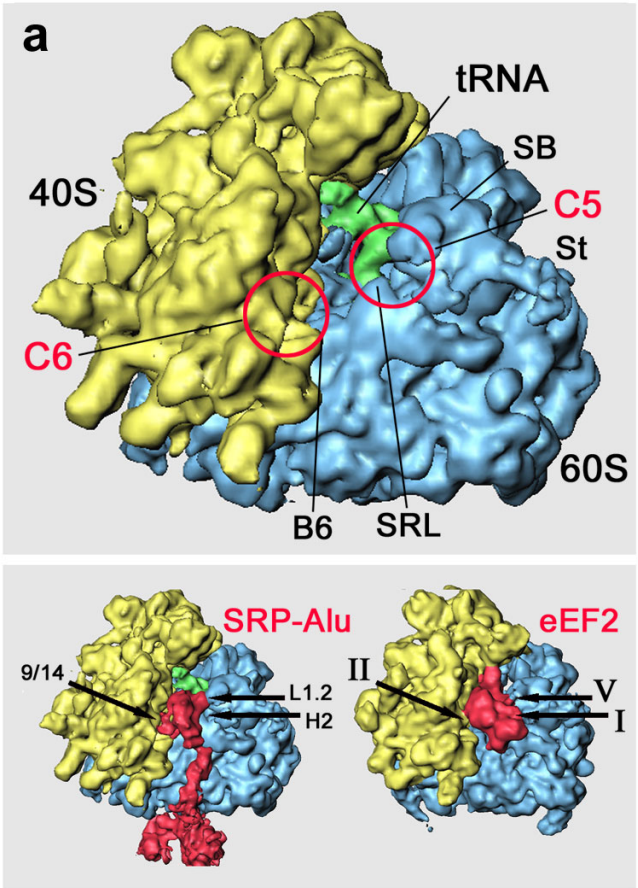

Figure 29: SRP Alu-domain interaction with 80S ribosome. a, Top: 80S RNC density without SRP, showing conserved contact sites of Alu-domain. B6, bridge 6. Bottom: Comparison of 80S RNC-SRP complex with 80S ribosome-eEF2 complex [126] in same orientation (SRP and eEF2 shown in red). Subunits of the Alu-domain and domains of eEF2 involved in similar contact sites are labelled. Colour code as in figure 12.

How can elongation arrest by the Alu-domain be controlled by the event of signal sequence binding, which occurs more than 250 Å away? Its binding has to induce or at least stabilize bending [130] of the particle at hinge 1 in order to promote Alu-domain binding (fig. 30). One possibility is that high-affinity binding of the S-domain simply tethers the Alu-domain in an appropriate position on the ribosome, and thereby favours the bound state conformation of SRP. However, another model can be suggested where recognition of a signal peptide produces specific positioning of the S-domain on the ribosome; this may lead to conformational changes of SRP68/72 that results in the hinge 1 stabilising a 90º angle and the Alu-domain closing into the factor binding site (fig. 30). In agreement with this idea is the brace-like localisation of SRP68/72 covering the hinge 1 region, its participation in connection 4 and the finding that SRP reconstituted without SRP68/72 lacks elongation arrest activity [18].

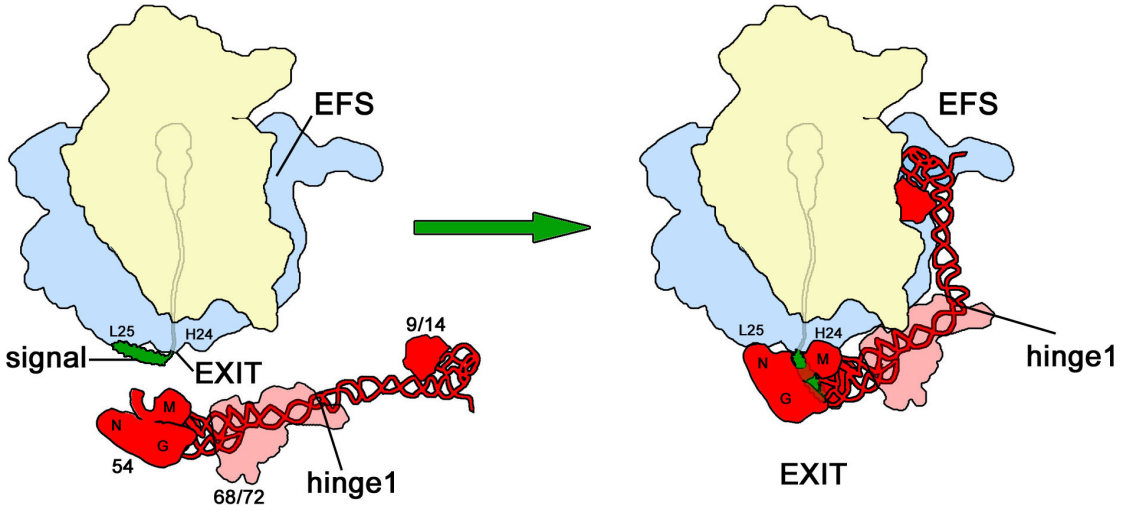

Figure 30: Signal sequence-dependent SRP-ribosome interaction. Upon signal sequence binding by SRP54, a kinked conformation of SRP is stabilized involving possibly SRP68/72 and a rotation around hinge 1. As a result, SRP interacts with the ribosome, stretching from the peptide exit (S-domain) to the elongation factor binding site in the intersubunit space (Alu-domain), where it causes elongation arrest by competition with elongation factors. Colour code as in figure 12; signal, signal sequence (green); EXIT, peptide tunnel exit; EFS, elongation factor binding site.

In homologous systems only a slowdown of translation, and not the complete arrest, is observed [16, 17, 55]. In order to continue translation it is necessary that the Alu-domain relocates on the ribosome, so that the required elongation factors can access the ribosome and translation can resume. It is not clear where the Alu-domain is located in this situation. It could be that it interacts with the ribosome in different position by forming new contacts or that it is simply flexible and disordered. The necessary plasticity of the Alu-domain could be also a result of flexibility around the hinge 2.

4.2 Model of the first steps of the SRP cycle

Based on those structural and previous biochemical data a more detailed mechanistic model can be presented describing the conformational changes within the SRP core which facilitate first steps of the SRP cycle (fig. 31).

(i) The free SRP core in solution most likely adopts a compact conformation similar as observed in the recent X-ray structure, and might be stabilized by an interaction of SRP54G with the SRP RNA [53]. A direct contact between the distal loop of SRP54N and helix αM1b of SRP54M is present and the finger loop of SRP54M is covering the hydrophobic groove to protect it from aqueous solvent. In this free state, SRP is indicated to be incapable of signal sequence binding [131] and the GTP affinity of SRP54 is low.

(ii) In the sampling mode, SRP binds with low affinity to the ribosome in order to probe it for the presence of a signal sequence [3]. Although there are no structural data available for this mode, biochemical cross-links indicate that the signal sequence-independent interaction is similar to that observed in the cryo-EM structure: the different ribosomal cross-link patterns of the mammalian Alu domain [132] as well as of SRP54 in mammalian [13] or E. coli SRP [103] do not change extensively between sampling and targeting mode. Therefore, the hydrophobic contact between the distal loop of SRP54N and the M domain might be lost already due to the interaction of SRP54N with L23p/L29p [13, 103, 106], which might prime SRP for signal sequence binding on the ribosome. Notably, signal sequences of RNCs could be cross-linked to the same site of the ribosome, the L23p protein [106], making this site ideally suited for probing by SRP54M. L23p functioning as a transitory binding site for signal sequences would be in agreement with a stabile affinity of SRP signal sequences independently of chain length [133]. However, without a signal sequence available at the tunnel exit, the SRP core adopts a conformation that allows only transient binding and that can not retard elongation nor target the RNC to the membrane.

(iii) In the targeting mode, SRP binds with high affinity to the RNC adopting the conformation observed in the cryo-EM structure. The SRP core is positioned with the SRP54N and the C-terminal SRP54M domains on opposite sides of the tunnel exit and the hydrophobic groove with the bound signal sequence directly on top (fig. 12, 17, 20b). It remains unclear, whether the conformational changes within SRP54 open the hydrophobic groove, or if the signal sequence shapes its binding groove. Yet, a hydrophobic groove exposed to the aqueous solvent without substrate would be energetically unfavourable, and therefore, signal sequence binding is likely to follow an induced fit mechanism. The signal sequence locks the ribosome-bound SRP54 in the open conformation as seen in the EM structure and increases the affinities of SRP for both the ribosome [3, 133] and GTP [71]. As a result, the SRP core is positioned on the ribosome in a way that allows the Alu domain to cause elongation arrest by binding in the orientation observed by cryo-EM.

(iv) Docking of the targeting complex to the SRP receptor is very likely to involve interaction of the NG domains and also direct interaction of SR with the ribosome [84, 85, 134]. The orientation of SRP54 on the ribosome is altered after SR binding as shown by cross-linking [13]. The RNC-SRP-

SR complex formation will have to re-arrange at least the SRP54NG domain away from the exit tunnel which in turn would enable the transfer of the RNC to the translocon. Notably, in the X-ray structures of the interacting NG domains of bacterial SRP and SR [77, 78] the N-terminal helix of both N domains is displaced and the C-terminal helix of the G-domain (adjacent to the 'LGMGD' linker) is shifted towards the NG interface. This might also be relevant for re-arranging the SRP54NG domain on the ribosome.

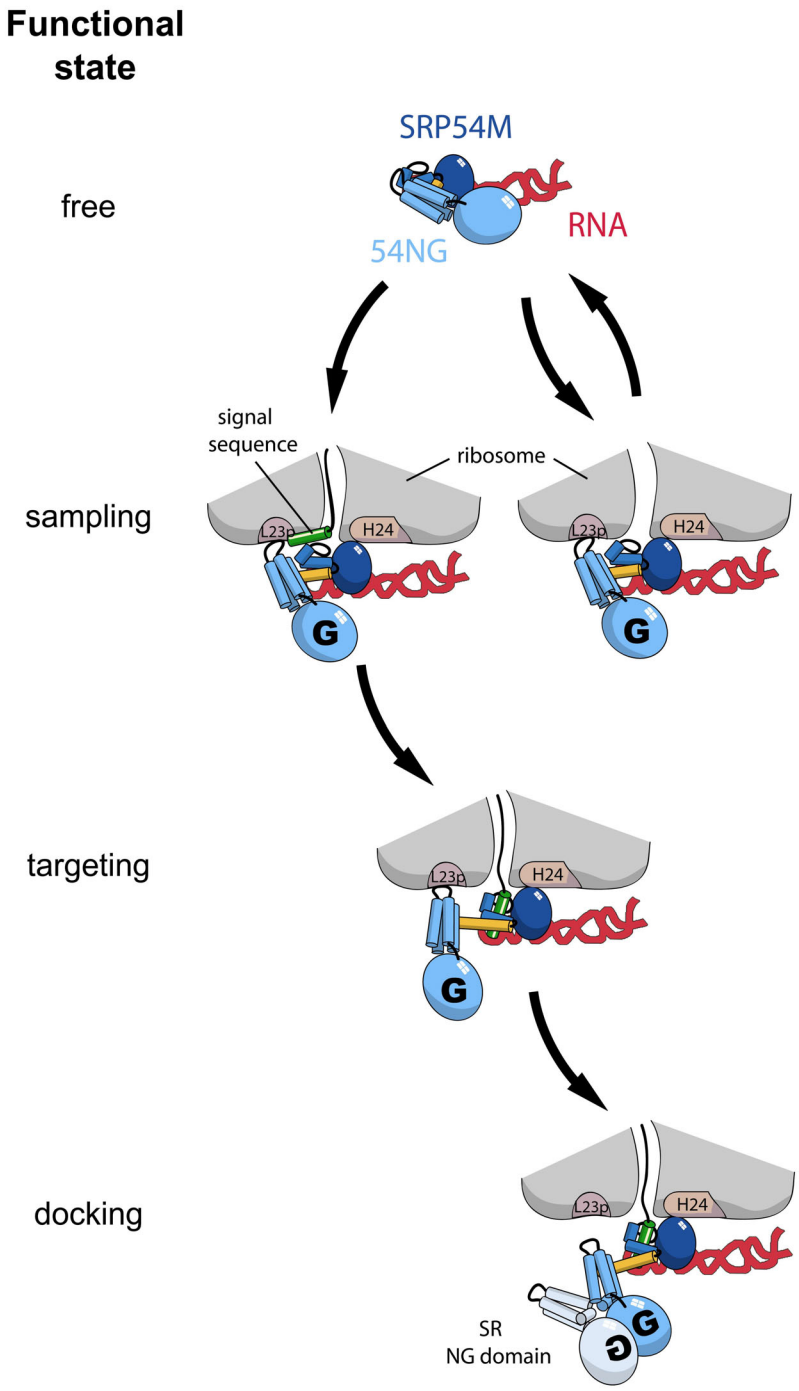

Figure 31: Model for the first steps of the SRP cycle. A detailed scheme of the conformational events of the SRP core during the first steps of cotranslational targeting can be modelled as follows: (i) In the free state, the SRP core adopts a compact conformation. A distal loop of SRP54N contacts SRP54MN, which is later on involved in signal sequence binding. SRP54G interacts with helix 8 of the SRP RNA and the nucleotide affinity is low. (ii) In the sampling mode, SRP interacts with low affinity and transiently with translating ribosomes in order to scan for signal sequences. The contact involves at least the L23p/L29p region (L23p) of the large ribosomal subunit and the distal loops of SRP54N. Ribosome binding induces a change in the SRP core towards a more open conformation, which probably leads already to a loss of the contact between the distal loop of SRP54N and SRP54MN and renders SRP capable for signal sequence recognition. The reorientation of SRP54NG allows for GTP binding. (iii) In the targeting mode, SRP interacts with high affinity with the ribosome-nascent-chain complex (including the L23p/L29p region and ribosomal RNA helix 24, H24). Signal sequence binding occurs to the hydrophobic binding groove of SRP54M and the binding is transmitted to SRP54NG by inter-domain communication. As a result, the RNC-bound SRP core changes to the fully open conformation by adjusting the flexible linker region between SRP54NG and SRP54M. The SRP-RNC targeting complex induces the high affinity GTP binding to SRP54NG, which is now primed for the interaction with the SRP receptor. (iv) The successive docking of the SRP-RNC complex to the translocon via SR is structurally unresolved. However, the interaction of the SRP-RNC complex with SR may lead to the twin-like arrangement of the SRP/SR NG-domains resulting in relocalization of the SRP54 NG domain. Colour code as in fig. 20 and 22.

4.2.1 Regulation of GTP affinity

Signal sequence binding to SRP54M must be followed by GTP binding to SRP54G in order to target the RNC to the translocation machinery at the membrane. SRP and the SRP receptor will form a complex only when the GTPases in both proteins bind GTP. The X-ray structures of the interacting NG domains of bacterial SRP and SR in the presence of a non-hydrolysable GTP analogue [77, 78] show the two nucleotides totally buried in the protein interface. This finding argues strongly in favour of GTP binding as a prerequisite for complex formation.

Although different models exist [63, 66, 134], there is strong evidence that the RNC complex stimulates GTP binding to SRP54 upon binding [71] and the question remains how that happens? The ribosome induced conformational change (most likely already in the sampling mode), and in particular the reorientation of the SRP54NG domain, is most likely the major trigger to increase GTP affinity. The observation that in the presence of ribosomes, but even in the absence of a signal sequence, the affinity of SRP54 for GTP is 10 times higher than in free SRP strongly supports this idea [71]. As already discussed previously, a tilt of SRP54N with respect to SRP54G seems to be responsible for a reorganisation of GTP binding determinants in SRP54G [135]. Only in the ribosome-bound state of SRP54, the rotation of SRP54N seems possible and can further on be communicated via conserved sequence motifs in the NG interface to the nucleotide binding pocket. However, in the absence of a signal sequence, SRP binding and therefore GTP binding remain transient. Only in the active SRP-RNC targeting complex, GTP binding to SRP54 is stabilized and targeting can proceed by docking to the SRP receptor.

4.3 Structure of SR-SRP-RNC complex

Although the resolution of the structure is not sufficient yet for complete interpretation and model building, a preliminary interpretation is already possible. When SRP-RNC complex interacts with

SR in presence of GTP, the NG-domains of SRP54 and SRα form a twin-like heterodimeric complex. Apparently this leads to delocalization of both NG-domains which dissociates SRP from binding site C1. This binding site involves ribosomal proteins L23e and L35 which provide, in addition, the binding site for the translocon and, thus, clearing of the binding site C1 allows spatial access of the translocon.

In the crystal structure of the yeast SRX-SRβ complex [81], SRβ is in the GTP-bound state, the same state as in the complex used for this cryo-EM structure. Nevertheless, it is not possible to dock the crystal structure of SRβ into the density without causing steric clashes with other structures. This leads to the assumption that SRβ may dissociate from SRα. To dissociate SRβ has to switch from the GTP-bound state to the GDP-bound state in which the affinity for SRα is several orders of magnitude lower [81]. Since SRβ is the only component in this ternary complex which is not loaded with GMP-PNP, but with GTP, nucleotide hydrolysis and the subsequent dissociation is possible. As a second prerequisite for the GTP hydrolysis, SRβ needs a GAP to function as a GTPase switch as it belongs to the Ras-like Arf-family of GTPases [81]. According to earlier biochemical studies, it may be indeed the ribosome which provides the GAP activity for SRβ [84]. Therefore, it appears to be the most likely scenario that after SRβ interaction with the ribosome-SRP complex, GTP hydrolysis takes place, followed by the dissociation of SRβ from SRα. It is intriguing that despite the dissociation from SRα, SRβ stays bound to the ribosome. This is in agreement not only with our binding assays (fig. 23) but also with earlier cross-linking experiments showing that SRβ, in its GDP or nucleotide free state, interacts with a 21kD protein of the large ribosomal subunit [85]. In the presence of GTP or GMP-PNP the cross-links were not observed. Thus, in its GDP form, SRβ would provide a second anchor point of the targeting complex on the ER membrane. More recent biochemical studies show that SR interacts strongly with both, SRP and the ribosome, and that SR by this dual recognition rejects ribosomes that lack bound SRP [134]. Taken together, it appears that in eukaryotes two different contacts are required for functional targeting, the contact between SRP and SRα, and the contact between the ribosome and SRα and SRβ. Here, SRβ could serve in a proofreading mechanism or simply by ensuring that the SRP-RNC complex is targeted to the correct membrane in the cell.

4.4 The next steps

Although the structural characterization of the first steps of the SRP cycle makes significant progress, many questions remain to be answered: Does the SRP54N domain in the ribosome-bound state indeed rotate with respect to the G domain and what is the exact conformation of the linker region? Is the signal sequence indeed bound to the hydrophobic groove of SRP54M as proposed, and what is the significance of the newly defined dynamic regions of the SRP core in different functional states? Mutational and biochemical analysis, more high resolution X-ray and cryo-EM structures should provide the missing details of what happens when SRP meets ribosome.

Following the SRP cycle further, the comparison of the SRP-RNC structure with the previously reported cryo-EM structure of the RNC in complex with the translocon [99] shows that both, SRP and the translocon, bind at the tunnel exit of the ribosome in a mutually exclusive way. Here, the question remains of how the transfer of the signal sequence and the entire RNC from SRP to the translocon is facilitated. The preliminary cryo-EM structure of SR-SRP-RNC complex provides more insights in the next step of protein targeting. Visualization of a Sec61-SR-SRP-RNC intermediate will be one of the next challenging tasks in order to build a more complete model of the SRP cycle.

Eidestattliche Erklärung:

Hiermit erkläre ich, die Dissertation selbständig und ohne unerlaubte Hilfe angefertigt zu haben.

References:

[1] Keenan, R. J.; Freymann, D. M.; Walter, P. and Stroud, R. M. (1998): Crystal structure of the signal sequence binding subunit of the signal recognition particle, Cell (vol. 94), No. 2, pp. 181-91.

[2] Blobel, G and Sabatini, DD (1971): Ribosome-membrane interaction in eucaryotic cells, Biomembranes, pp. 193-195.

[3] Walter, P.; Ibrahimi, I. and Blobel, G. (1981): Translocation of proteins across the endoplasmic reticulum. I. Signal recognition protein (SRP) binds to in-vitro-assembled polysomes synthesizing secretory protein, J Cell Biol (vol. 91), No. 2 Pt 1, pp. 545-50.

[4] Koch, H. G.; Moser, M. and Muller, M. (2003): Signal recognition particle-dependent protein targeting, universal to all kingdoms of life, Rev Physiol Biochem Pharmacol (vol. 146:55-94.), No. 10.

[5] Gundelfinger, E. D.; Krause, E.; Melli, M. and Dobberstein, B. (1983): The organization of the 7SL RNA in the signal recognition particle, Nucleic Acids Res (vol. 11), No. 21, pp. 7363-74.

[6] Siegel, V. and Walter, P. (1988): Each of the activities of signal recognition particle (SRP) is contained within a distinct domain: analysis of biochemical mutants of SRP, Cell (vol. 52), No. 1, pp. 39-49.

[7] Walter, P. and Blobel, G. (1983): Disassembly and reconstitution of signal recognition particle, Cell (vol. 34), No. 2, pp. 525-33.

[8] Connolly, T. and Gilmore, R. (1989): The signal recognition particle receptor mediates the GTP-dependent displacement of SRP from the signal sequence of the nascent polypeptide, Cell (vol. 57), No. 4, pp. 599-610.

[9] Bernstein, H. D.; Poritz, M. A.; Strub, K.; Hoben, P. J.; Brenner, S. and Walter, P. (1989): Model for signal sequence recognition from amino-acid sequence of 54K subunit of signal recognition particle, Nature (vol. 340), No. 6233, pp. 482-6.

[10] Romisch, K.; Webb, J.; Lingelbach, K.; Gausepohl, H. and Dobberstein, B. (1990): The 54-kD protein of signal recognition particle contains a methionine-rich RNA binding domain, J Cell Biol (vol. 111), No. 5 Pt 1, pp. 1793-802.

[11] Batey, R. T.; Rambo, R. P.; Lucast, L.; Rha, B. and Doudna, J. A. (2000): Crystal structure of the ribonucleoprotein core of the signal recognition particle, Science (vol. 287), No. 5456, pp. 1232-9.

[12] Zopf, D.; Bernstein, H. D.; Johnson, A. E. and Walter, P. (1990): The methionine-rich domain of the 54 kd protein subunit of the signal recognition particle contains an RNA binding site and can be crosslinked to a signal sequence, Embo J (vol. 9), No. 13, pp. 4511-7.

[13] Pool, M. R.; Stumm, J.; Fulga, T. A.; Sinning, I. and Dobberstein, B. (2002): Distinct modes of signal recognition particle interaction with the ribosome, Science (vol. 297), No. 5585, pp. 1345-8.

[14] Siegel, V. and Walter, P. (1986): Removal of the Alu structural domain from signal recognition particle leaves its protein translocation activity intact, Nature (vol. 320), No. 6057, pp. 81-4.

[15] Walter, P. and Blobel, G. (1981): Translocation of proteins across the endoplasmic reticulum III. Signal recognition protein (SRP) causes signal sequence-dependent and site-specific arrest of chain elongation that is released by microsomal membranes, J Cell Biol (vol. 91), No. 2 Pt 1, pp. 557-61.

[16] Wolin, S. L. and Walter, P. (1989): Signal recognition particle mediates a transient elongation arrest of preprolactin in reticulocyte lysate, J Cell Biol (vol. 109), No. 6 Pt 1, pp. 2617-22.
[17] Mason, N.; Ciufo, L. F. and Brown, J. D. (2000): Elongation arrest is a physiologically important function of signal recognition particle, Embo J (vol. 19), No. 15, pp. 4164-74.
[18] Siegel, V. and Walter, P. (1985): Elongation arrest is not a prerequisite for secretory protein translocation across the microsomal membrane, J Cell Biol (vol. 100), No. 6, pp. 1913-21.
[19] Zheng, N. and Gierasch, L. M. (1997): Domain interactions in E. coli SRP: stabilization of M domain by RNA is required for effective signal sequence modulation of NG domain, Mol Cell (vol. 1), No. 1, pp. 79-87.
[20] Cleverley, R. M.; Zheng, N. and Gierasch, L. M. (2001): The cost of exposing a hydrophobic loop and implications for the functional role of 4.5 S RNA in the Escherichia coli signal recognition particle, J Biol Chem (vol. 276), No. 22, pp. 19327-31.
[21] Larsen, N. and Zwieb, C. (1991): SRP-RNA sequence alignment and secondary structure, Nucleic Acids Res (vol. 19), No. 2, pp. 209-15.
[22] Poritz, M. A.; Strub, K. and Walter, P. (1988): Human SRP RNA and E. coli 4.5S RNA contain a highly homologous structural domain, Cell (vol. 55), No. 1, pp. 4-6.
[23] Honda, K.; Nakamura, K.; Nishiguchi, M. and Yamane, K. (1993): Cloning and characterization of a Bacillus subtilis gene encoding a homolog of the 54-kilodalton subunit of mammalian signal recognition particle and Escherichia coli Ffh, J Bacteriol (vol. 175), No. 15, pp. 4885-94.
[24] Nakamura, K.; Yahagi, S.; Yamazaki, T. and Yamane, K. (1999): Bacillus subtilis histone-like protein, HBsu, is an integral component of a SRP-like particle that can bind the Alu domain of small cytoplasmic RNA, J Biol Chem (vol. 274), No. 19, pp. 13569-76.
[25] Wild, K.; Weichenrieder, O.; Strub, K.; Sinning, I. and Cusack, S. (2002): Towards the structure of the mammalian signal recognition particle, Curr Opin Struct Biol (vol. 12), No. 1, pp. 72-81.
[26] Keenan, R. J.; Freymann, D. M.; Stroud, R. M. and Walter, P. (2001): The signal recognition particle, Annu Rev Biochem (vol. 70:755-75.), No. 52.
[27] Bhuiyan, S. H.; Gowda, K.; Hotokezaka, H. and Zwieb, C. (2000): Assembly of archaeal signal recognition particle from recombinant components, Nucleic Acids Res (vol. 28), No. 6, pp. 1365-73.
[28] Van Nues, R. W. and Brown, J. D. (2004): Saccharomyces SRP RNA secondary structures: a conserved S-domain and extended Alu-domain, Rna (vol. 10), No. 1, pp. 75-89.
[29] Bernstein, H. D.; Zopf, D.; Freymann, D. M. and Walter, P. (1993): Functional substitution of the signal recognition particle 54-kDa subunit by its Escherichia coli homolog, Proc Natl Acad Sci U S A (vol. 90), No. 11, pp. 5229-33.
[30] Schuenemann, D.; Gupta, S.; Persello-Cartieaux, F.; Klimyuk, Vi Vi; Jones, J. D. G.; Nussaume, L. and Hoffman, N. E. (1998): A novel signal recognition particle targets light-harvesting proteins to the thylakoid membranes, Proc Natl Acad Sci U S A (vol. 95), No. 17, pp. 10312-6.
[31] Eichacker, L. A. and Henry, R. (2001): Function of a chloroplast SRP in thylakoid protein export, Biochim Biophys Acta (vol. 1541), No. 1-2, pp. 120-34.
[32] Zhang, L.; Paakkarinen, V.; van Wijk, K. J. and Aro, E. M. (1999): Co-translational assembly of the D1 protein into photosystem II, J Biol Chem (vol. 274), No. 23, pp. 16062-7.

[33] Zhang, L.; Paakkarinen, V.; Suorsa, M. and Aro, E. M. (2001): A SecY homologue is involved in chloroplast-encoded D1 protein biogenesis, J Biol Chem (vol. 276), No. 41, pp. 37809-14.
[34] Nilsson, R.; Brunner, J.; Hoffman, N. E. and van Wijk, K. J. (1999): Interactions of ribosome nascent chain complexes of the chloroplast-encoded D1 thylakoid membrane protein with cpSRP54, Embo J (vol. 18), No. 3, pp. 733-42.
[35] Li, X.; Henry, R.; Yuan, J.; Cline, K. and Hoffman, N. E. (1995): A chloroplast homologue of the signal recognition particle subunit SRP54 is involved in the posttranslational integration of a protein into thylakoid membranes, Proc Natl Acad Sci U S A (vol. 92), No. 9, pp. 3789-93.
[36] Groves, M. R.; Mant, A.; Kuhn, A.; Koch, J.; Dubel, S.; Robinson, C. and Sinning, I. (2001): Functional characterization of recombinant chloroplast signal recognition particle, J Biol Chem (vol. 276), No. 30, pp. 27778-86.
[37] Politz, J. C.; Yarovoi, S.; Kilroy, S. M.; Gowda, K.; Zwieb, C. and Pederson, T. (2000): Signal recognition particle components in the nucleolus, Proc Natl Acad Sci U S A (vol. 97), No. 1, pp. 55-60.
[38] Grosshans, H.; Deinert, K.; Hurt, E. and Simos, G. (2001): Biogenesis of the signal recognition particle (SRP) involves import of SRP proteins into the nucleolus, assembly with the SRP-RNA, and Xpo1p-mediated export, J Cell Biol (vol. 153), No. 4, pp. 745-62.
[39] Strub, K. and Walter, P. (1990): Assembly of the Alu domain of the signal recognition particle (SRP): dimerization of the two protein components is required for efficient binding to SRP RNA, Mol Cell Biol (vol. 10), No. 2, pp. 777-84.
[40] Weichenrieder, O.; Wild, K.; Strub, K. and Cusack, S. (2000): Structure and assembly of the Alu domain of the mammalian signal recognition particle, Nature (vol. 408), No. 6809, pp. 167-73.
[41] Chen, Y.; Sinha, K.; Perumal, K.; Gu, J. and Reddy, R. (1998): Accurate 3' end processing and adenylation of human signal recognition particle RNA and alu RNA in vitro, J Biol Chem (vol. 273), No. 52, pp. 35023-31.
[42] Emde, G.; Frontzek, A. and Benecke, B. J. (1997): Secondary structure of the nascent 7S L RNA mediates efficient transcription by RNA polymerase III, Rna (vol. 3), No. 5, pp. 538-49.
[43] Weiner, A. M.; Deininger, P. L. and Efstratiadis, A. (1986): Nonviral retroposons: genes, pseudogenes, and transposable elements generated by the reverse flow of genetic information, Annu Rev Biochem (vol. 55), pp. 631-61.
[44] Mighell, A. J.; Markham, A. F. and Robinson, P. A. (1997): Alu sequences, FEBS Lett (vol. 417), No. 1, pp. 1-5.
[45] Wild, K.; Sinning, I. and Cusack, S. (2001): Crystal structure of an early protein-RNA assembly complex of the signal recognition particle, Science (vol. 294), No. 5542, pp. 598-601.
[46] Kuglstatter, A.; Oubridge, C. and Nagai, K. (2002): Induced structural changes of 7SL RNA during the assembly of human signal recognition particle, Nat Struct Biol (vol. 9), No. 10, pp. 740-4.
[47] Nagai, K.; Oubridge, C.; Kuglstatter, A.; Menichelli, E.; Isel, C. and Jovine, L. (2003): Structure, function and evolution of the signal recognition particle, Embo J (vol. 22), No. 14, pp. 3479-85.
[48] Lutcke, H.; Prehn, S.; Ashford, A. J.; Remus, M.; Frank, R. and Dobberstein, B. (1993): Assembly of the 68- and 72-kD proteins of signal recognition particle with 7S RNA, J Cell Biol (vol. 121), No. 5, pp. 977-85.

[49] Siegel, V. and Walter, P. (1988): Binding sites of the 19-kDa and 68/72-kDa signal recognition particle (SRP) proteins on SRP RNA as determined in protein-RNA "footprinting", Proc Natl Acad Sci U S A (vol. 85), No. 6, pp. 1801-5.
[50] Althoff, S.; Selinger, D. and Wise, J. A. (1994): Molecular evolution of SRP cycle components: functional implications, Nucleic Acids Res (vol. 22), No. 11, pp. 1933-47.
[51] Gellman, S. H. (1991): On the role of methionine residues in the sequence-independent recognition of nonpolar protein surfaces, Biochemistry (vol. 30), No. 27, pp. 6633-6.
[52] Luirink, J.; High, S.; Wood, H.; Giner, A.; Tollervey, D. and Dobberstein, B. (1992): Signal-sequence recognition by an Escherichia coli ribonucleoprotein complex, Nature (vol. 359), No. 6397, pp. 741-3.
[53] Rosendal, K. R.; Wild, K.; Montoya, G. and Sinning, I. (2003): Crystal structure of the complete core of archaeal signal recognition particle and implications for interdomain communication, Proc Natl Acad Sci U S A (vol. 100), No. 25, pp. 14701-6.
[54] Schmitz, U.; James, T. L.; Lukavsky, P. and Walter, P. (1999): Structure of the most conserved internal loop in SRP RNA, Nat Struct Biol (vol. 6), No. 7, pp. 634-8.
[55] Yaver, D. S.; Matoba, S. and Ogrydziak, D. M. (1992): A mutation in the signal recognition particle 7S RNA of the yeast Yarrowia lipolytica preferentially affects synthesis of the alkaline extracellular protease: in vivo evidence for translational arrest, J Cell Biol (vol. 116), No. 3, pp. 605-16.
[56] Raine, A.; Ullers, R.; Pavlov, M.; Luirink, J.; Wikberg, J. E. and Ehrenberg, M. (2003): Targeting and insertion of heterologous membrane proteins in E. coli, Biochimie (vol. 85), No. 7, pp. 659-68.
[57] Gilmore, R.; Blobel, G. and Walter, P. (1982): Protein translocation across the endoplasmic reticulum. I. Detection in the microsomal membrane of a receptor for the signal recognition particle, J Cell Biol (vol. 95), No. 2 Pt 1, pp. 463-9.
[58] Young, J. C. and Andrews, D. W. (1996): The signal recognition particle receptor alpha subunit assembles co-translationally on the endoplasmic reticulum membrane during an mRNA-encoded translation pause in vitro, Embo J (vol. 15), No. 1, pp. 172-81.
[59] Bourne, H. R.; Sanders, D. A. and McCormick, F. (1990): The GTPase superfamily: a conserved switch for diverse cell functions, Nature (vol. 348), No. 6297, pp. 125-32.
[60] Millman, J. S. and Andrews, D. W. (1997): Switching the model: a concerted mechanism for GTPases in protein targeting, Cell (vol. 89), No. 5, pp. 673-6.
[61] Montoya, G.; Svensson, C.; Luirink, J. and Sinning, I. (1997): Crystal structure of the NG domain from the signal-recognition particle receptor FtsY, Nature (vol. 385), No. 6614, pp. 365-8.
[62] Freymann, D. M.; Keenan, R. J.; Stroud, R. M. and Walter, P. (1997): Structure of the conserved GTPase domain of the signal recognition particle, Nature (vol. 385), No. 6614, pp. 361-4.
[63] Miller, J. D.; Wilhelm, H.; Gierasch, L.; Gilmore, R. and Walter, P. (1993): GTP binding and hydrolysis by the signal recognition particle during initiation of protein translocation, Nature (vol. 366), No. 6453, pp. 351-4.
[64] Miller, J. D.; Bernstein, H. D. and Walter, P. (1994): Interaction of E. coli Ffh/4.5S ribonucleoprotein and FtsY mimics that of mammalian signal recognition particle and its receptor, Nature (vol. 367), No. 6464, pp. 657-9.

[65] Moser, C.; Mol, O.; Goody, R. S. and Sinning, I. (1997): The signal recognition particle receptor of Escherichia coli (FtsY) has a nucleotide exchange factor built into the GTPase domain, Proc Natl Acad Sci U S A (vol. 94), No. 21, pp. 11339-44.
[66] Jagath, J. R.; Rodnina, M. V.; Lentzen, G. and Wintermeyer, W. (1998): Interaction of guanine nucleotides with the signal recognition particle from Escherichia coli, Biochemistry (vol. 37), No. 44, pp. 15408-13.
[67] Newitt, J. A. and Bernstein, H. D. (1997): The N-domain of the signal recognition particle 54-kDa subunit promotes efficient signal sequence binding, Eur J Biochem (vol. 245), No. 3, pp. 720-9.
[68] Zopf, D.; Bernstein, H. D. and Walter, P. (1993): GTPase domain of the 54-kD subunit of the mammalian signal recognition particle is required for protein translocation but not for signal sequence binding, J Cell Biol (vol. 120), No. 5, pp. 1113-21.
[69] Peluso, P.; Herschlag, D.; Nock, S.; Freymann, D. M.; Johnson, A. E. and Walter, P. (2000): Role of 4.5S RNA in assembly of the bacterial signal recognition particle with its receptor, Science (vol. 288), No. 5471, pp. 1640-3.
[70] Jagath, J. R.; Matassova, N. B.; de Leeuw, E.; Warnecke, J. M.; Lentzen, G.; Rodnina, M. V.; Luirink, J. and Wintermeyer, W. (2001): Important role of the tetraloop region of 4.5S RNA in SRP binding to its receptor FtsY, Rna (vol. 7), No. 2, pp. 293-301.
[71] Bacher, G.; Lutcke, H.; Jungnickel, B.; Rapoport, T. A. and Dobberstein, B. (1996): Regulation by the ribosome of the GTPase of the signal-recognition particle during protein targeting, Nature (vol. 381), No. 6579, pp. 248-51.
[72] de Leeuw, E.; Poland, D.; Mol, O.; Sinning, I.; ten Hagen-Jongman, C. M.; Oudega, B. and Luirink, J. (1997): Membrane association of FtsY, the E. coli SRP receptor, FEBS Lett (vol. 416), No. 3, pp. 225-9.
[73] de Leeuw, E.; te Kaat, K.; Moser, C.; Menestrina, G.; Demel, R.; de Kruijff, B.; Oudega, B.; Luirink, J. and Sinning, I. (2000): Anionic phospholipids are involved in membrane association of FtsY and stimulate its GTPase activity, Embo J (vol. 19), No. 4, pp. 531-41.
[74] Song, W.; Raden, D.; Mandon, E. C. and Gilmore, R. (2000): Role of Sec61alpha in the regulated transfer of the ribosome-nascent chain complex from the signal recognition particle to the translocation channel, Cell (vol. 100), No. 3, pp. 333-43.
[75] Shepotinovskaya, I. V. and Freymann, D. M. (2002): Conformational change of the N-domain on formation of the complex between the GTPase domains of Thermus aquaticus Ffh and FtsY, Biochim Biophys Acta (vol. 1597), No. 1, pp. 107-14.
[76] Powers, T. and Walter, P. (1995): Reciprocal stimulation of GTP hydrolysis by two directly interacting GTPases, Science (vol. 269), No. 5229, pp. 1422-4.
[77] Focia, P. J.; Shepotinovskaya, I. V.; Seidler, J. A. and Freymann, D. M. (2004): Heterodimeric GTPase core of the SRP targeting complex, Science (vol. 303), No. 5656, pp. 373-7.
[78] Egea, P. F.; Shan, S. O.; Napetschnig, J.; Savage, D. F.; Walter, P. and Stroud, R. M. (2004): Substrate twinning activates the signal recognition particle and its receptor, Nature (vol. 427), No. 6971, pp. 215-21.
[79] Shan, S. O.; Stroud, R. M. and Walter, P. (2004): Mechanism of association and reciprocal activation of two GTPases, PLoS Biol (vol. 2), No. 10, p. e320.
[80] Caldon, C. E.; Yoong, P. and March, P. E. (2001): Evolution of a molecular switch: universal bacterial GTPases regulate ribosome function, Mol Microbiol (vol. 41), No. 2, pp. 289-97.

[81] Schwartz, T. and Blobel, G. (2003): Structural basis for the function of the beta subunit of the eukaryotic signal recognition particle receptor, Cell (vol. 112), No. 6, pp. 793-803.
[82] Legate, K. R.; Falcone, D. and Andrews, D. W. (2000): Nucleotide-dependent binding of the GTPase domain of the signal recognition particle receptor beta-subunit to the alpha-subunit, J Biol Chem (vol. 275), No. 35, pp. 27439-46.
[83] Helmers, J.; Schmidt, D.; Glavy, J. S.; Blobel, G. and Schwartz, T. (2003): The beta-subunit of the protein-conducting channel of the endoplasmic reticulum functions as the guanine nucleotide exchange factor for the beta-subunit of the signal recognition particle receptor, J Biol Chem (vol. 278), No. 26, pp. 23686-90.
[84] Bacher, G.; Pool, M. and Dobberstein, B. (1999): The ribosome regulates the GTPase of the beta-subunit of the signal recognition particle receptor, J Cell Biol (vol. 146), No. 4, pp. 723-30.
[85] Fulga, T. A.; Sinning, I.; Dobberstein, B. and Pool, M. R. (2001): SRbeta coordinates signal sequence release from SRP with ribosome binding to the translocon, Embo J (vol. 20), No. 9, pp. 2338-47.
[86] Martoglio, B.; Hauser, S. and Dobberstein, B. (1997), Celis, J.C., Cell Biology: A Laboratory Handbook (vol. 34) pp. 265-273., Academic Press, San Diego.
[87] Walter, P. and Blobel, G. (1983): Signal recognition particle: a ribonucleoprotein required for cotranslational translocation of proteins, isolation and properties, Methods Enzymol (vol. 96), pp. 682-91.
[88] Wagenknecht, T.; Grassucci, R. and Frank, J. (1988): Electron microscopy and computer image averaging of ice-embedded large ribosomal subunits from Escherichia coli, J Mol Biol (vol. 199), No. 1, pp. 137-47.
[89] Frank, J.; Radermacher, M.; Penczek, P.; Zhu, J.; Li, Y.; Ladjadj, M. and Leith, A. (1996): SPIDER and WEB: processing and visualization of images in 3D electron microscopy and related fields, J Struct Biol (vol. 116), No. 1, pp. 190-9.
[90] Mindell, J. A. and Grigorieff, N. (2003): Accurate determination of local defocus and specimen tilt in electron microscopy, J Struct Biol (vol. 142), No. 3, pp. 334-47.
[91] Roseman, A. M. (2003): Particle finding in electron micrographs using a fast local correlation algorithm, Ultramicroscopy (vol. 94), No. 3-4, pp. 225-36.
[92] Jones, T.A.; Zhou, J.Y.; Cowan, S.W. and Kjeldgaard, M. (1991): Improved methods for building protein models in electron density maps and the location of errors in these models., Acta Crystallogr. A (vol. A47), pp. 110-119.
[93] Huang, Q.; Abdulrahman, S.; Yin, J. and Zwieb, C. (2002): Systematic site-directed mutagenesis of human protein SRP54: interactions with signal recognition particle RNA and modes of signal peptide recognition, Biochemistry (vol. 41), No. 38, pp. 11362-71.
[94] Padmanabhan, S. and Freymann, D. M. (2001): The conformation of bound GMPPNP suggests a mechanism for gating the active site of the SRP GTPase, Structure (Camb) (vol. 9), No. 9, pp. 859-67.
[95] Rosenblad, M. A.; Gorodkin, J.; Knudsen, B.; Zwieb, C. and Samuelsson, T. (2003): SRPDB: Signal Recognition Particle Database, Nucleic Acids Res (vol. 31), No. 1, pp. 363-4. 12:.
[96] Rath, B. K.; Hegerl, R.; Leith, A.; Shaikh, T. R.; Wagenknecht, T. and Frank, J. (2003): Fast 3D motif search of EM density maps using a locally normalized cross-correlation function, J Struct Biol (vol. 144), No. 1-2, pp. 95-103.
[97] Chao, J. A.; Prasad, G. S.; White, S. A.; Stout, C. D. and Williamson, J. R. (2003): Inherent protein structural flexibility at the RNA-binding interface of L30e, J Mol Biol (vol. 326), No. 4, pp. 999-1004.

[98] Walter, P. and Blobel, G. (1983): Subcellular distribution of signal recognition particle and 7SL-RNA determined with polypeptide-specific antibodies and complementary DNA probe, J Cell Biol (vol. 97), No. 6, pp. 1693-9.
[99] Beckmann, R.; Spahn, C. M.; Eswar, N.; Helmers, J.; Penczek, P. A.; Sali, A.; Frank, J. and Blobel, G. (2001): Architecture of the protein-conducting channel associated with the translating 80S ribosome, Cell (vol. 107), No. 3, pp. 361-72.
[100] Spahn, C. M.; Beckmann, R.; Eswar, N.; Penczek, P. A.; Sali, A.; Blobel, G. and Frank, J. (2001): Structure of the 80S ribosome from Saccharomyces cerevisiae--tRNA-ribosome and subunit-subunit interactions, Cell (vol. 107), No. 3, pp. 373-86.
[101] Ban, N.; Nissen, P.; Hansen, J.; Moore, P. B. and Steitz, T. A. (2000): The complete atomic structure of the large ribosomal subunit at 2.4 A resolution, Science (vol. 289), No. 5481, pp. 905-20.
[102] Thomas, Y.; Bui, N. and Strub, K. (1997): A truncation in the 14 kDa protein of the signal recognition particle leads to tertiary structure changes in the RNA and abolishes the elongation arrest activity of the particle, Nucleic Acids Res (vol. 25), No. 10, pp. 1920-9.
[103] Gu, S. Q.; Peske, F.; Wieden, H. J.; Rodnina, M. V. and Wintermeyer, W. (2003): The signal recognition particle binds to protein L23 at the peptide exit of the Escherichia coli ribosome, Rna (vol. 9), No. 5, pp. 566-73.
[104] Eisner, G.; Koch, H. G.; Beck, K.; Brunner, J. and Muller, M. (2003): Ligand crowding at a nascent signal sequence, J Cell Biol (vol. 163), No. 1, pp. 35-44.
[105] Kramer, G.; Rauch, T.; Rist, W.; Vorderwulbecke, S.; Patzelt, H.; Schulze-Specking, A.; Ban, N.; Deuerling, E. and Bukau, B. (2002): L23 protein functions as a chaperone docking site on the ribosome, Nature (vol. 419), No. 6903, pp. 171-4.
[106] Ullers, R. S.; Houben, E. N.; Raine, A.; ten Hagen-Jongman, C. M.; Ehrenberg, M.; Brunner, J.; Oudega, B.; Harms, N. and Luirink, J. (2003): Interplay of signal recognition particle and trigger factor at L23 near the nascent chain exit site on the Escherichia coli ribosome, J Cell Biol (vol. 161), No. 4, pp. 679-84.
[107] Rinke-Appel, J.; Osswald, M.; von Knoblauch, K.; Mueller, F.; Brimacombe, R.; Sergiev, P.; Avdeeva, O.; Bogdanov, A. and Dontsova, O. (2002): Crosslinking of 4.5S RNA to the Escherichia coli ribosome in the presence or absence of the protein Ffh, Rna (vol. 8), No. 5, pp. 612-25.
[108] Diener, J. L. and Wilson, C. (2000): Role of SRP19 in assembly of the Archaeoglobus fulgidus signal recognition particle, Biochemistry (vol. 39), No. 42, pp. 12862-74.
[109] Esnouf, R. M. (1997): An extensively modified version of MolScript that includes greatly enhanced coloring capabilities, J Mol Graph Model (vol. 15), No. 2, pp. 132-4, 112-3.
[110] Merritt and Bacon (1997): Raster 3D, Macromolecular Crystallography (vol. 277), No. 277, pp. 505-524.
[111] Cleverley, R. M. and Gierasch, L. M. (2002): Mapping the signal sequence-binding site on SRP reveals a significant role for the NG domain, J Biol Chem (vol. 277), No. 48, pp. 46763-8.
[112] Eng, F. J. and Warner, J. R. (1991): Structural basis for the regulation of splicing of a yeast messenger RNA, Cell (vol. 65), No. 5, pp. 797-804.
[113] Vilardell, J. and Warner, J. R. (1994): Regulation of splicing at an intermediate step in the formation of the spliceosome, Genes Dev (vol. 8), No. 2, pp. 211-20.
[114] Dabeva, M. D. and Warner, J. R. (1993): Ribosomal protein L32 of Saccharomyces cerevisiae regulates both splicing and translation of its own transcript, J Biol Chem (vol. 268), No. 26, pp. 19669-74.

[115] Li, B.; Vilardell, J. and Warner, J. R. (1996): An RNA structure involved in feedback regulation of splicing and of translation is critical for biological fitness, Proc Natl Acad Sci U S A (vol. 93), No. 4, pp. 1596-600.
[116] Vilardell, J.; Yu, S. J. and Warner, J. R. (2000): Multiple functions of an evolutionarily conserved RNA binding domain, Mol Cell (vol. 5), No. 4, pp. 761-6.
[117] Chen, Y. W.; Bycroft, M. and Wong, K. B. (2003): Crystal structure of ribosomal protein L30e from the extreme thermophile Thermococcus celer: thermal stability and RNA binding, Biochemistry (vol. 42), No. 10, pp. 2857-65.
[118] Bates, P. A.; Kelley, L. A.; MacCallum, R. M. and Sternberg, M. J. (2001): Enhancement of protein modeling by human intervention in applying the automatic programs 3D-JIGSAW and 3D-PSSM, Proteins (vol. Suppl 5), pp. 39-46.
[119] Baronas-Lowell, D. M. and Warner, J. R. (1990): Ribosomal protein L30 is dispensable in the yeast Saccharomyces cerevisiae, Mol Cell Biol (vol. 10), No. 10, pp. 5235-43.
[120] Spahn, C. M.; Gomez-Lorenzo, M. G.; Grassucci, R. A.; Jorgensen, R.; Andersen, G. R.; Beckmann, R.; Penczek, P. A.; Ballesta, J. P. and Frank, J. (2004): Domain movements of elongation factor eEF2 and the eukaryotic 80S ribosome facilitate tRNA translocation, Embo J (vol. 23), No. 5, pp. 1008-1019.
[121] Andrews, D. W.; Walter, P. and Ottensmeyer, F. P. (1987): Evidence for an extended 7SL RNA structure in the signal recognition particle, Embo J (vol. 6), No. 11, pp. 3471-7.
[122] Morgan, D. G.; Menetret, J. F.; Neuhof, A.; Rapoport, T. A. and Akey, C. W. (2002): Structure of the mammalian ribosome-channel complex at 17A resolution, J Mol Biol (vol. 324), No. 4, pp. 871-86.
[123] Moller, I.; Jung, M.; Beatrix, B.; Levy, R.; Kreibich, G.; Zimmermann, R.; Wiedmann, M. and Lauring, B. (1998): A general mechanism for regulation of access to the translocon: competition for a membrane attachment site on ribosomes, Proc Natl Acad Sci U S A (vol. 95), No. 23, pp. 13425-30.
[124] Wilson, D. N.; Blaha, G.; Connell, S. R.; Ivanov, P. V.; Jenke, H.; Stelzl, U.; Teraoka, Y. and Nierhaus, K. H. (2002): Protein synthesis at atomic resolution: mechanistics of translation in the light of highly resolved structures for the ribosome, Curr Protein Pept Sci (vol. 3), No. 1, pp. 1-53.
[125] Gomez-Lorenzo, M. G.; Spahn, C. M.; Agrawal, R. K.; Grassucci, R. A.; Penczek, P.; Chakraburtty, K.; Ballesta, J. P.; Lavandera, J. L.; Garcia-Bustos, J. F. and Frank, J. (2000): Three-dimensional cryo-electron microscopy localization of EF2 in the Saccharomyces cerevisiae 80S ribosome at 17.5 A resolution, Embo J (vol. 19), No. 11, pp. 2710-8.
[126] Spahn, Christian; Gomez-Lorenzo, Maria G.; Grassucci, Robert A.; Jørgensen, Rene; Andersen, Gregers R.; Beckmann, Roland; Penczek, Pawel A.; Ballesta, Juan P. G. and Frank, Joachim Domain movements of elongation factor eEF2 and the eukaryotic 80S ribosome facilitate tRNA translocation, EMBO J. in press.
[127] Valle, M.; Zavialov, A.; Li, W.; Stagg, S. M.; Sengupta, J.; Nielsen, R. C.; Nissen, P.; Harvey, S. C.; Ehrenberg, M. and Frank, J. (2003): Incorporation of aminoacyl-tRNA into the ribosome as seen by cryo-electron microscopy, Nat Struct Biol (vol. 10), No. 11, pp. 899-906.
[128] Wolin, S. L. and Walter, P. (1988): Ribosome pausing and stacking during translation of a eukaryotic mRNA, Embo J (vol. 7), No. 11, pp. 3559-69.
[129] Ogg, S. C. and Walter, P. (1995): SRP samples nascent chains for the presence of signal sequences by interacting with ribosomes at a discrete step during translation elongation, Cell (vol. 81), No. 7, pp. 1075-84.

[130] Andreazzoli, M. and Gerbi, S. A. (1991): Changes in 7SL RNA conformation during the signal recognition particle cycle, Embo J (vol. 10), No. 4, pp. 767-77.
[131] Wiedmann, M.; Kurzchalia, T. V.; Bielka, H. and Rapoport, T. A. (1987): Direct probing of the interaction between the signal sequence of nascent preprolactin and the signal recognition particle by specific cross-linking, J Cell Biol (vol. 104), No. 2, pp. 201-8.
[132] Terzi, L.; Pool, M. R.; Dobberstein, B. and Strub, K. (2004): Signal recognition particle Alu domain occupies a defined site at the ribosomal subunit interface upon signal sequence recognition, Biochemistry (vol. 43), No. 1, pp. 107-17.
[133] Flanagan, J. J.; Chen, J. C.; Miao, Y.; Shao, Y.; Lin, J.; Bock, P. E. and Johnson, A. E. (2003): Signal recognition particle binds to ribosome-bound signal sequences with fluorescence-detected subnanomolar affinity that does not diminish as the nascent chain lengthens, J Biol Chem (vol. 278), No. 20, pp. 18628-37.
[134] Mandon, E. C.; Jiang, Y. and Gilmore, R. (2003): Dual recognition of the ribosome and the signal recognition particle by the SRP receptor during protein targeting to the endoplasmic reticulum, J Cell Biol (vol. 162), No. 4, pp. 575-85.
[135] Wild, K.; Rosendal, KR. and I., Sinning (2004): A structural step into the SRP cycle (vol. In press).